SIMILITUDE STUDY OF FLEXIBLE BURIED ARCHES SUBJECTED TO BLAST LOADS

Jimmy Piroshaw Balsara

Army Engineer Waterways Experiment Station
Vicksburg, Mississippi

January 1968

17

TECHNICAL REPORT NO. 1-807

SIMILITUDE STUDY OF FLEXIBLE BURIED ARCHES SUBJECTED TO BLAST LOADS

by

J. P. Balsara

January 1968

Sponsored by

Defense Atomic Support Agency

Conducted by

U. S. Army Engineer Waterways Experiment Station
CORPS OF ENGINEERS
Vicksburg, Mississippi

145

Destroy this report when no longer needed. Do not return it to the originator.

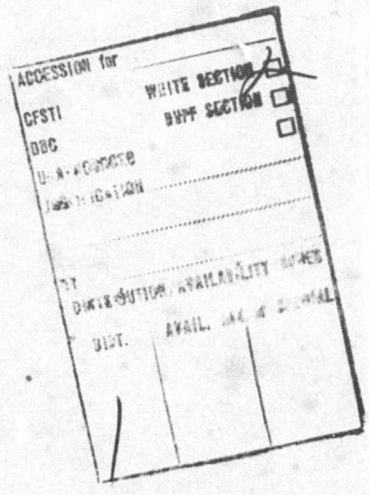

The findings in this report are not to be construed as an official Department of the Army position, unless so designated by other authorized documents.

TECHNICAL REPORT NO. 1-807

SIMILITUDE STUDY OF FLEXIBLE BURIED ARCHES SUBJECTED TO BLAST LOADS

by

J. P. Balsara

January 1968

Sponsored by

Defense Atomic Support Agency
NWER Subtask 13.010

Conducted by

U. S. Army Engineer Waterways Experiment Station
CORPS OF ENGINEERS
Vicksburg, Mississippi

ARMY-MRC VICKSBURG, MISS.

SIMILITUDE STUDY OF FLEXIBLE BURIED ARCHES SUBJECTED TO BLAST LOADS

Dissertation

Submitted in Partial Fulfillment
of the Requirements for the Degree of
Doctor of Philosophy
to the
Faculty of the Graduate School
of
West Virginia University

by

Jimmy Piroshaw Balsara, M.S.

Morgantown
West Virginia
1967

ACKNOWLEDGMENTS

This dissertation is based upon experiments conducted at the U. S. Army Engineer Waterways Experiment Station (WES), Vicksburg, Mississippi.

The investigation was conducted under the supervision of Mr. W. J. Flathau, Chief, Protective Structures Branch, WES, and Professor J. H. McElhaney of the Department of Theoretical and Applied Mechanics, West Virginia University.

Acknowledgment is made to Mr. W. J. Flathau for his comments and encouragement, to Mr. D. R. Denton who helped get the author started in this study, to the members of the Materials Section and the Instrumentation Branch for their support in carrying out the tests and their comments on interpreting the test data, and to the staff of the Reproduction and Reports Branch for their assistance in the preparation of the manuscript.

PREFACE

This study was conducted in the Nuclear Weapons Effects Division, U. S. Army Engineer Waterways Experiment Station, under the sponsorship of the Defense Atomic Support Agency (DASA) as part of NWER Subtask 13.010, Similitude Studies. The work was accomplished during the period June 1966 through September 1967.

Colonel John R. Oswalt, Jr., CE, was the Director of the Waterways Experiment Station during the period of this study. Mr. J. B. Tiffany was the Technical Director, and Mr. G. L. Arbuthnot, Jr., was Chief of the Nuclear Weapons Effects Division.

TABLE OF CONTENTS

LIST OF FIGURES

Figure Page

NOTATION

$a_1, a_2, \ldots a_n$	Physical quantities
a	Acceleration
$b_1, b_2, \ldots b_n$	Exponents
c	Velocity of propagation of waves
$c_1, c_2, \ldots c_n$	Exponents
D	Arch diameter
E	Modulus of elasticity
F	Force
g	Acceleration due to gravity
h	Arch thickness
H	Depth of soil cover
k	Number of independent fundamental dimensions
K	Constant
$K_{subscript}$	Scale factor
L	Length
m	Mass
M	Bending moment per unit length
n	Length scale
p	Pressure at any time
p_{so}	Peak surface overpressure
R	Arch radius

t	Time
t_+	Positive phase duration
T	Thrust per unit length
u_1, u_2, u_3	Displacements in x_1, x_2, x_3 directions, respectively, in cartesian coordinates
v	Velocity, in general
V	Particle velocity
w_o	Radial displacement of arch crown with respect to floor plate
γ_d	Dry unit weight
δ	Displacement of arch roof with respect to floor plate
ϵ	Strain
ϵ_{ij}	Strain components in cartesian coordinates
η_1	Soil modulus
η_2	Mass density of soil
ν	Poisson's ratio
π	Dimensionless product
ρ	Mass density
σ	Stress
σ_{ij}	Stress components in cartesian coordinates
ϕ	Angle of internal friction

BLANK PAGE

I

INTRODUCTION

A. Background

In recent years a number of laboratory facilities have been developed for studying the response of buried protective structures subjected to blast forces of nuclear devices. Many scale models of these structures, such as command centers, and other underground facilities, will probably be tested in the field or in these laboratory simulation facilities because of their importance to the defense of the United States.[26] Scale models have been used in many areas in engineering, especially where the systems were complex and not readily amenable to theory. Model testing in the laboratory allows closer control over important variables influencing the problem and it also becomes possible to repeat tests. Before model test results are used to predict the response of a prototype, scaling relations must be verified under simulated nuclear blast conditions. The length scale for the verification study must be practical for laboratory tests and large enough for scaling up to field prototypes.

Loading on the model required the pressure-time history to simulate the blast produced by the detonation of a nuclear weapon: a near instantaneous rise time to peak pressure followed by a relatively long positive pressure duration. The table in Figure 1

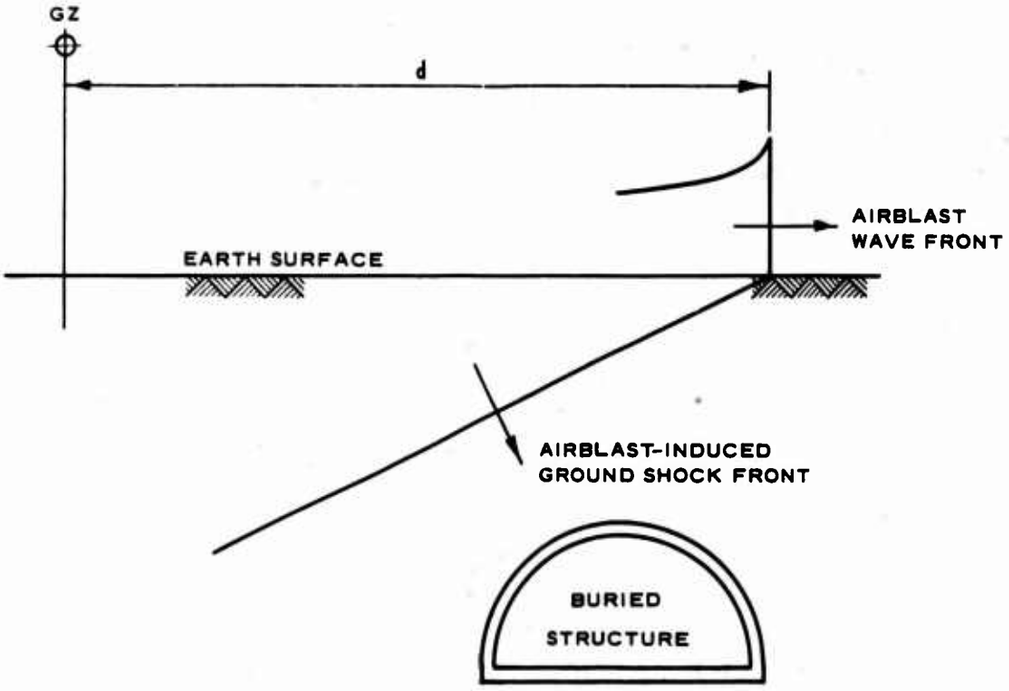

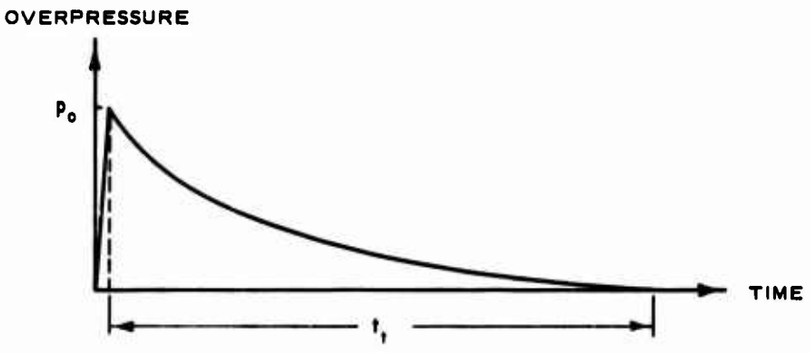

20-MT DEVICE

DISTANCE FROM GROUND ZERO d, FT	PEAK OVERPRESSURE p_o, PSI	POSITIVE PHASE t_t, SEC
4,700	500	3.6
6,700	200	3.7
12,000	50	4.6

Fig. 1

Air-Induced Ground Shock

illustrates values for distance from ground zero, peak overpressure, and duration time for a 20-MT (20 million tons of TNT) surface burst.[10] The maximum stress induced in the soil by the airblast wave from the surface burst traveling over the surface is nearly vertical, with no significant attenuation of medium to high, i.e. greater than 100 psi, airblast overpressure at the surface for moderate depths.

The next requirement in scaling airblast-induced ground shock problems is to define appropriate soil properties. The kind of stress waves produced and their propagation velocity depend on the magnitude of the surface air overpressure and on the properties of the soil. Should the stress-strain curve be concave about the stress axis, the velocity of propagation increases with increasing stress and the wave is shocked-up. When the shock wave engulfs the structure, the interaction or coupling of energy between the surrounding soil and the structure is complex. The surrounding soil redistributes the pressure in response to relative displacement of the structure and this input pressure to the structure then depends on the structural geometry, the structural flexibility, the pressure-time history and the soil characteristics.

Generally, a structure with a cylindrical geometry is able to transmit external loads by membrane stresses. In a buried configuration, this property makes the cylindrical shell structure extremely rigid when subjected to blast forces. Current

emphasis in protective structure research is therefore being placed on arch-type structures.[13,20]

B. Review of Pertinent Literature

Much literature exists on the theory and experiments of dynamically loaded structures. This section summarizes some of the more recent references pertinent to the development of scaling laws for blast-loaded structures.

Jones[14] discusses the problems involved in using high explosives and model structures to simulate nuclear weapons and full-scale structures, and the difficulties encountered in satisfying full dynamic similarity. Certain classes of targets and their applicability to model studies are discussed.

Baker[4] develops a model law for scaling of response to blast loading of structures which undergo large elastic and plastic deformations. The scaling of the response predicted by this law was verified by experiments on geometrically scaled cantilever beams. The beams were made from 6061-T6 aluminum alloy with 6-, 12-, and 24-inch lengths. Spherical Pentolite explosive charges detonated in air provided the blast load.

Ahlers[1] extensively reviews the problem areas involved in blast-loaded underground structures, the theoretical approaches to the problem and model testing. The modeling treatment deals with the limitations in scaling up to a prototype.

Murphy and Young[22] develop scaling laws for dynamically loaded underground structures. As an initial step towards verifying the scaling laws, 1- and 2-inch-diameter cylinders were

embedded in soil at various depths and impact loads applied to the soil surface by a falling weight.

American Machine and Foundry Co., Mechanics Research Division,[24] presents scaling laws for blast-loaded underground structures. The laws are developed from a consideration of the basic conditions involved in the response of buried shell-type structures to a shock wave. Physical properties of some materials are presented as a guide to select a soil simulant.

Allgood and others[3] conducted tests on small, two-hinged arches buried in dry sand and subjected to loads from a blast simulator. Deflections of the model arch were scaled up and compared to the deflections of arches tested in a full-scale nuclear field test (Operation PLUMBOB[12]). Comparison showed scaled deflections of the same order of magnitude.

Murphy, Young, and Martin[23] investigated similitude requirements for dynamically loaded structures and verified model requirements experimentally. Tests were run on 1-, 2-, and 4-inch-diameter cylinders buried in dry Ottawa sand in a drop-weight loader, a vertical shock tube and a horizontal shock tube. Peak strain and complete strain-time histories were obtained for various depths of burial. The tests indicated that the similitude requirements for geometrically scaled models were satisfactory.

Tener[25] presented design and prediction equations for semicircular aluminum alloy arches subjected to dynamic overpressures. Five geometrically similar arches with 8-, 12-, 16-, 20-,

and 24-inch diameters were buried in dense, dry sand and tested in the Large Blast Load Generator (LBLG) at the U. S. Army Engineer Waterways Experiment Station (WES). Sixteen dynamic tests at overpressures ranging from 30 to 220 psi were conducted for two different depths of burial. Peak elastic deflections and strains were compared. The results verified the model theory.

Denton and Flathau[9] tested a series of models in the LBLG at the WES to evaluate scale-model techniques for predicting the response of laboratory-size prototypes. Three metal arches having 8-, 16-, and 24-inch diameters were subjected to surface overpressures ranging from 57 to 196 psi. Peak dynamic deflections, strains, thrusts, and moments were adequately predicted. The effect of depth of burial on the response of the structures was also examined.

C. Objectives

The objective of this study is to further examine the parameters associated with model to prototype scaling relations for blast-loaded buried structures and to verify experimentally the validity of the scaling procedures for length ratios up to 9. The objectives were as follows:

1. To outline a theory sufficient to indicate the important variables which enter the problem of blast-loaded buried structures that respond both elastically and inelastically.

2. To develop scaling relations for geometrically scaled arches buried in dense, dry sand and loaded dynamically in the elastic and inelastic ranges of response.

3. To test four geometrically scaled arches buried in the same soil and subjected to airblast-induced surface overpressures.

4. To verify the scaling relations.

D. Scope

Four semicircular fixed-end arches with 4-, 8-, 12-, and 36-inch diameters were buried in dense, dry sand at a depth of burial of 1/2 diameter and subjected to overpressures ranging from 70 to 300 psi. All four arches were buried simultaneously in the LBLG located at the WES.

The arches were instrumented to measure strains on the arch surfaces, relative deflection between arches and the base plate, and accelerations of the crown and floor. The free field was instrumented for surface overpressures and soil stress. Moments and thrusts at various sections of the arch were calculated from back-to-back strain measurements.

Although it is recognized that prototype protective structures will be fabricated from reinforced concrete or structural steel, aluminum was selected as the arch material because of its low elastic modulus and because its material properties are not sensitive under dynamic loads.[9]

II

THEORY

A. Background

Dimensional analysis is developed from a consideration of physical quantities associated with a problem which are then combined into a functional relation based on their dimensions. The theory of models, from which prediction equations and similarity conditions are developed, is based on dimensional analysis.

The first step in the dimensional analysis of any problem is to determine the variables associated with the problem. To achieve this it becomes necessary to investigate analytical concepts which govern the problem.

B. Analytical Concepts

The development in this section is based on one-dimensional wave propagation.[5] The equation of motion is given by

$$\frac{\partial \sigma}{\partial x} = \rho \frac{\partial^2 u}{\partial t^2} \tag{1}$$

The strain in the body in terms of the displacement is given by

$$\epsilon = \frac{\partial u}{\partial x} \tag{2}$$

Equation 1 can be written as

$$\frac{d\sigma}{d\epsilon} \frac{\partial \epsilon}{\partial x} = \rho \frac{\partial^2 u}{\partial t^2} \tag{3}$$

$$\frac{\partial^2 u}{\partial x^2} = \frac{1}{c^2} \frac{\partial^2 u}{\partial t^2} \tag{4}$$

Equation 4 is the one-dimensional wave equation where

$$c = \left(\frac{1}{\rho} \frac{d\sigma}{d\epsilon}\right)^{1/2}$$

is the velocity of the stress wave. When the stress-strain relation is linear, as in the case of an elastic media, the wave velocity is constant.

$$c = \left(\frac{E}{\rho}\right)^{1/2} \tag{5}$$

The particle velocity is given by

$$V = \frac{\sigma}{\rho c} \tag{6}$$

The term ρc is known as the characteristic impedance of the media.

The propagation of plastic deformation in one dimension is given by von Karman and Duwez.[17] The wave velocity c and the particle velocity V are given by

$$c = \left(\frac{S}{\rho_o}\right)^{1/2} \tag{7}$$

and

$$V = \int_o^{\epsilon_1} \left(\frac{S}{\rho_o}\right)^{1/2} d\epsilon \tag{8}$$

where $S = \frac{d\sigma}{d\epsilon}$ is the modulus of deformation, elastic or plastic.

If the stress-strain relation for the media is such that increasing strains are accompanied by increasing values of $\frac{d\sigma}{d\epsilon}$, then large strains travel faster than smaller strains and the pulse develops shorter rise times. The fundamental shock-wave equations,

known as the Rankine-Hugoniot equations, are derived from the equations for conservation of mass, momentum, and energy.

If an instantaneous rise time develops, consideration of impulse-momentum[16] leads to the relation

$$\sigma = \rho_o c V \tag{9}$$

The strain in an infinitesimal volume is given by

$$\epsilon = \frac{V}{c} \tag{10}$$

Combining the two equations, the shock propagation velocity is given by

$$c = \left(\frac{\frac{\sigma}{\epsilon}}{\rho_o} \right)^{1/2} \tag{11}$$

where $\frac{\sigma}{\epsilon}$ represents the secant modulus for the material.

When the wave reaches a boundary, reflected and refracted waves are generated. The amplitudes of these waves depend on the mismatch of characteristic impedances of the two media.

Assuming a slip-free boundary, the normal and tangential displacements and the normal and tangential stresses must be equal at the interface. In addition, boundary conditions for the constraints need to be expressed mathematically.

The equations of motion and strain-displacement and the stress-strain law for deformable bodies are given in texts on the theory of elasticity. The equations of motion are:

$$\sum_{i=1}^{3} \frac{\partial \sigma_{ij}}{\partial x_i} + \rho F_j = 0 \tag{12}$$

The rectangular coordinates (x_1, x_2, and x_3) are referred to the deformed body, and the body force component F_j includes inertial force. The components of strain in terms of displacement components are given for fixed rectangular coordinates by

$$\epsilon_{ii} = \frac{\partial u_i}{\partial x_i} + \frac{1}{2}\sum_{n=1}^{3}\left(\frac{\partial u_n}{\partial x_i}\right)^2$$

$$\epsilon_{ij} = \frac{\partial u_i}{\partial x_j} + \frac{\partial u_j}{\partial x_i} + \sum_{n=1}^{3}\frac{\partial u_n}{\partial x_i}\frac{\partial u_n}{\partial x_j} \qquad (13)$$

For infinitely small strains, the general relation between the stress and strain components becomes

$$\sigma_{ii} = \frac{E}{(1+\nu)}\left(\epsilon_{ii} + \frac{\nu}{(1-2\nu)}\, e\right)$$

$$\sigma_{ij} = \frac{E}{2(1+\nu)}\,\epsilon_{ij} \qquad (14)$$

where

$$e = \epsilon_{11} + \epsilon_{22} + \epsilon_{33}$$

The two equations express Hooke's law in which E and ν are Young's modulus and Poisson's ratio.

The equations outlined above are for large displacement-elastic response.

C. Physical Systems

Let the number of physical quantities involved in the problem under consideration be represented by $a_1, a_2, \ldots a_n$, where

$$F(a_1, a_2, \ldots a_n) = 0 \qquad (15)$$

All equations involving physical quantities must be dimensionally homogeneous, i.e., all terms in the equation must have the same resultant dimension. A physical equation in which the coefficients are dimensionless can be expressed as

$$\sum_{j} \left(K a_1^{b_1} a_2^{b_2} \dots a_n^{b_n} \right) = 0 \qquad (16)$$

where K is a constant, and j, the number of terms in the physical equation.

Dividing equation 16 by any one term, the form of the equation becomes

$$\sum_{j-1} \left(K^1 a_1^{c_1} a_2^{c_2} \dots a_n^{c_n} \right) + 1 = 0 \qquad (17)$$

The exponents $c_1, c_2, c_3, \dots c_n$ must be such that each term of equation 17 has no dimension or the dimensional equation

$$[\pi] = 1 \qquad (18)$$

where $\pi = a_1^{c_1} a_2^{c_2} \dots a_n^{c_n}$ must be satisfied.[6]

D. The Method of E. Buckingham[6]

Let k be the number of independent fundamental dimensions by which the a's are measured. The number of dimensionless products π_i which appear as independent variables in an equation of the form

$$\phi(\pi_1, \pi_2, \pi_3, \dots \pi_i) = 0 \qquad (19)$$

is $n - k$. Among the n quantities, k dimensionally independent

quantities may be used as principal quantities with the remaining $(n - k)$ being secondary quantities. Let $a_1, a_2, \ldots a_k$ represent the principal quantities and $a_{k+1} \ldots a_n$ represent the remaining secondary quantities; then i equations of the form of equation 18 may be written

$$[\pi_1] = \left[a_1^{c_1^1} \cdot a_2^{c_2^1} \ldots a_k^{c_k^1} \cdot a_{k+1} \right] = [1]$$

$$[\pi_2] = \left[a_1^{c_1^2} \cdot a_2^{c_2^2} \ldots a_k^{c_k^2} \cdot a_{k+2} \right] = [1] \qquad (20)$$

$$\cdots\cdots\cdots\cdots\cdots\cdots\cdots\cdots$$

$$[\pi_i] = \left[a_1^{c_1^i} \cdot a_2^{c_2^i} \ldots a_k^{c_k^i} \cdot a_n \right] = [1]$$

If the a's are replaced by the k fundamental dimensions, then k linear homogeneous equations for the exponents of each of the i equations will result. The solution of the equations will result in the formulation of one dimensionless product. The procedure is repeated until all the $(n - k)$ dimensionless products are obtained.

E. Theory of Models

An equation equivalent to equation 19 may be expressed as

$$\pi_1 = \phi(\pi_2, \pi_3, \ldots \pi_i) \qquad (21)$$

This equation is general and applies to any system which is a function of the same variables. Let it apply to a model which is also a function of the same variables.

$$\pi_{1m} = \phi(\pi_{2m}, \pi_{3m}, \ldots \pi_{im})$$

where the subscript m denotes the model.

Now if

$$\pi_{2m} = \pi_2 \qquad (22)$$

$$\pi_{3m} = \pi_3$$

$$\cdots$$

$$\cdots$$

$$\pi_{im} = \pi_i$$

then

$$\phi(\pi_2, \pi_3, \ldots \pi_i) = \phi(\pi_{2m}, \pi_{3m}, \ldots \pi_{im}) \qquad (23)$$

hence,

$$\pi_1 = \pi_{1m} \qquad (24)$$

Equation 22 is the conditions which dictate the design of the model; if all these design conditions are met, the model and the prototype are completely similar.[21] In many instances complete similarity cannot be achieved, and as a result the effect on the dependent dimensionless product has to be evaluated. If the effect is not significant, the term involved may be omitted. Care must be exercised in neglecting dimensionless products since forces that have no significant effect on the prototype may affect the behavior of the model. This type of influence greatly depends on the size of the model and is called "scale effects."[19]

F. Development of Dimensionless Products

The physical quantities associated with arches buried in

dense, dry sand and subjected to a surface blast load are listed below:

Physical Quantity	Notation	Dimension
Independent Variables		
1. Arch diameter	D	L
2. Arch thickness	h	L
3. Any length	L	L
4. Poisson's ratio	ν	None
5. Modulus of arch material	E	FL^{-2}
6. Mass density of arch material	ρ	$FL^{-4}T^2$
7. Depth of soil cover	H	L
8. Peak surface overpressure	p_o	FL^{-2}
9. Time	t	T
10. Soil modulus	η_1	FL^{-2}
11. Mass density of soil	η_2	$FL^{-4}T^2$
12. Angle of internal friction	ϕ	None
Dependent Variables		
1. Acceleration	a	LT^{-2}
2. Velocity	v	LT^{-1}
3. Displacement	s	L
4. Strains	ϵ	None
5. Thrust per unit length	T	FL^{-1}
6. Moment per unit length	M	FL

The fundamental dimensions are F, L, and T. To find a specific form corresponding to equation [illegible], [illegible] are selected as the principal variables. These three variables

will appear in all the dimensional equations and one or more will appear in all the dimensionless products. Consider a dimensional equation in a form corresponding to equation 19.

$$[\pi_1] = \left[D^{c_1} \cdot E^{c_2} \cdot \rho^{c_3} \cdot \delta \right] = [1] \qquad (25)$$

Substituting the dimensions of D, E, ρ, and δ, we have

$$\left[L^{c_1} \cdot F^{c_2} L^{-2c_2} \cdot F^{c_3} L^{-4c_3} T^{2c_3} \cdot L \right] = [1] \qquad (26)$$

from which

$$\left[L^{c_1 - 2c_2 - 4c_3 + 1} \cdot F^{c_2 + c_3} \cdot T^{2c_3} \right] = [1] \qquad (27)$$

Equation 27 can be satisfied if

$$c_1 - 2c_2 - 4c_3 + 1 = 0$$

$$c_2 + c_3 = 0$$

$$2c_3 = 0$$

or

$$c_1 = -1, \; c_2 = 0, \; c_3 = 0$$

We obtain $\pi_1 = \frac{\delta}{D}$. Following a similar process the ten $(n - k)$ dimensionless products can be obtained. They are

$$\pi_2 = \frac{h}{D} \; ; \; \pi_3 = \frac{L}{D} \; ; \; \pi_4 = \nu \; ; \; \pi_5 = \frac{H}{D} \; ; \; \pi_6 = \frac{p_o}{E}$$

$$\pi_7 = \frac{t}{D}\sqrt{\left(\frac{E}{\rho}\right)} \; , \; \pi_8 = \frac{\eta_1}{E} \; , \; \pi_9 = \frac{\eta_2}{\rho} \; , \; \pi_{10} = \phi$$

and equation 20 takes the form

$$\frac{\delta}{D} = \phi\left(\frac{h}{D} \; , \; \frac{L}{D} \; , \; \nu \; , \; \frac{H}{D} \; , \; \frac{p_o}{E} \; , \; \frac{t}{D}\sqrt{\frac{E}{\rho}} \; , \; \frac{\eta_1}{E} \; , \; \frac{\eta_2}{\rho} \; , \; \phi\right) \qquad (28)$$

G. Similitude Conditions

If equation 28 represents the equation for a prototype, a similar equation is valid for a model. If the material properties defined by E, ρ, and ν are the same for model and prototype and a length scale is defined by

$$n = \frac{D}{D_m} \tag{29}$$

the prediction equation

$$\frac{\delta}{D} = \frac{\delta_m}{D_m} \tag{30}$$

or

$$\delta = n\delta_m$$

is true, if the following conditions are met

1. $\frac{h}{D} = \frac{h_m}{D_m}$ $\qquad h = nh_m$

2. $\frac{L}{D} = \frac{L_m}{D_m}$ $\qquad L = nL_m$

3. $\nu = \nu_m$ $\qquad \nu = \nu_m$

4. $\frac{H}{D} = \frac{H_m}{D_m}$ $\qquad H = nH_m$

5. $\frac{p_o}{E} = \frac{p_{om}}{E_m}$ $\qquad p_o = p_{om}$

6. $\frac{t}{D}\sqrt{\frac{E}{\rho}} = \frac{t_m}{D_m}\sqrt{\frac{E_m}{\rho_m}}$ $\qquad t = nt_m$

7. $\frac{\eta_1}{E} = \frac{\eta_{1m}}{E_m}$ $\qquad \eta_1 = \eta_{1m}$

$$8.\quad \frac{\eta_2}{\rho} = \frac{\eta_{2m}}{\rho_m} \qquad\qquad \eta_2 = \eta_{2m}$$

$$9.\quad \phi = \phi_m \qquad\qquad \phi = \phi_m$$

Conditions 1 and 2 require geometric similarity. Condition 4 requires that the depth of burial be scaled according to the length scale. The same overpressure for model and prototype is dictated by condition 5. Condition 6 requires that the time scale be the same as the length scale. Finally conditions 7, 8, and 9 specify the same soil for the model and prototype.

If gravitational acceleration was included in the analysis, a dimensionless term of the form $\frac{g\rho D}{E}$ would result, and the condition

$$\frac{g\rho D}{E} = \frac{g_m \rho_m D_m}{E_m} \qquad\qquad g = \frac{g_m}{n}$$

that gravity or specific weights γ scales as one over the length scale would have to be met; however, the effect of gravity is to induce dead-load stresses and since dead-load stresses are small compared to the stresses induced by overpressure loads, the dimensionless product containing gravity can be neglected.

H. Scale Factors[19]

Let the cartesian coordinates x, y, and z designate points on the prototype and x', y', and z' represent similar points on the model. Then $x = K_x x'$, $y = K_y y'$, and $z = K_z z'$ where the constants K_x, K_y, and K_z are the scale factors for length. In our case

$$K_x = K_y = K_z = K_L = n \tag{31}$$

If the two systems are kinematically similar, then

$$t = K_t t' = nt' \tag{32}$$

The scale factor for velocity is

$$K_v = \frac{K_L}{K_t} = 1 \tag{33}$$

Accordingly the scale factor for acceleration is

$$K_a = \frac{K_L}{K_t^2} = \frac{1}{n} \tag{34}$$

By Newton's second law the scale factor for forces acting on similar cross sections is

$$K_F = K_m K_a = \frac{K_m K_L}{K_t^2} = \frac{K_\rho K_L^3 K_L}{K_t^2} \tag{35}$$

Since the mass densities are the same, $K_\rho = 1$; K_F then becomes

$$K_F = \frac{K_L^4}{K_t^2} = n^2 \tag{36}$$

The scale factors for stress, strain, radial deflection, thrust per unit length, and moment per unit length can be expressed as

$$K_\sigma = \frac{K_F}{K_L^2} = 1 \tag{37}$$

$$K_\epsilon = \frac{K_L}{K_L} = 1 \tag{38}$$

$$K_w = K_L = n \tag{39}$$

$$K_T = \frac{K_F}{K_L} = n \tag{40}$$

$$K_M = \frac{K_F K_L}{K_L} = n^2 \tag{41}$$

I. Scaling of Elastic-Plastic Response

The equations of motion and the strain-displacement relations in section B are completely general. The stress-strain relation for strains exceeding the elastic limit is unique only when the stresses increase slowly and monotonically during loading. If the dimensionless stress-strain curves ($\frac{\sigma}{E}$ versus ϵ) are identical, then the materials have the same type of stress-strain relation, and when the model and prototype structures are made of the same material, or have the same type of stress-strain relation, the distinction between elastic and inelastic material is eliminated.[19]

According to the scale factors, the strains in the model and prototype are the same and time scales as the length scale. The structures are strained at different rates, and strain-rate sensitivity effects a change in material properties. To investigate strain-rate effects, assume that

$$\sigma_{yd} = \sigma_{ys} f(\dot{\epsilon}) \tag{42}$$

where σ_{yd} and σ_{ys} represent the dynamic and static yield stresses and $f(\dot{\epsilon})$ is a function of strain rate. It follows that if equation 37 is to hold true

$$f(\dot{\epsilon}) = f(\dot{\epsilon})_m \tag{43}$$

which gives

$$K_{\dot{\epsilon}} = 1 \tag{44}$$

and

$$K_t = K_{\dot{\epsilon}}^{-1} = 1 \tag{45}$$

which contradicts similitude condition that time scales according to length scale. The similitude condition for mass density (inertial effects) cannot be satisfied simultaneously with strain-rate effects.

Some of the common structural materials like steel show significant increases in yield stress for high strain rates; on the other hand, some of the aluminum alloys show no appreciable strain-rate sensitivity.[7]

In view of the above considerations, it appears that the similitude conditions for geometric scaling for elastic-plastic strains due to dynamic loads are valid if the same material is used in the model and prototype and if the material is not sensitive to strain rate.

III

PROCEDURE

A. Model Fabrication

The structure geometry selected for verification of the model theory was semicircular fixed-end arches. Four arches with diameters of 4, 8, 12, and 36 inches and lengths equal to 2 diameters were tested. A length scale of 9 was considered as practical for laboratory testing and large enough for scaling to a field prototype.

The arch roof and floor plate were fabricated from 5086-H32 aluminum alloy. As a model material, aluminum alloy is easily machined, has a low modulus of elasticity, and can be loaded repeatedly. The arches were constructed commercially to the specifications shown in Figure 2. The four arches (without strain gages) are shown in Figure 3. The semicircular roofs were rolled and fitted into grooves machined in the floor plate. The roof-floor plate joint was secured by screws. End walls were cut from 6061-T6 aluminum alloy with the same outer radius as the arch roof. The end walls were spaced by a spacer strip and braced by tie bars so that the arch roof could deflect freely. The gaps between the end walls and arch were sealed by tape and the gaps around the instrumentation cables were filled with a silastic compound. The locations of the tie bars and end walls are shown in Figure 4.

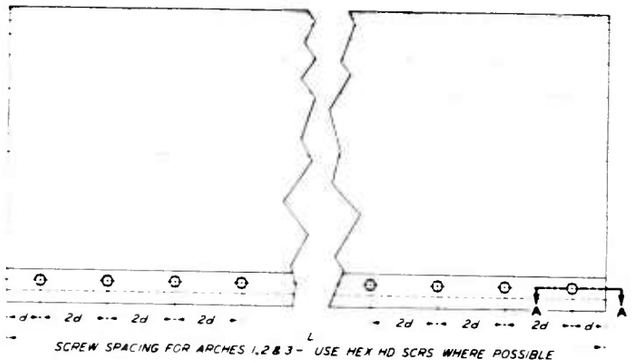

ELEVATION

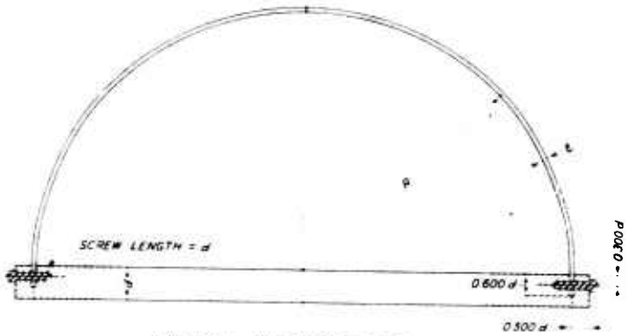

TYPICAL SECTION THROUGH ARCH

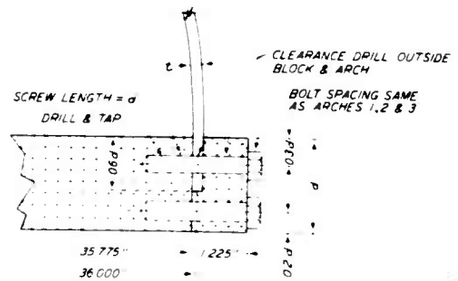

MOUNTING DETAIL - END SECTION
ARCH 4 TO FLOOR PLATE 4

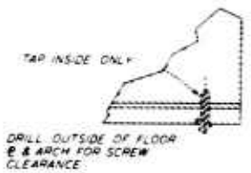

SECTION A-A

ARCH	1	2	3	*4
R	2.000 ± 0.010	4.000 ± 0.010	6.000 ± 0.015	18.000 ± 0.015
t	0.025 ± 0.002	0.050 ± 0.002	0.075 ± 0.003	0.225 ± 0.003
d	0.250 ± 0.010	0.500 ± 0.020	0.750 ± 0.030	2.250 ± 0.015
0.600 d	0.150	0.300	0.450	1.350
0.500 d	0.125	0.250	0.375	1.125
0.300 d	0.075	0.150	0.225	0.675
L	8.000	16.000	24.000	72.000
SCREW SIZE	1-64 NC	4-40 NC	8-32 NC	7/16-14 NC

ALL DIMENSIONS IN INCHES

NOTE

MATERIAL: ALUMINUM - 5086-H32
YIELD STRENGTH 28,000 PSI
ULTIMATE STRENGTH 40,000 PSI

MODULUS OF ELASTICITY MUST BE UNIFORM WITHIN ± 2% BETWEEN SPECIMENS

FINISH ±16 MICRO INCHES

HARDNESS, CORROSION RESISTANCE AND TEMPERATURE CHARACTERISTICS NOT CRITICAL

* METHOD OF FIXING ARCH TO FLOOR PLATE WILL DIFFER ON THIS MODEL ONLY SEE DETAILS - THIS SHEET

Fig. 2

Model Arch Specifications

Fig. 3

Geometrically Scaled Model Arches

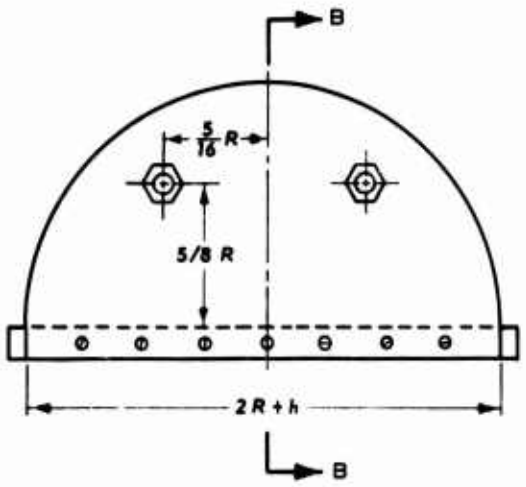

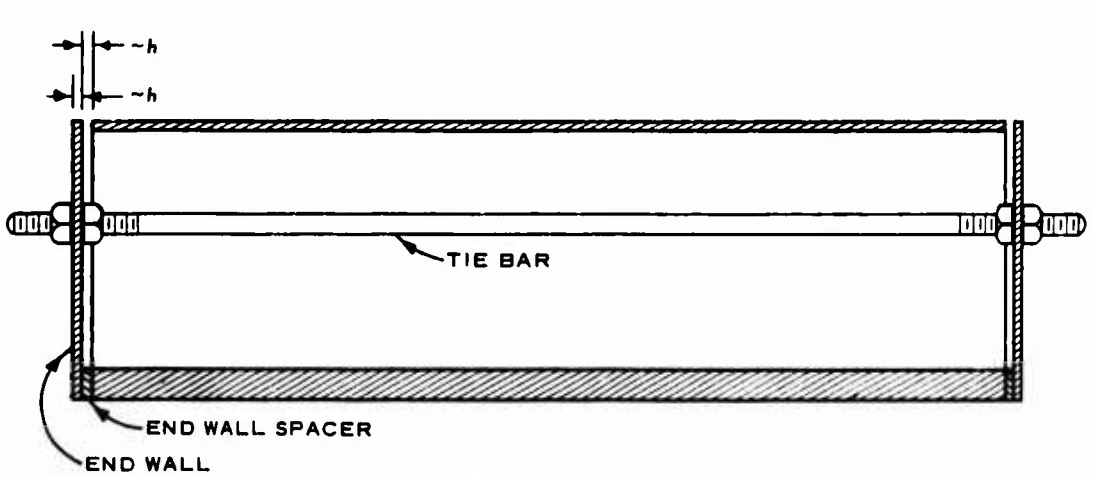

SECTION B-B

Fig. 4

Location of End Walls and Tie Bars

B. Large Blast Load Generator

The LBLG is a device capable of simulating pressures produced by kiloton and megaton nuclear devices. It is designed primarily to test underground structures subjected to airblast-induced ground shock loads. Surface airblast pressures ranging from 30 to 500 psi with rise times of approximately 1 msec and decay times over several hundred milliseconds can be reproduced.

The two basic components of the LBLG are the central firing station and the test chamber (Figure 5). The central firing station is a massive, posttensioned, prestressed concrete reaction structure designed to resist the static or dynamic loads generated in the test chamber. The test chamber is a cylindrical bin 23 feet in diameter and 10 feet deep.

In preparing for a test, three C rings are stacked on a movable platen (Figure 6). The structure and the selected soil are placed in the chamber at the desired levels. The proper quantity of explosive to produce the desired overpressure is inserted in each of the fifteen firing tubes. The B ring is placed on top of the C rings and the firing tube assembly is lowered into the B ring. The lid or A ring is then placed in the circumferential slot in the B ring. The platen supporting the test chamber is drawn into the firing station on rails. The rails are lowered, allowing the platen to rest on the floor. Nitrogen gas under pressure is forced into the slot in the B ring causing the lid to move upward so that it comes in contact with the roof of the central firing station. Horizontal jacks are then extended to rest on steel plates

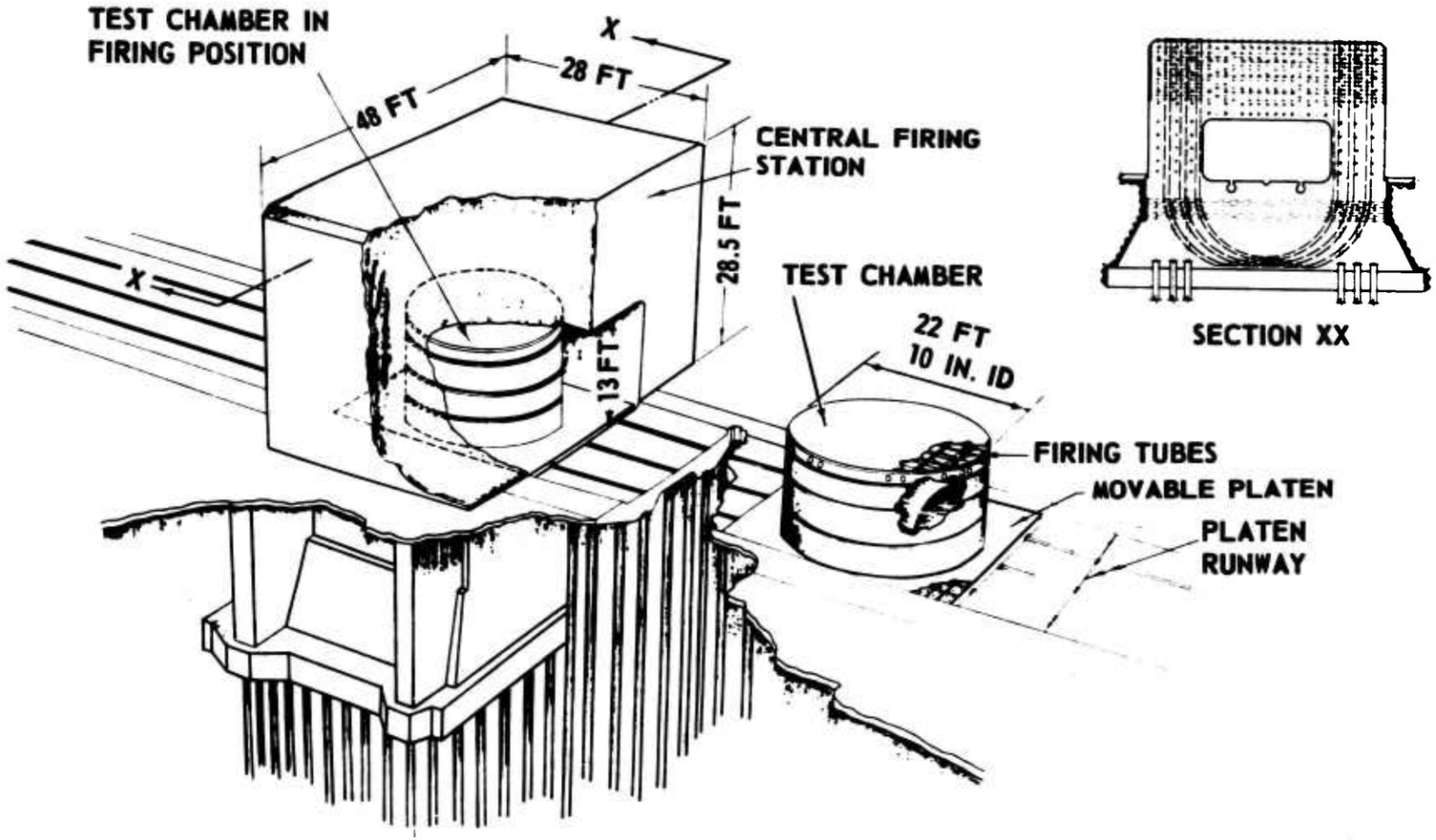

Fig. 5

Large Blast Load Generator

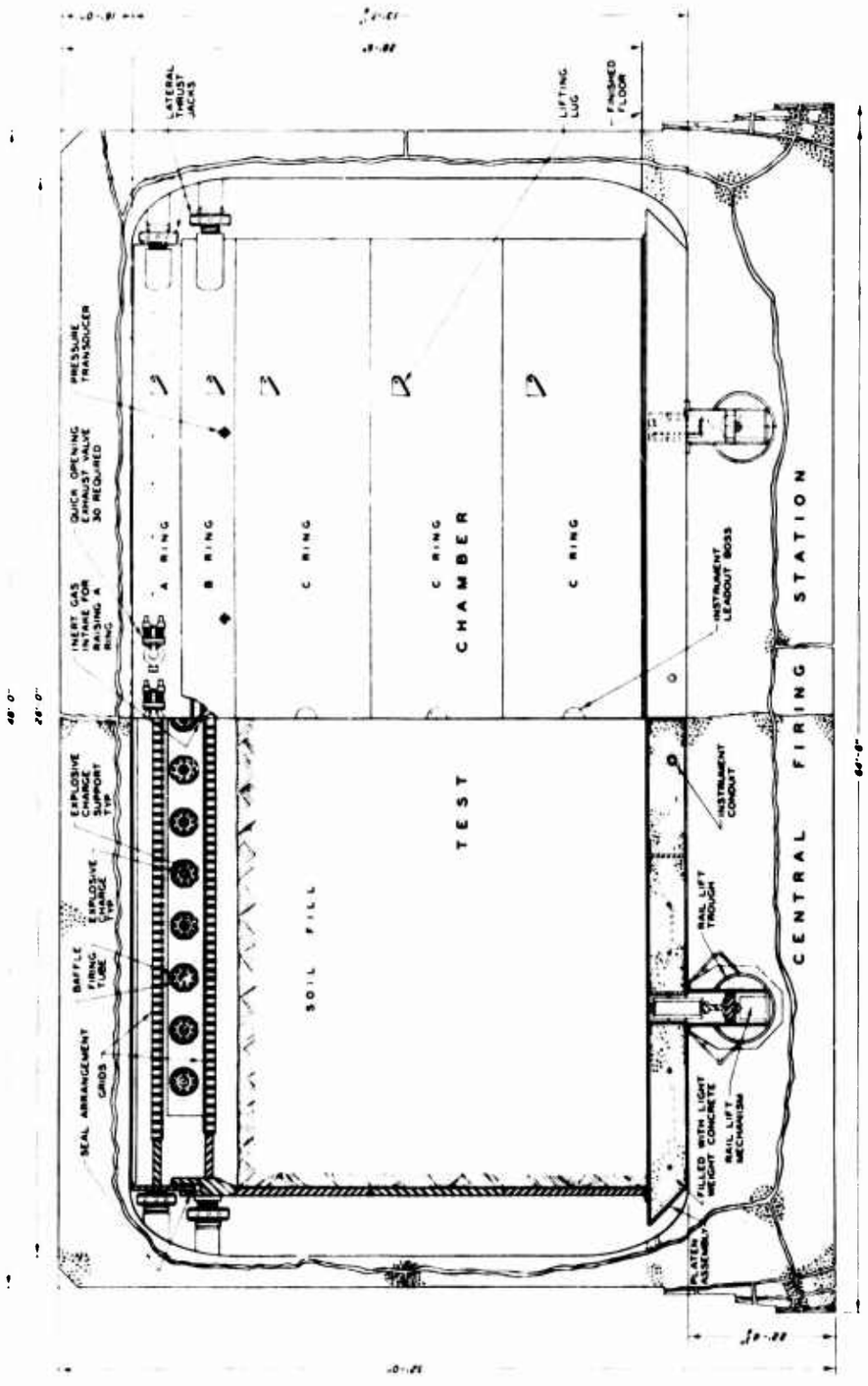

Fig. 6

Half-Section of the Blast Load Generator

in the side walls of the firing station to prevent any lateral movement. The explosives in the firing tube are detonated electrically by a standard engineer blasting cap connected to a leader strand of Primacord. A more complete description and evaluation of the LBLG is given by Albritton.[2]

C. Arch and Free-Field Instrumentation

The arch and free field were instrumented differently for the series of shots in the elastic and inelastic ranges of response. The gage locations (Figure 7) remained the same for the two series, and the changes in the transducers shown in Figure 8 will be described herein.

Strain gages on the arch midsection were placed on the inside and outside surfaces to provide data for use in computing thrusts and moments. Although symmetry of loading in the LBLG has been verified by previous tests, strain gages were localized symmetrically at 5 degrees from the springing line to average out any localized action at the joints. Longitudinal strain gages were installed at the crown to detect the end walls striking the arch. The strain gages used were metal film gages, epoxy backed, and compensated for use with aluminum. The gages were bonded to the structure with Armstrong C-2 and Activator E using the recommended application and curing techniques. Scaled gage lengths of 0.125, 0.250, 0.375, and 1.00 inches were used on the 4-, 8-, 12-, and 36-inch-diameter arches. The required gage length of 1.125 inches for the 36-inch-diameter arch was not available; therefore a 1.000-inch gage length was used. It was believed that this discrepancy could be neglected.

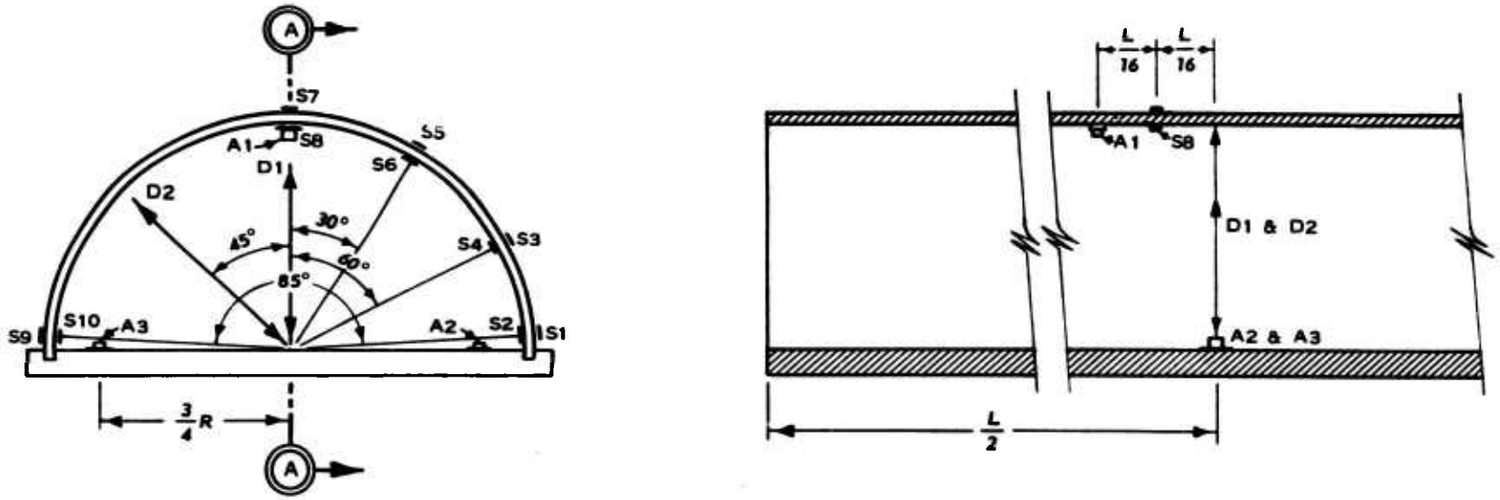

SECTION A-A

LEGEND

S1-S14	STRAIN GAGES
D1, D2	DEFLECTION GAGES
A1, A2, A3	ACCELEROMETERS

Fig. 7

Gage Locations

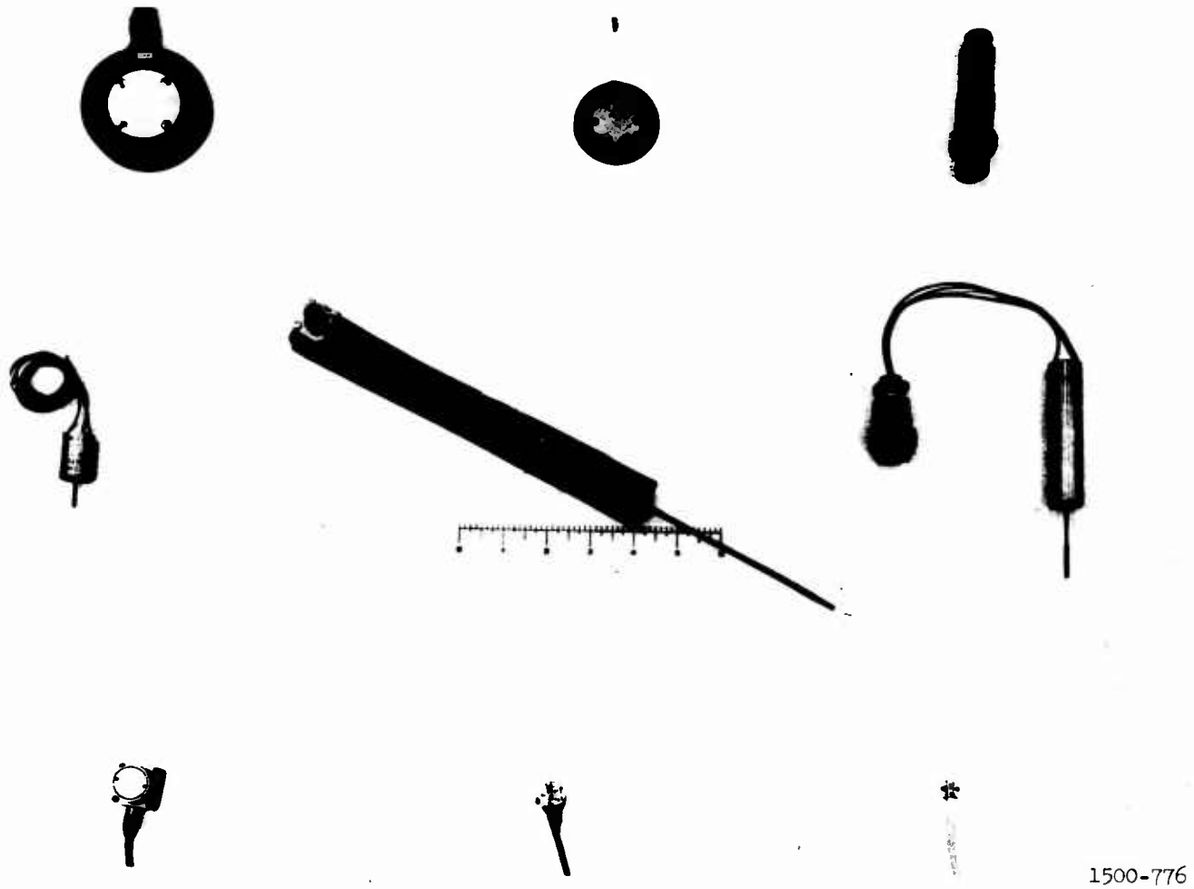

1500-776

Fig. 8

Transducers Used in the Test Series

The three dummy gages required to complete the full bridge were mounted on aluminum alloy blocks which were free to slide on the tie bars. Two blocks with 36 dummy gages were made up for each arch. The bridge was completed inside the arch and the signal carried out by Belden 21 AWG stranded 4-conductor, shielded, plastic-jacketed cables.

The deflection between the arch roof and floor was measured along the vertical radius and at 45 degrees from the vertical by linear variable differential transformers (LVDT) with ranges of ±1/10, ±5/8, and ±2 inches. The gage mounts for the displacement transducers were bolted to the floor plate at midlength.

The arches were also instrumented with accelero ers at the crown and at 3/4 radius on the floor plate. The 4-inch-diameter arch was instrumented with a 20,000-g piezoelectric accelerometer at the crown and two 1000-g accelerometers on the floor plate. The crown of the 8-, 12-, and 36-inch-diameter arches were instrumented with 2500-g piezoresistive accelerometers and the floor plate with 1000-, 500-, and 250-g accelerometers. For the next series of shots, 10,000-g solid-state accelerometers were used at the crown, and 2500-g piezoresistive accelerometers were used on the floor of all four arches. In this series 10,000-g accelerometers, potted in a weak plaster-sand mix about 2 inches in diameter, were used to measure free-field accelerations at the floor level of each arch.

The free field around each arch was instrumented with soil-stress gages developed at WES. The gages were placed at crown

level of each arch at the locations shown in Figure 9.

Bonded-strain-gage pressure transducers were used to monitor surface pressures. The transducers were mounted on wooden trusses to prevent them from being driven into the soil under repeated loads. The locations of the gages are shown in Figure 10.

Prior to burying the arches in the LBLG test chamber, their natural periods of vibration were determined. The crown of each arch was struck at midlength with a plastic mallet and the response of strain gages at the crown (S3) and at 60 degrees from the crown (S7) were recorded on a Consolidated Electrodynamics Corporation (CEC) oscillograph at a paper speed of 64 in/sec.

D. Data Recording Instrumentation

The recording system consisted of four CEC 36-channel galvanometer oscillographs recording on photographic paper with a maximum speed of 160 in/sec, and four Sangamo 14-channel magnetic tape recorders with recording speeds of 60 in/sec. The strain, acceleration, soil stress, and pressure signals were amplified on Dana differential d-c amplifiers and ALINCO Sensor Analog Module (SAM) amplifiers in conjunction with B & F Instruments, Inc., strain conditioning equipment. The signal from seven LVDT's were fed through galvodrivers and CEC 1-118 carrier amplifiers. The signal from the piezoelectric accelerometer was fed through a Kistler charge amplifier.

For tests 1, 2, and 3, 80 channels of instrumentation were used, and for tests 5, 6, and 7, 57 channels were used. The instrumentation used in the tests and schematics of the hook-ups

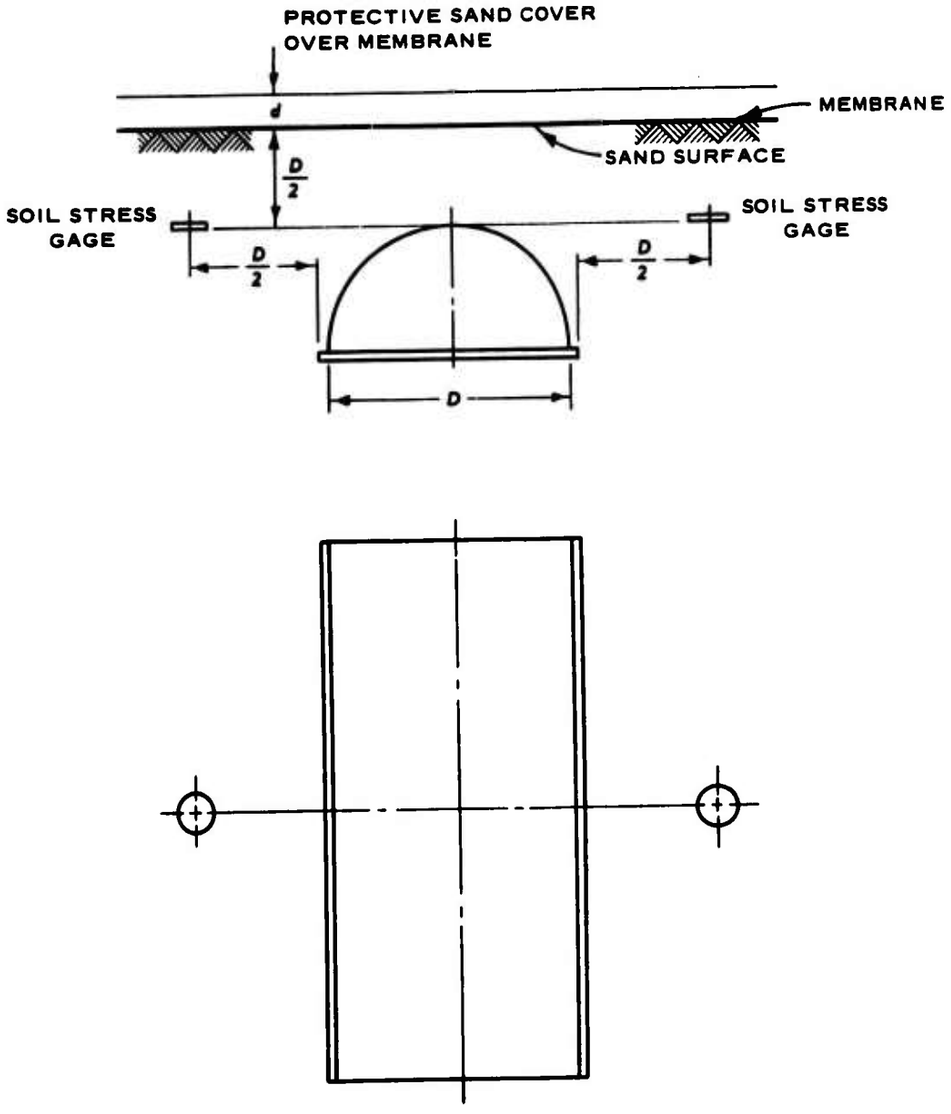

Fig. 9

Location of Arches and Soil Stress Gages in LBLG

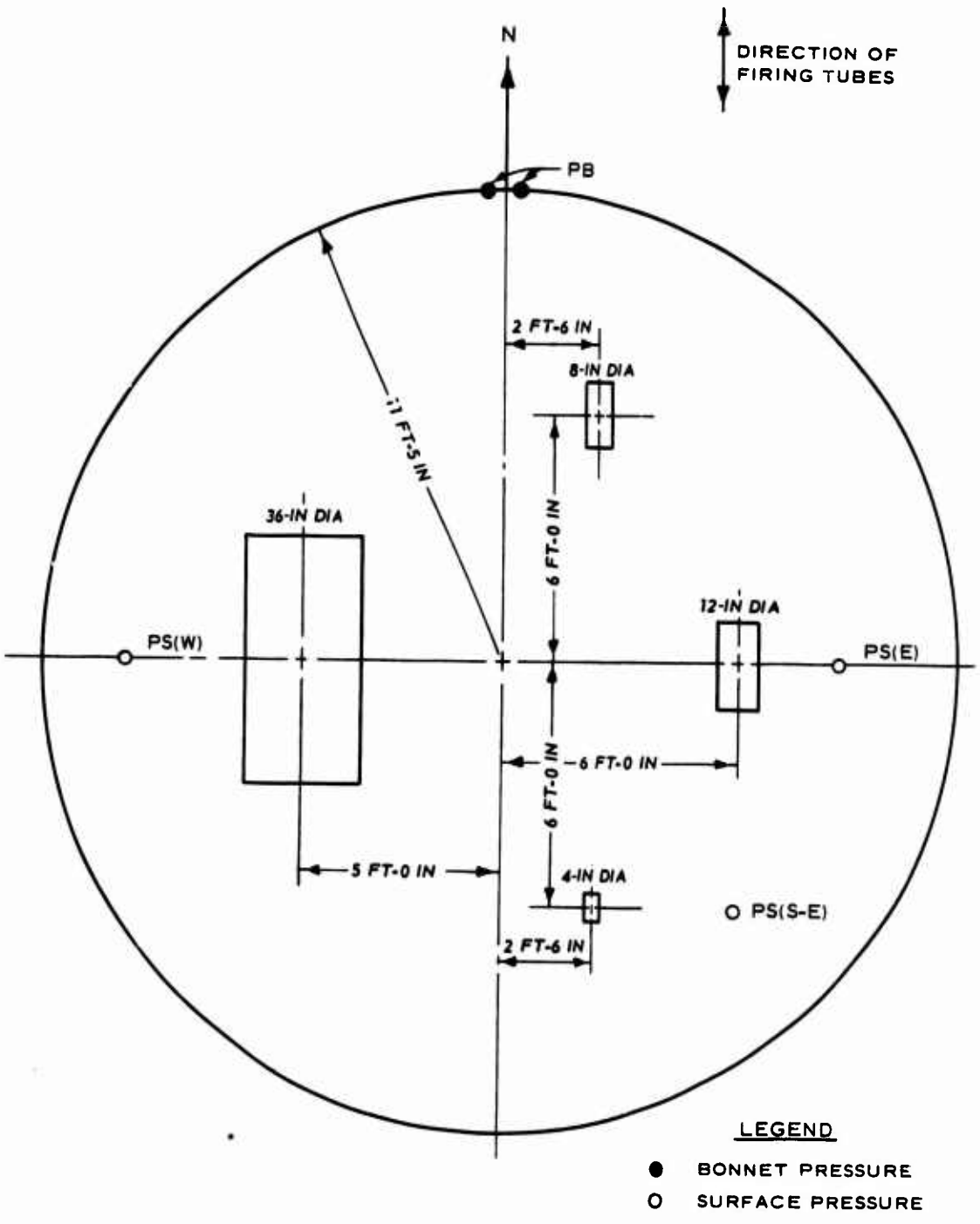

Fig. 10

Location of Arches and Pressure Gages in LBLG

are shown in Figures 11, 12, and 13. Minor changes were made between shots as necessary.

E. Soil Placement

One of the similitude requirements was that the soil density be the same around each arch. Special vibration and showering techniques in placing sand were used to assure that proper densities were achieved. Since the floor of the largest arch was at a depth of 3 feet, density was controlled from this level by showering. The sand was built up by vibrating 6- or 12-inch lifts by a vibrator mounted on a 16- by 36-inch curved, steel plate. Calibration tests for the sprinkled sand showed that the density could be maintained between 108.1 and 109.5 pcf for a height of fall ranging from 2 to 4 feet. Box density tests at various locations around the arches were taken before and after each series of shots.

A copper screen was placed over the sand surface to serve as a shield that would ground electromagnetic disturbances generated when the explosive charge was detonated. Such disturbances if not grounded produce spurious signals on the records obtained from unshielded gages.

A 1/16-inch polyethylene membrane was placed over the copper screen to prevent the flow of pressure in the soil skeleton from producing dynamic pore pressure that would disturb the buried arches. A cover of loose sand was placed directly on the membrane to protect it from the heat generated by the explosion. To satisfy the scaling relation, the cover over the membrane was scaled up from 1/4 inch over the 4-inch-diameter arch according to the length

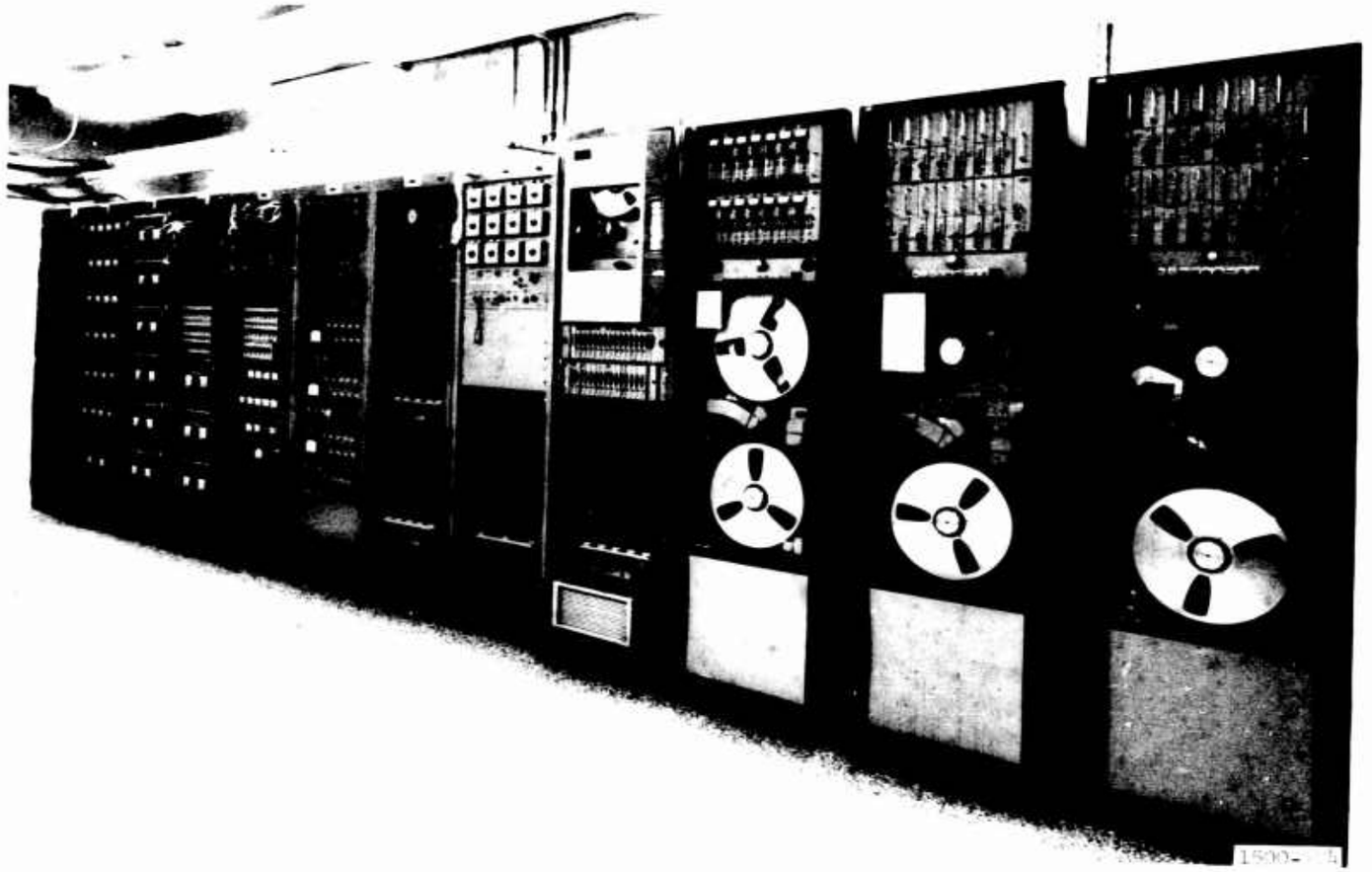

Fig. 11

Data Recording Instrumentation

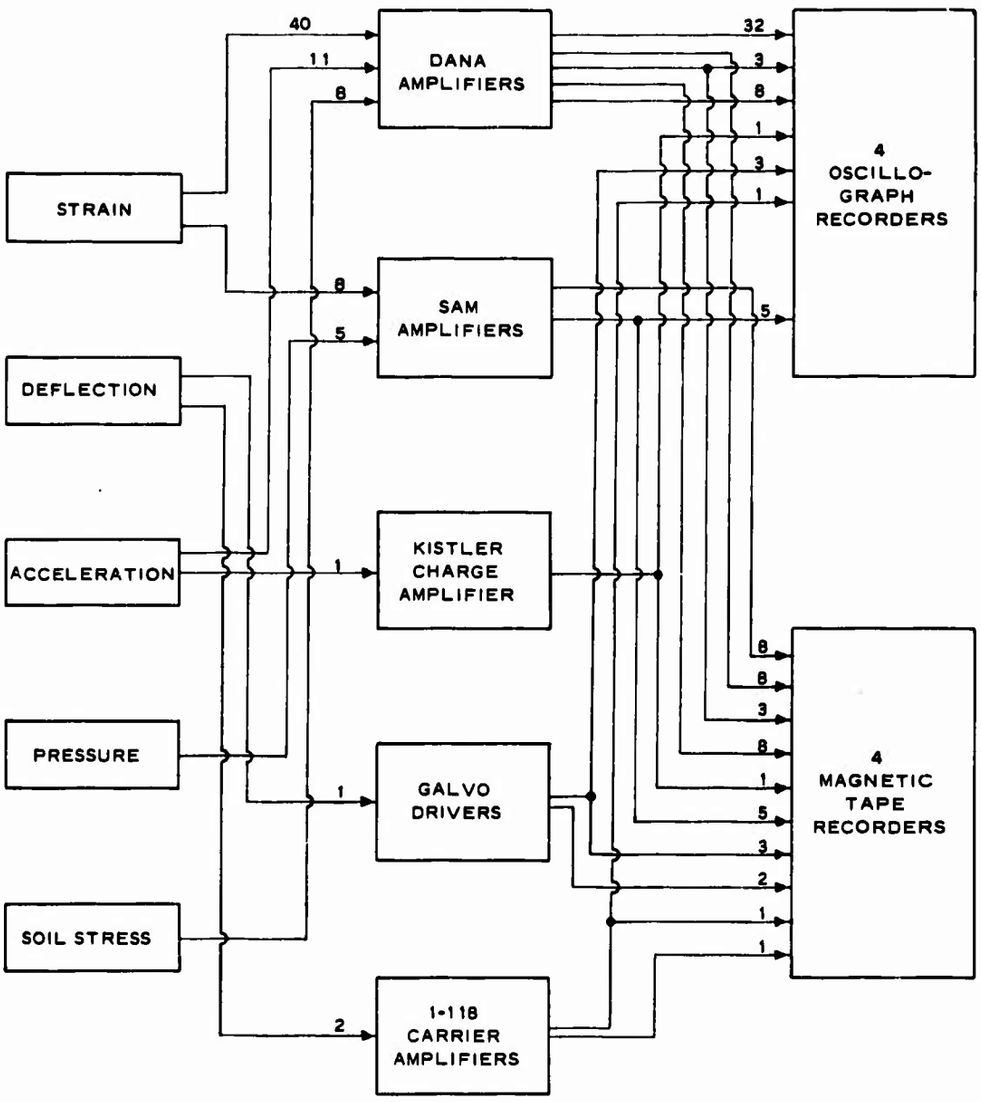

INSTRUMENTATION SCHEMATIC

Fig. 12

Instrumentation Schematic, Series 1

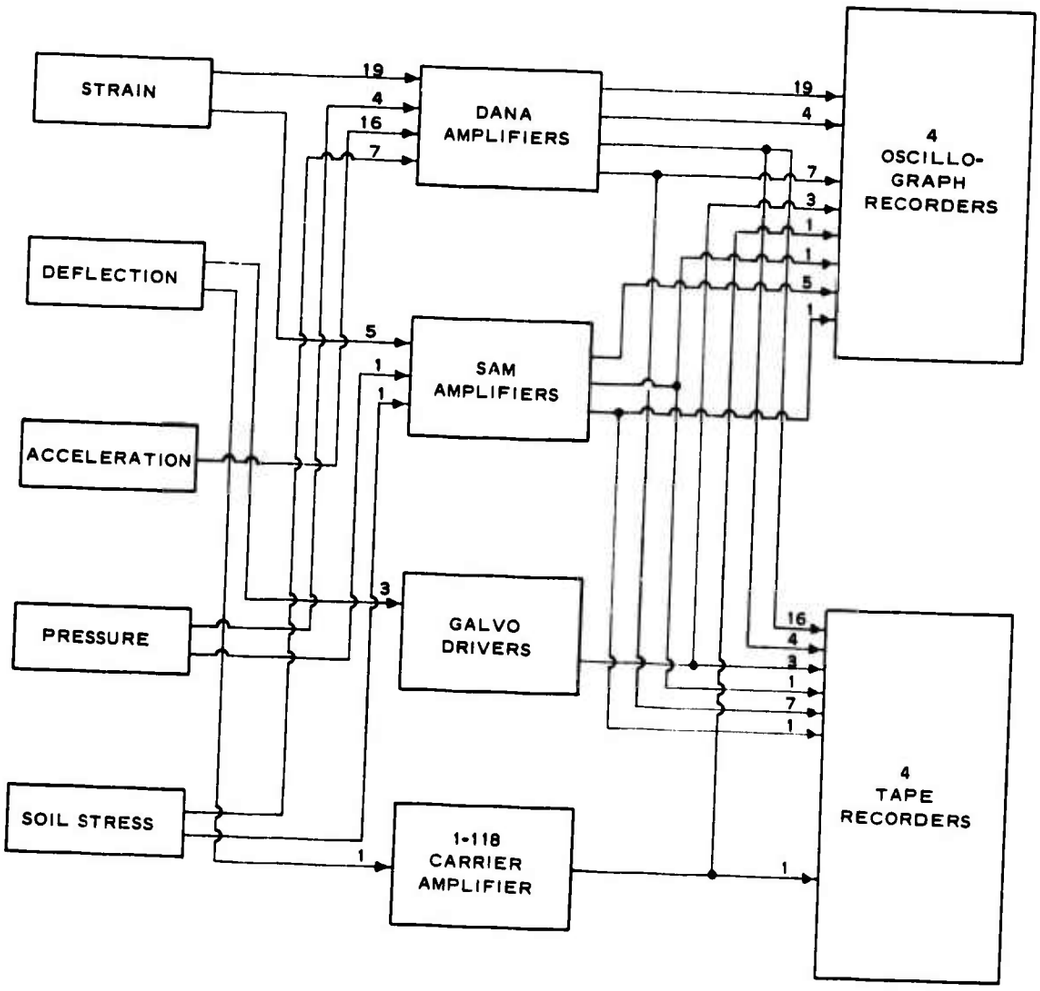

INSTRUMENTATION SCHEMATIC

Fig. 13

Instrumentation Schematic, Series 2

scale. The arches were located a sufficient distance from the walls of the test chamber to minimize the sidewall-friction effect on the load.

F. Operations

After the instrumentation hook-up was completed, preshot calibration steps were performed with the recorders running at slow speed. At shot time minus 15 seconds the tape recorders were turned on. At shot time minus 1 second the oscillograph recorders were turned on. At zero time the generator was fired and 0.3 second later the exhaust valves were opened. At plus 0.5 second the oscillograph recorders were turned off, and at plus 8 seconds the tape recorders stopped.

IV

RESULTS

A. Presentation

Results are presented for two series of tests, each consisting of three shots. Results of investigations to determine properties of the sand and the stress-strain relation of the aluminum alloy are given in Appendix A. Appendix B contains reproductions of the oscillograph records for all tests.

B. Test Series in Elastic Range

This series consisted of three repeated shots having average airblast overpressures at the surface of 70, 120, and 153 psi. The oscillograph records in Appendix B show the strain, soil pressures, surface and bonnet pressures with respect to time. The traces of relative displacement between the arch crown and floor are not shown. These data, from the LVDT's, were considered erroneous as it seemed that the spring-loaded probe separated from the arch roof.

The acceleration records were obtained from magnetic tape playbacks on an expanded time scale. The floor acceleration together with the velocity and displacement obtained by integrating acceleration-time records are shown in Chapter V. The surface pressure records from magnetic tape playback for condensed time and the crown accelerations for an expanded time are also shown in Appendix B.

C. Test Series in Inelastic Range

Three repeated shots having average surface airblast overpressures of 209, 239, and 300 psi were fired in this series. The oscillograph records of strain, soil pressure, surface and bonnet pressures, and relative displacement are shown in Appendix B. The floor acceleration-time records are shown in Chapter V. Usable crown and free-field acceleration data from two of the three shots were not obtained. The damage sustained by the arches is shown in Figures 14 and 15. The 4- and 12-inch-diameter arches buckled at the springing line, the 8-inch-diameter arch seemed to be on the verge of developing a local buckle, and on the 36-inch-diameter arch the bolts which join the arch roof to the floor plate were sheared. The method of fixing the arch roof to the floor plate was different for this particular arch, as shown in Figure 2. The post-shot photographs also show that the 4- and 8-inch-diameter arches were tilted in varying degrees along their longitudinal axes.

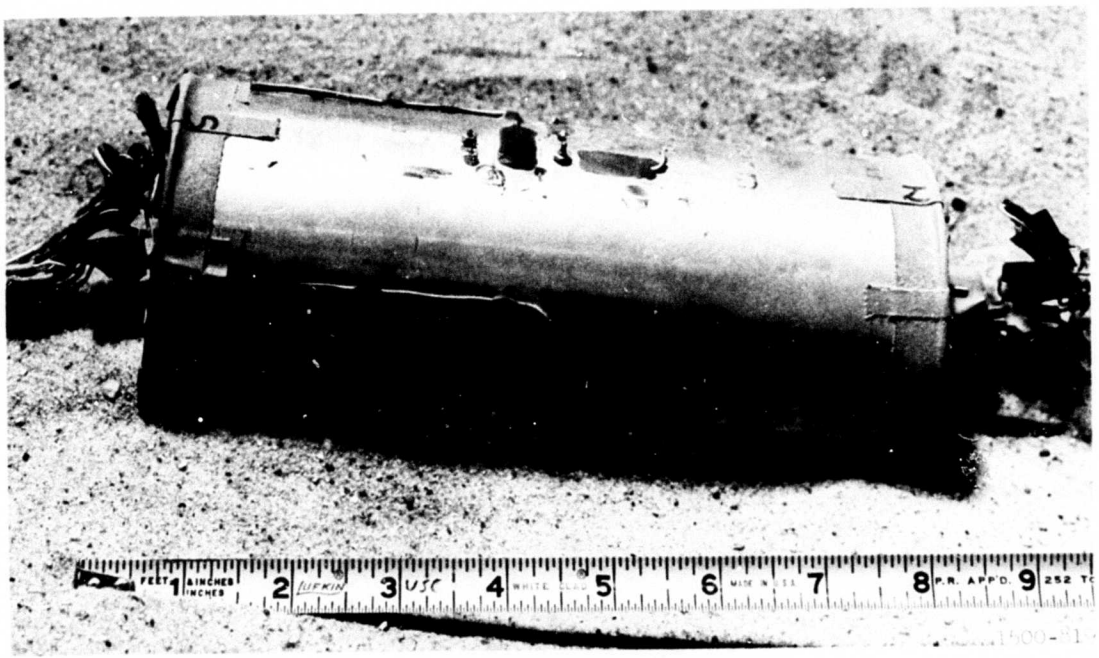

a. Four-Inch-Diameter Arch

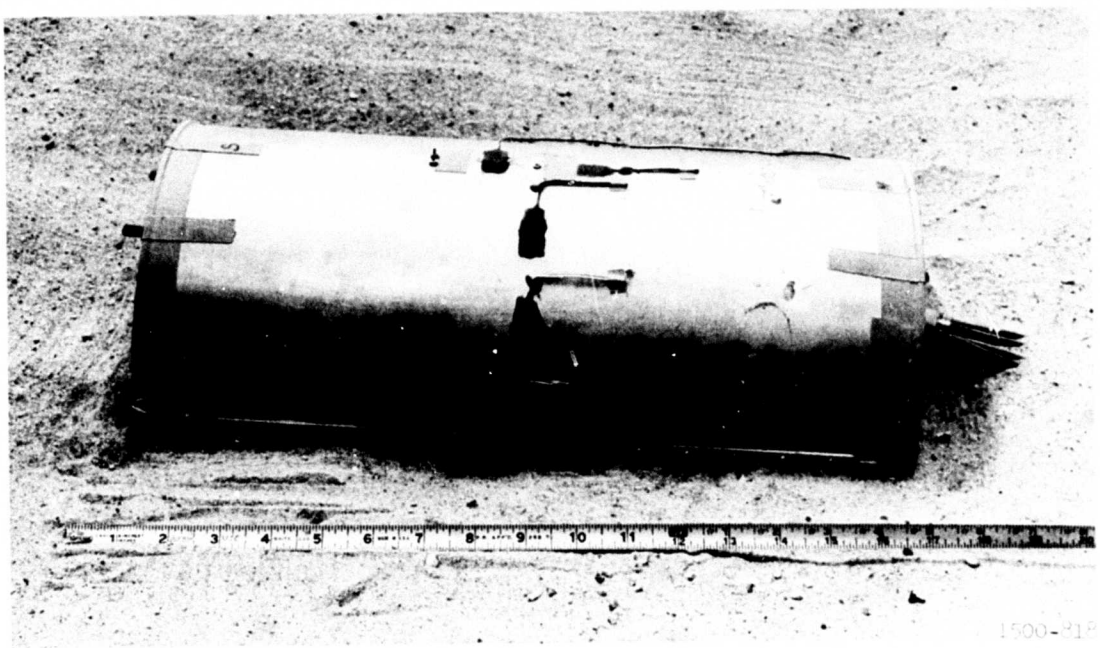

b. Eight-Inch-Diameter Arch

Fig. 14

Four- and Eight-Inch-Diameter Arches in LBLG Test Chamber After 300-psi Test

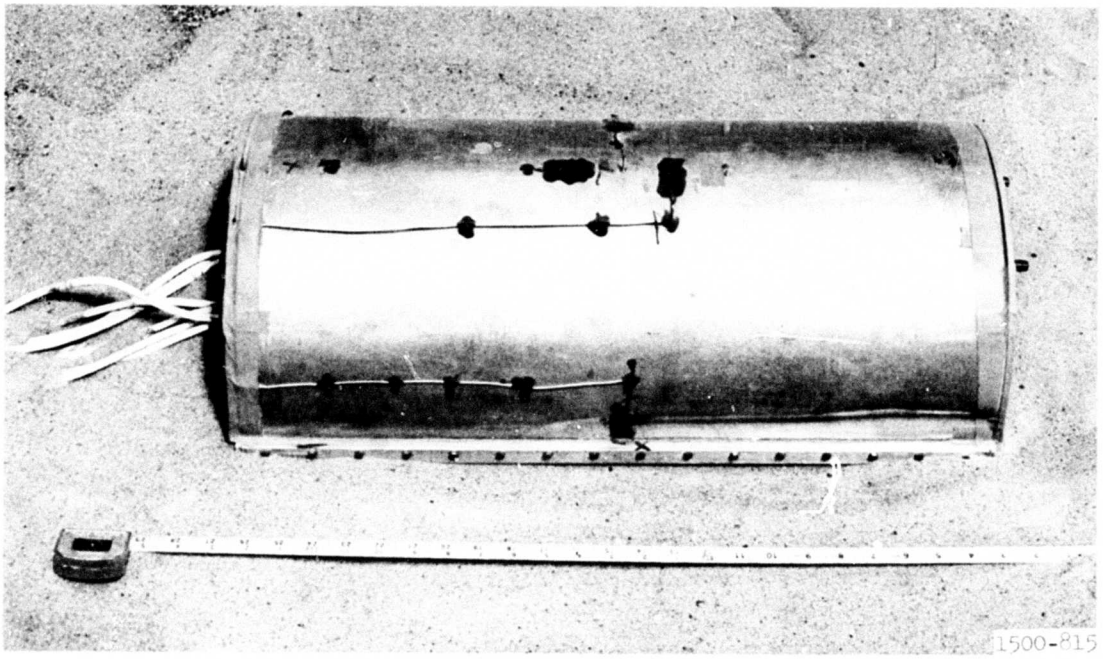

a. Twelve-Inch-Diameter Arch

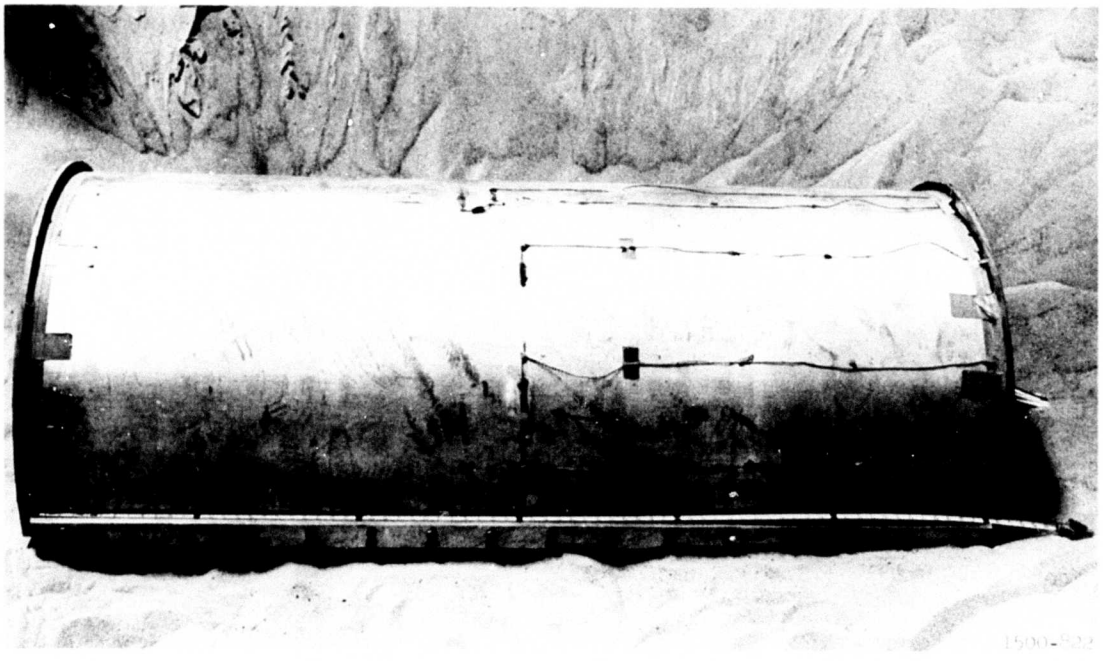

b. Thirty-Six-Inch-Diameter Arch

Fig. 15

Twelve- and Thirty-Six-Inch-Diameter Arches in LBLG Test Chamber After 300-psi Test

V

INTERPRETATION AND ANALYSIS OF RESULTS

A. Scaling Independent Variables

The independent variables are associated with the structure and test geometry, the material properties of the structure and the surrounding media, and the pressure-time history on the sand surface. Geometric scaling of the arches and the test geometry was maintained for all tests. The material properties of the arches and surrounding soil were the same since the model and prototype were fabricated from the same material and were buried in the same type of sand at maximum density.

The similitude condition requiring that the peak pressure be the same on all four arches was met by testing the arches simultaneously in the test chamber. In addition to the three surface-pressure gages, two pressure transducers were mounted in the bonnet of the test chamber. These bonnet gages, by virtue of their different location, had values approximately 10 percent higher than the surface-pressure gages. A large amount of scatter was present in the surface-pressure data from the second shot, and one of the surface-pressure gages during the sixth shot read substantially lower than the others. The data from this gage were not used in determining the average surface pressure. The location of the gages with respect to the firing tubes and gage damage caused by

debris could account for the scatter. Several gages also recorded negative pressures after 400 msec (see condensed pressure-time records in Appendix B). The negative pressures could be attributed to the severe temperature environment due to the explosive detonation. At best, duration times ranging from 1100 to 1700 msec were determined from the soil stress gages located 2 inches below the sand surface. The effect of the pulse reflected from the bottom of the test chamber is evident in almost all the traces. If a stress wave velocity is approximated by 1 ft/msec, the effect of the reflection should occur at about 16 msec from zero time.

Since the four arches were subjected to an airblast-induced pressure, the rise and decay times of the surface pressures were the same for all of the arches. This violates the similitude condition that the time scale should be the same as the length scale. This distortion in time of response for the structure was considered insignificant since the rise time measured by the soil-stress gages was approximately 50 μsec, which is much less than the natural period of vibration of the smallest arch, and the duration time was much larger. The magnitudes of the free-field stresses as recorded were consistently higher than the surface pressures. Transducer placement, gage overregistration, and transmission and distribution of pressure through sand account somewhat for the inconsistent data between the free-field stress gages.

The natural periods of vibration of the arch structures were determined by the method described in the previous chapter. Figure 1[illegible] shows that the natural period without cover varies

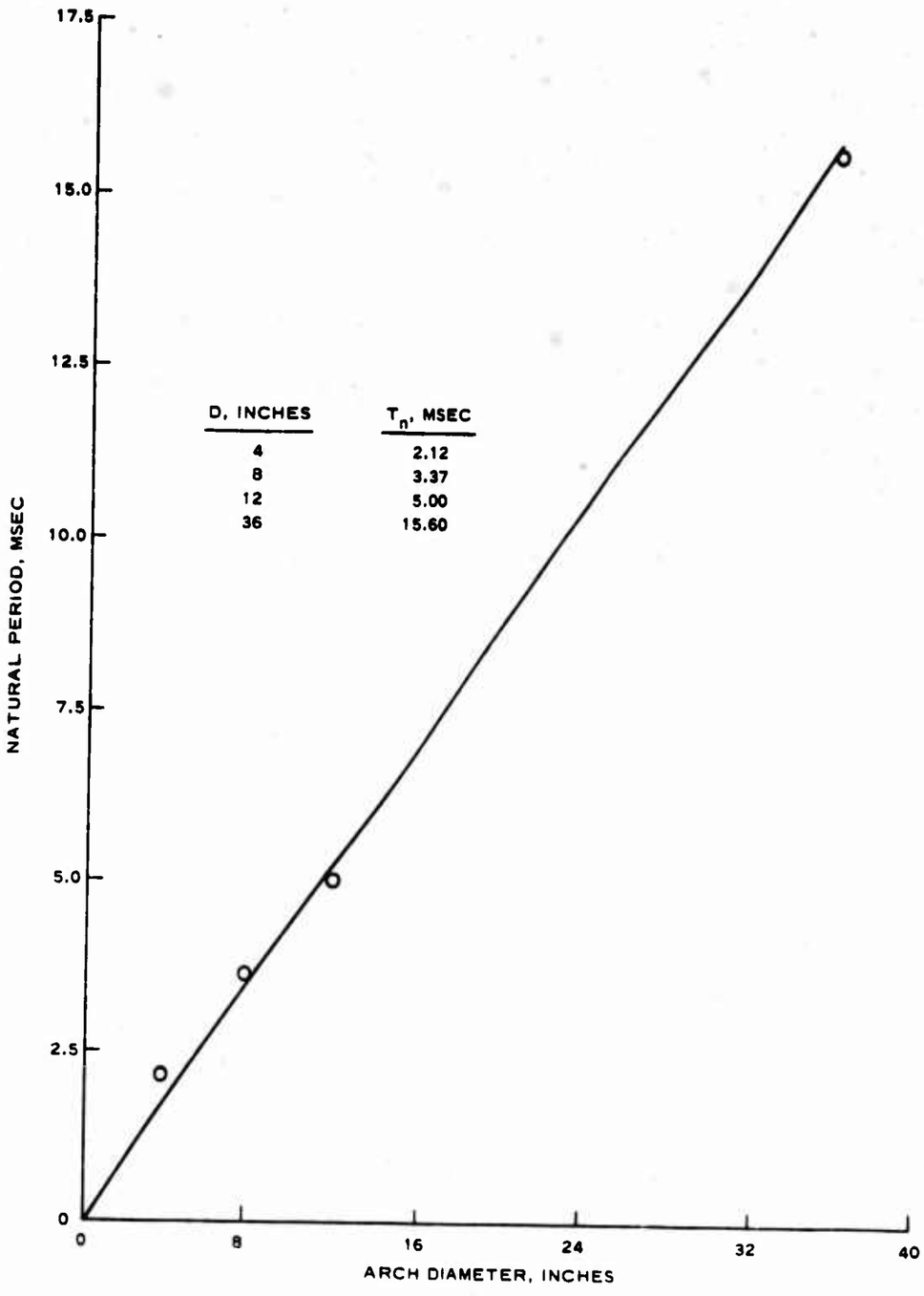

Fig. 16

Natural Period of Vibration of Arches Without Soil Cover

linearly with the arch diameter. The mode of vibration excited by striking the crown was probably the first symmetric bending mode. However, the arch in the buried configuration vibrates in a primarily compressive mode at a higher frequency.

B. Scaling Dependent Variables

Figures 17 through 25 show the acceleration, velocity, and displacement-time plots for the arch floors for the six shots from the two series of tests. The accelerometers with 1000- to 250-g range used in the first three shots had fluid damping varying from 0.6 to 0.79 of critical and natural frequencies varying from 1200 to 3800 cps. The signals were recorded on magnetic tape and played back at expanded time with signal reproduction frequencies of 3000 cps. The ordinates and abscissa of the acceleration-time plots have been constructed according to the scaling relations. When plotted in this manner, the acceleration-time for the 4-, 8-, 12-, and 36-inch-diameter arches should appear identical. The same holds true for the velocity- and displacement-time plots. For the first three shots of the series, the scaled acceleration-time trace of the 4-inch arch floor shows an acceleration of lower amplitude and larger duration than those experienced by the other three arches at the same overpressure. To scale correctly, the acceleration-time trace should have a frequency of over 4000 cps, which indicates that the transducer was frequency overranged. For the three subsequent tests in which accelerometers were used that had a frequency response of 6000 cps, damping of 0.03 critical, and a signal reproduction capability of 8000 cps, signal frequencies of over 4000 cps

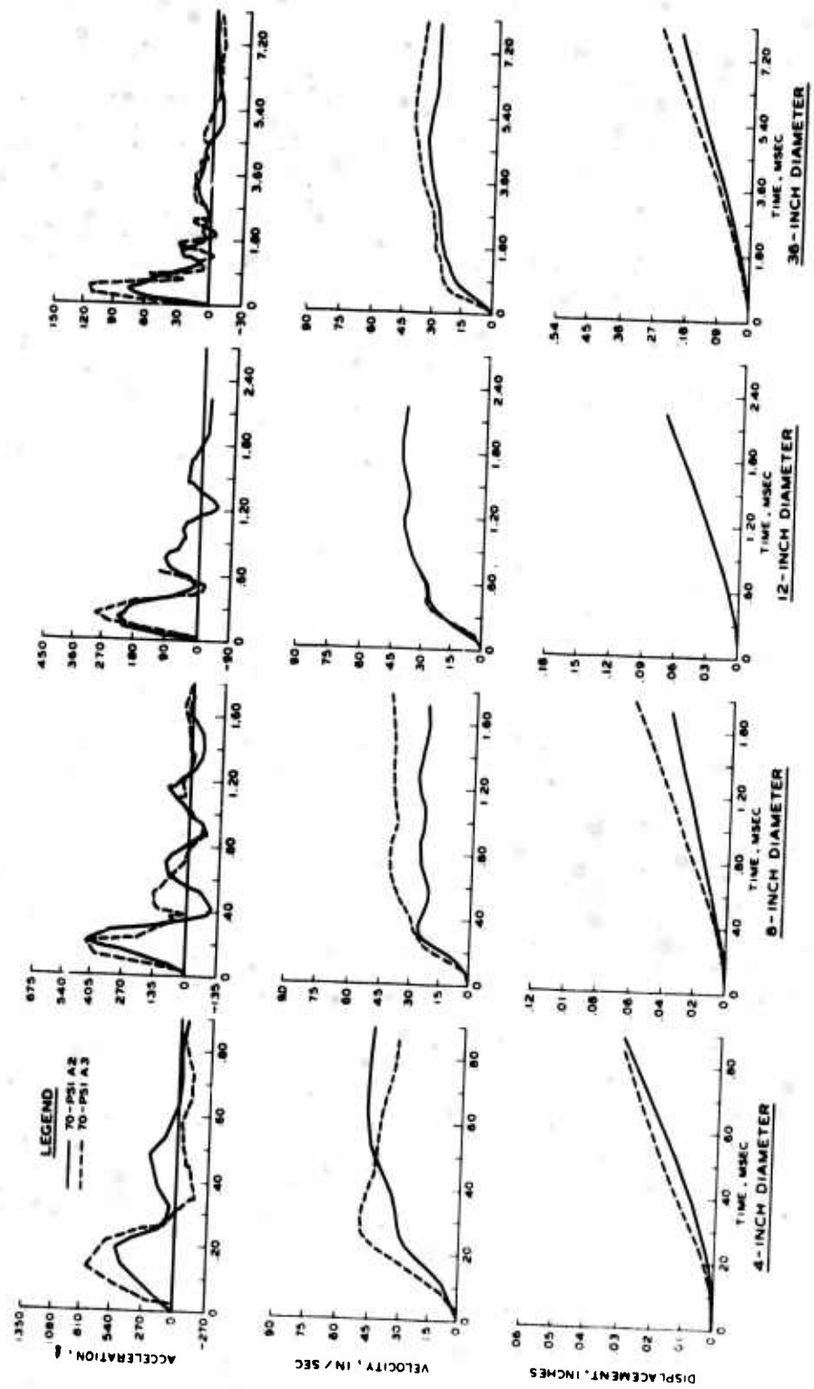

Fig. 17

Accelerations, Velocities, and Displacements of Arch Floors, P_{so} = 70 psi

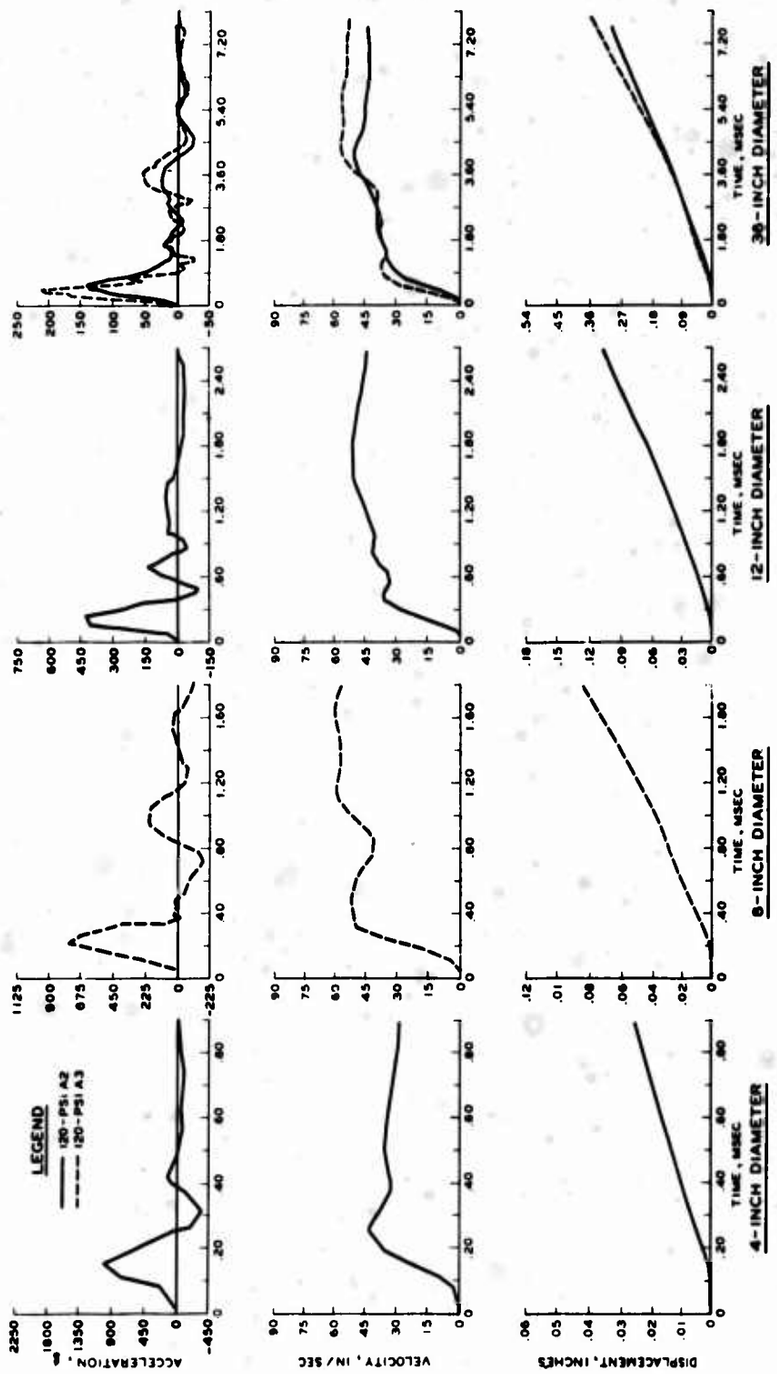

Fig. 18

Accelerations, Velocities, and Displacements of Arch Floors, p_{so} = 120 psi

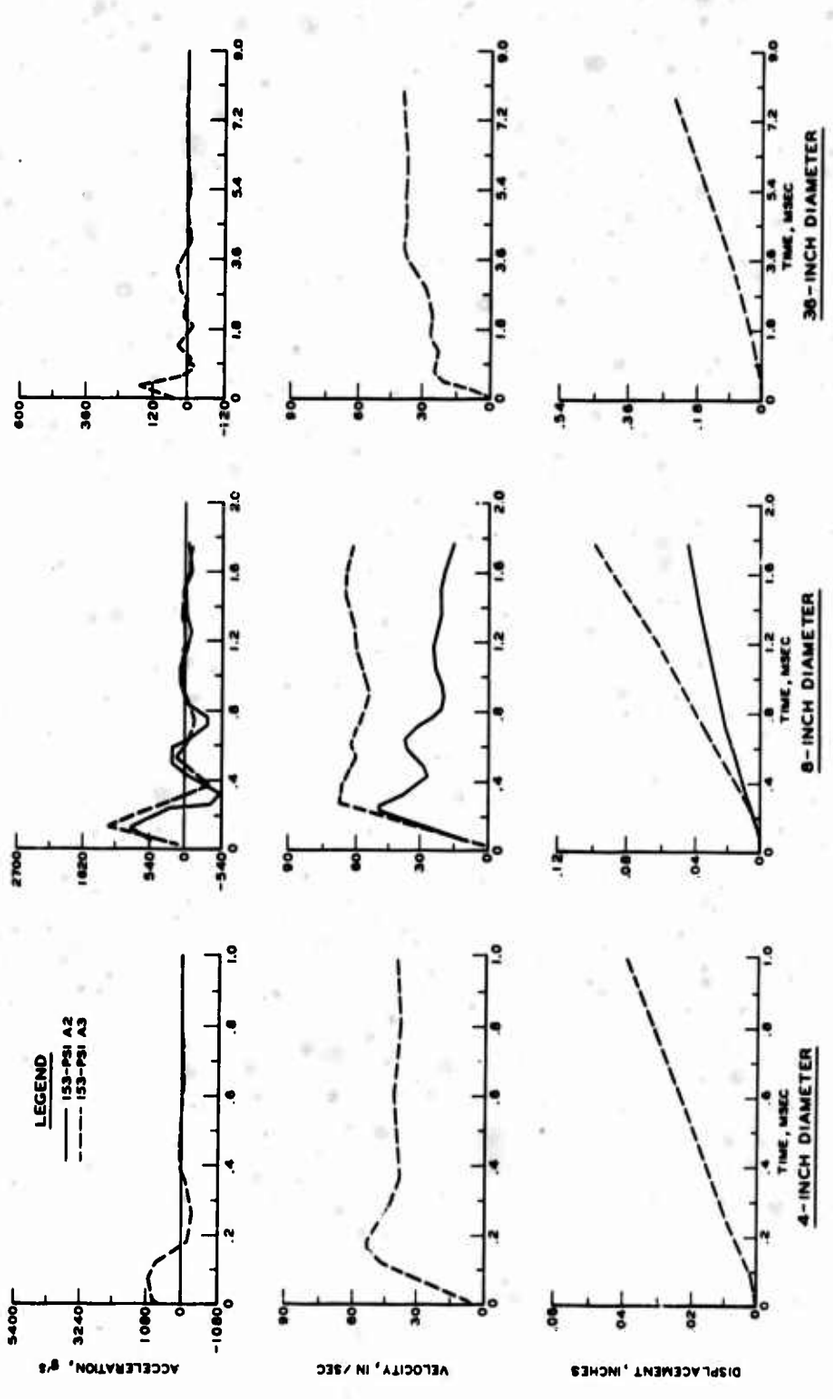

Fig. 19

Accelerations, Velocities, and Displacements of Arch Floors, p_{so} = 153 psi

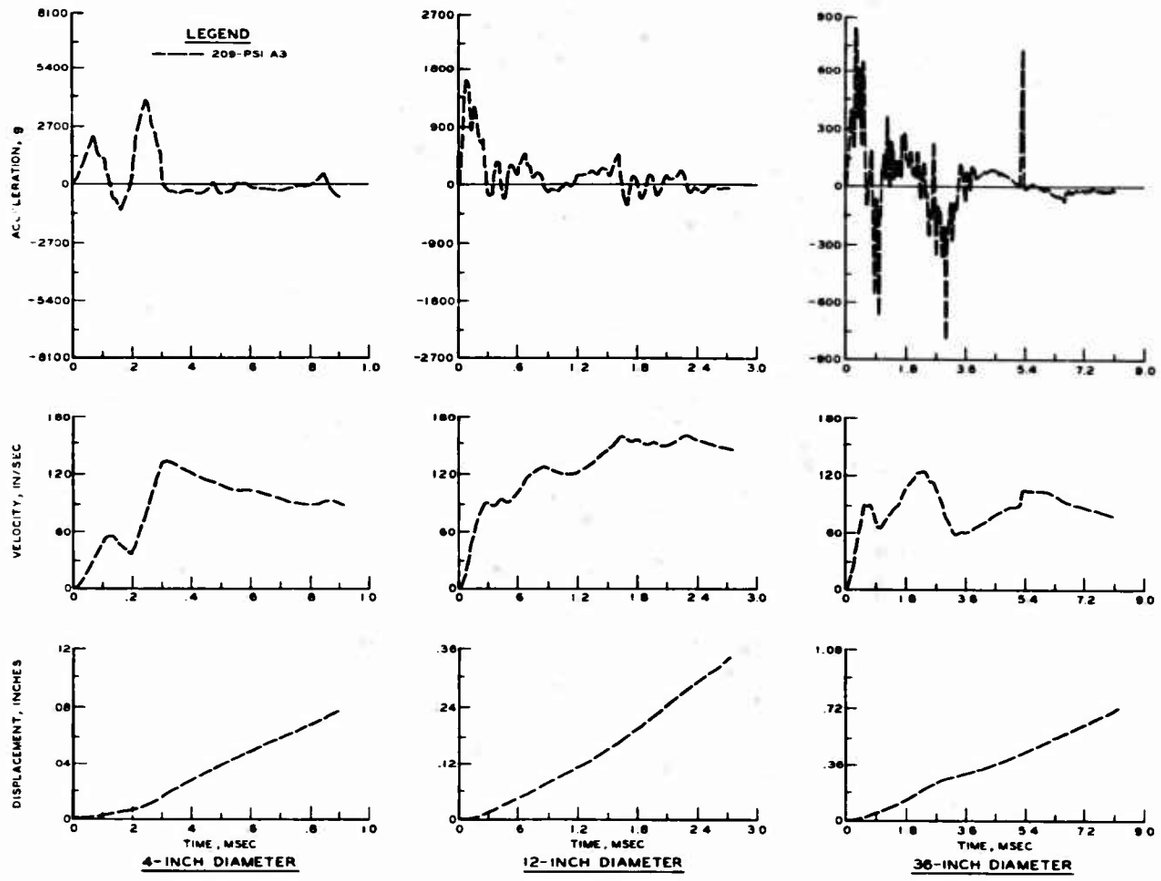

Fig. 20

Accelerations, Velocities, and Displacements of 4-, 12-, and 36-Inch-Diameter Arch Floors, Gage A3, p_{so} = 209 psi

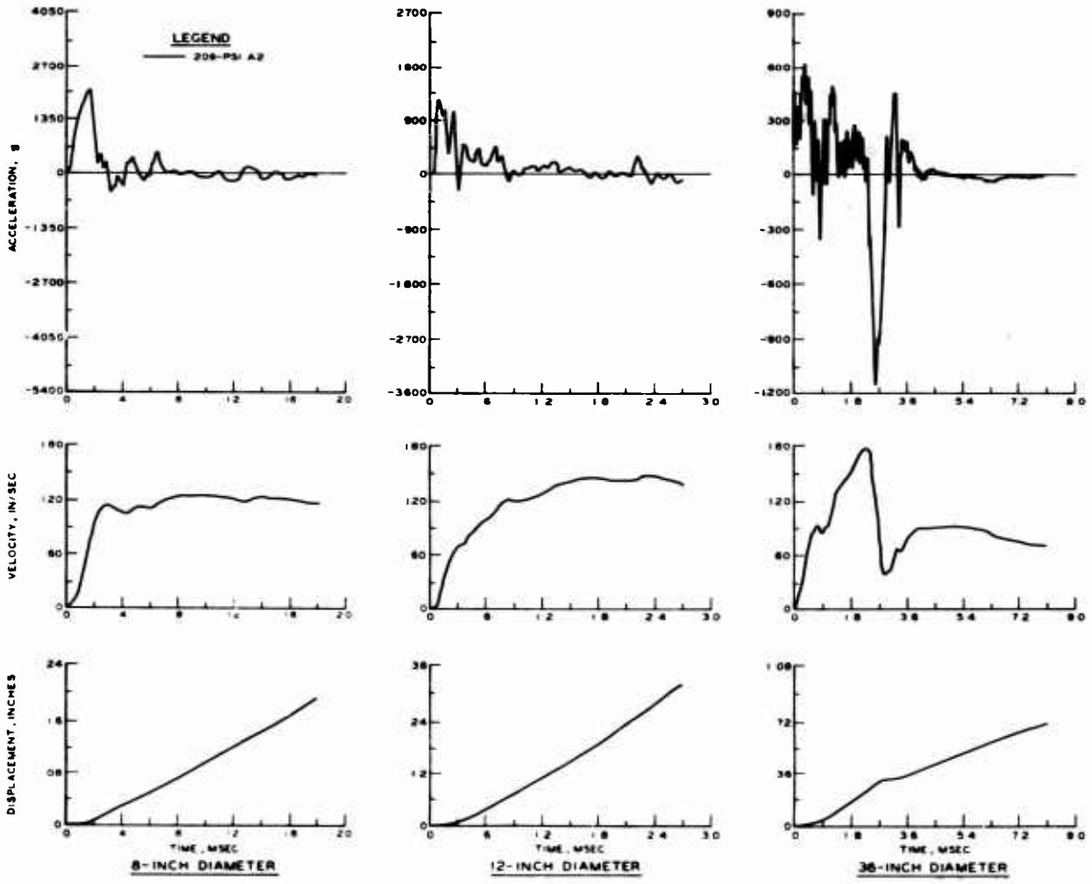

Fig. 21

Accelerations, Velocities, and Displacements of 8-, 12-, and 36-Inch-Diameter Arch Floors, Gage A2, p_{so} = 209 psi

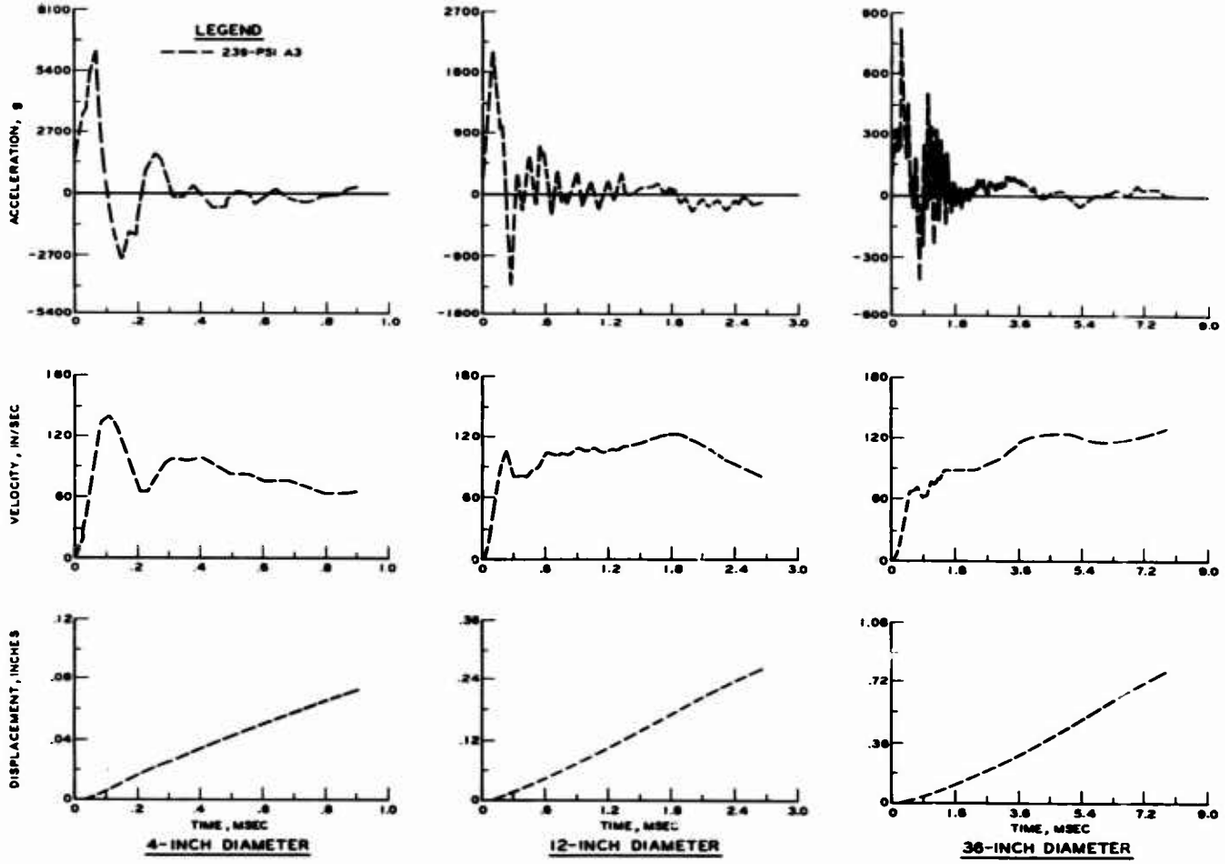

Fig. 22

Accelerations, Velocities, and Displacements of 4-, 12-, and 36-Inch-Diameter Arch Floors, Gage A3, p_{so} = 239 psi

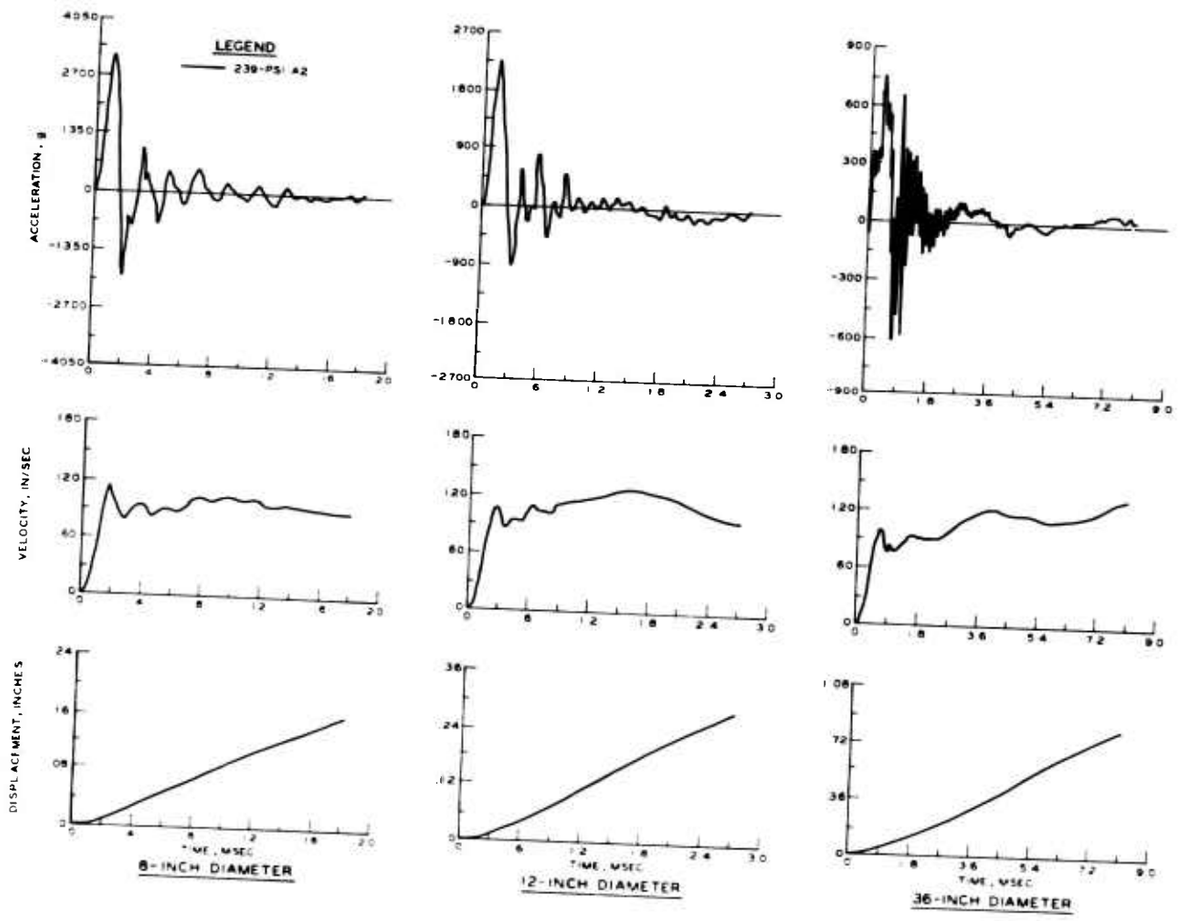

Fig. 23

Accelerations, Velocities, and Displacements of 8-, 12-, and 36-Inch-Diameter Arch Floors, Gage A2, p_{so} = 239 psi

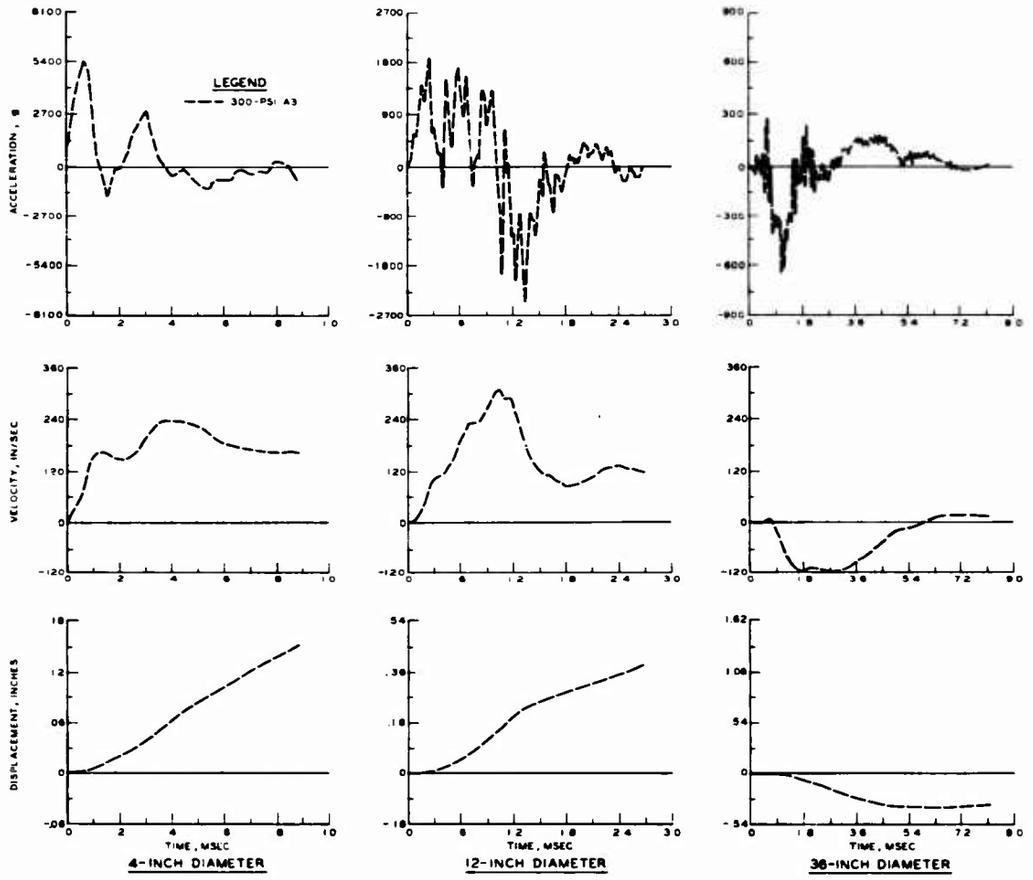

Fig. 24

Accelerations, Velocities, and Displacements of 4-, 12-, and 36-Inch-Diameter Arch Floors, Gage A3, p_{so} = 300 psi

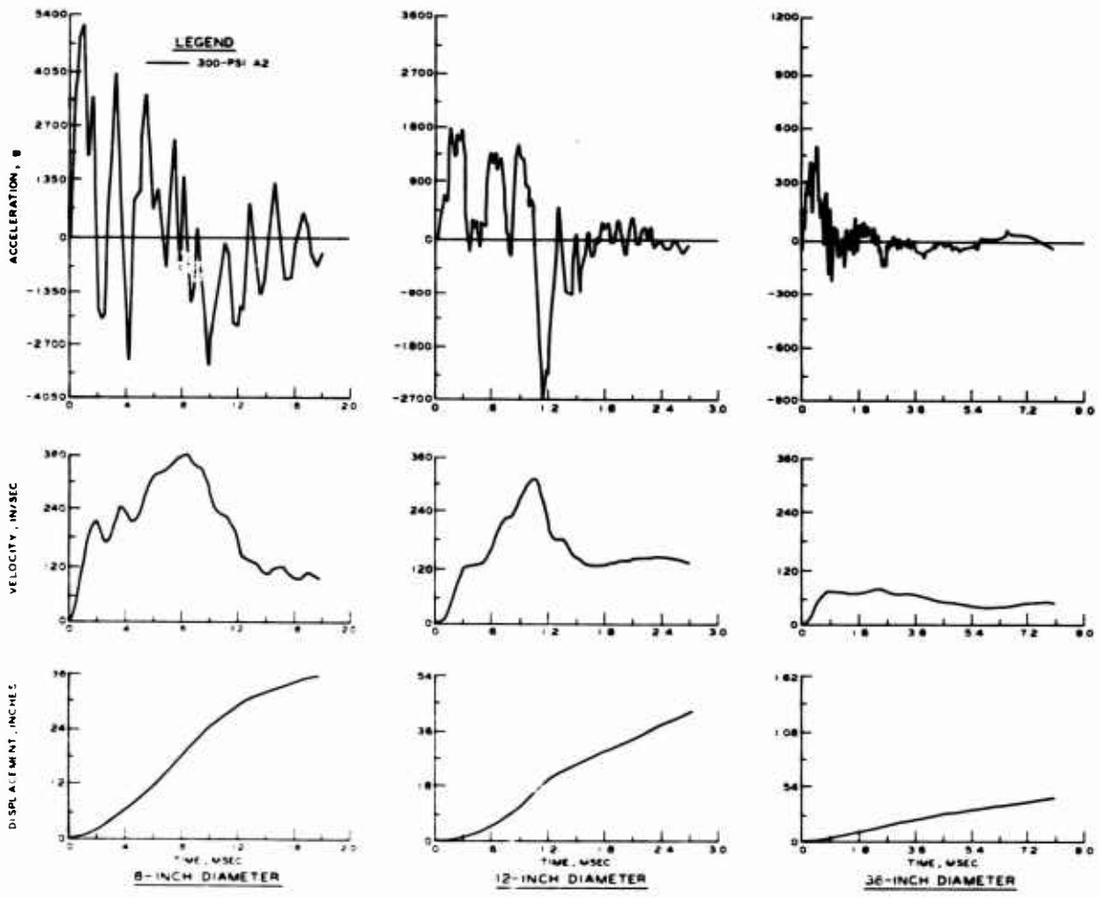

Fig. 25

Accelerations, Velocities, and Displacements of 8-, 12-, and 36-Inch-Diameter Arch Floors, Gage A2, p_{so} = 300 psi

for the 4-inch-diameter arch were recorded. It should also be pointed out that the 2500-g accelerometers were overranged. However, they are rated for a shock environment at 7500-g half-sine pulse at 150-μsec or more duration without damage, and it is estimated that the calibration remained fairly linear. The velocity and displacement of the arch floors were obtained by integrating acceleration-time records. The oscillograph records were digitized and integrated on the Waterways Experiment Station computer, and the output was plotted on a Calcomp plotter.

Figures 26 and 27 show the peak value of the floor acceleration plotted against the arch diameter for each surface overpressure. A rectangular hyperbola, which is predicted from the scaling relations, is plotted through the data points. Figures 28 through 32 show the predicted linear floor displacement at homoiogous times.

The crown accelerations of the arches for the first three shots are plotted in Figure 33. The predicted rectangular hyperbola is fitted through the data points. The traced acceleration-time playbacks are shown in Appendix B. Much of these data were considered unreliable for integrating to obtain velocities and displacements. In obtaining peak values, the source of error seems to be in overdriving the tape system. This is generally indicated by an abrupt flattening of the initial acceleration peak.

The thrust T and bending moments M were calculated from back-to-back strain gages by using the following relations:

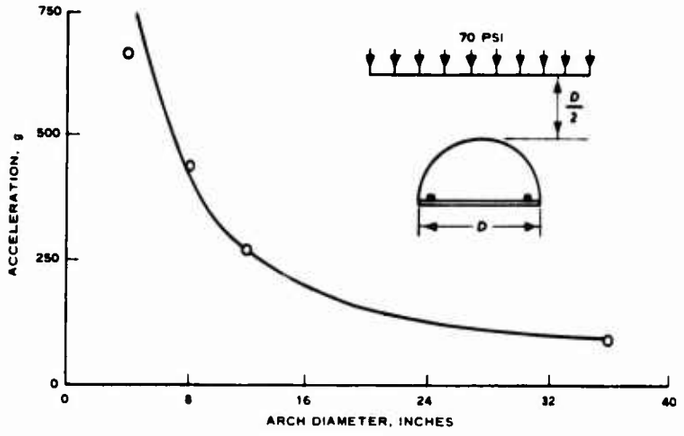

a. p_{so} = 70 psi

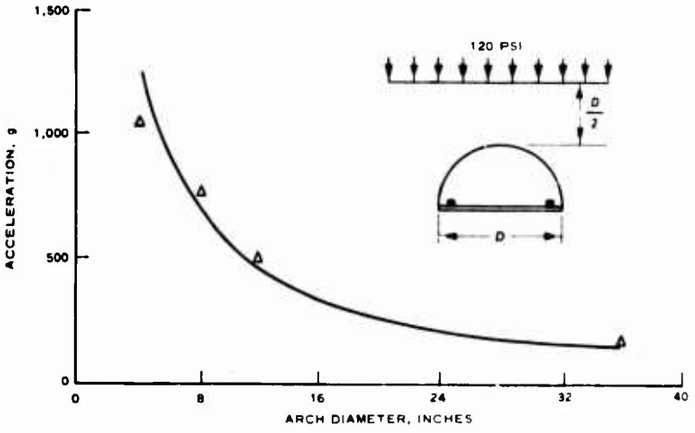

b. p_{so} = 120 psi

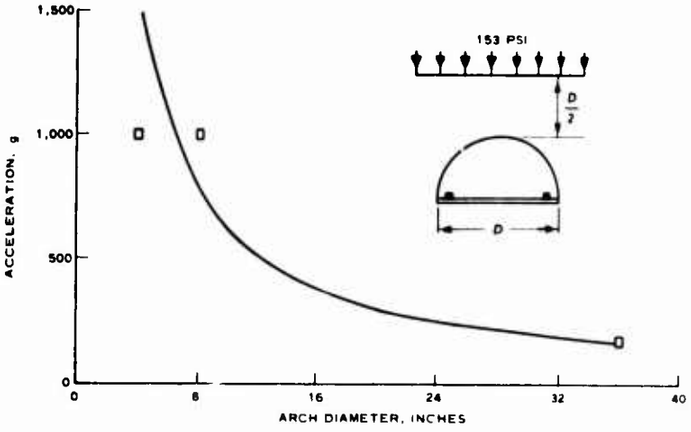

c. p_{so} = 153 psi

Fig. 26

Peak Floor Accelerations, p_{so} = 70, 120, and 153 psi

a. p_{so} = 209 psi

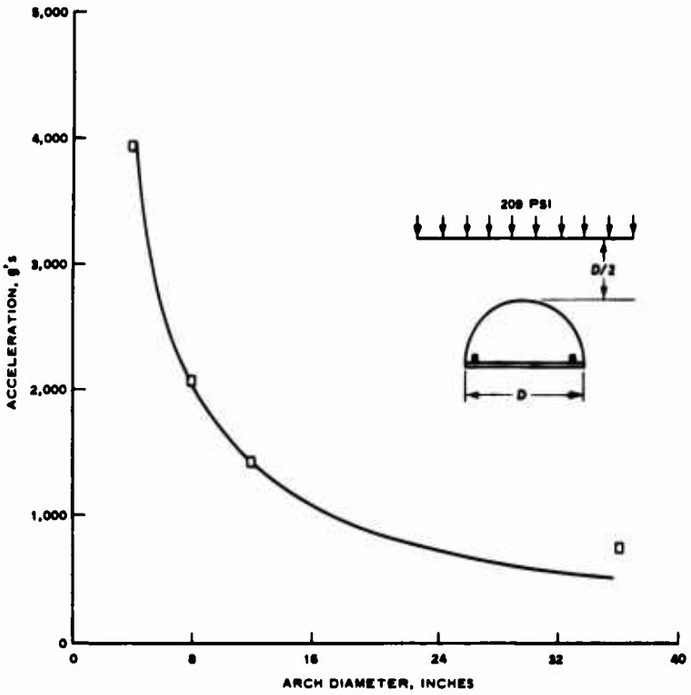

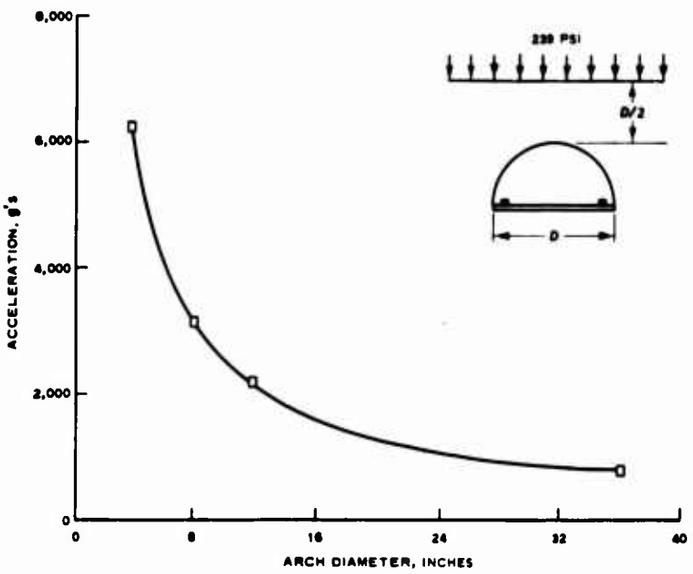

b. p_{so} = 239 psi

Fig. 27

Peak Floor Accelerations, p_{so} = 209 and 239 psi

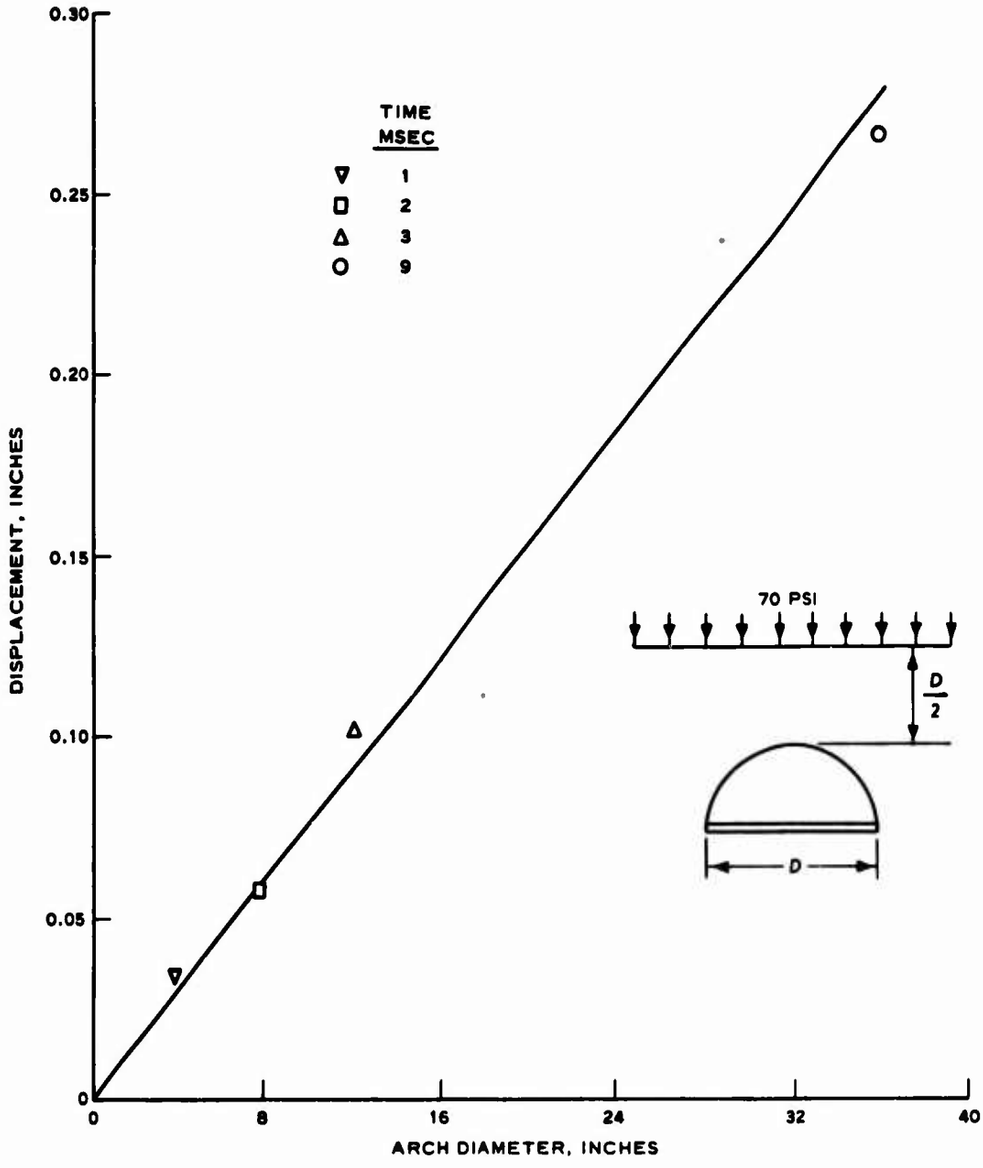

Fig. 28

Floor Displacement at Scaled Time, p_{so} = 70 psi

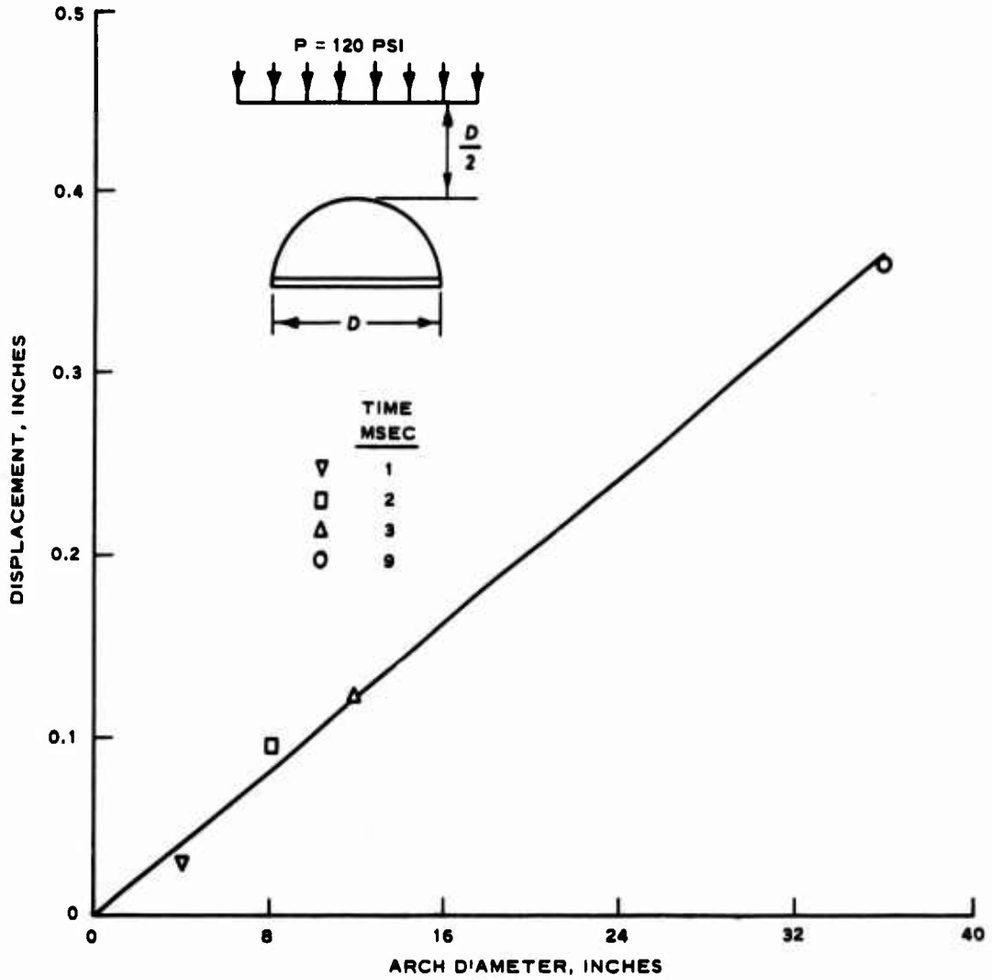

Fig. 29

Floor Displacement at Scaled Time, p_{so} = 120 psi

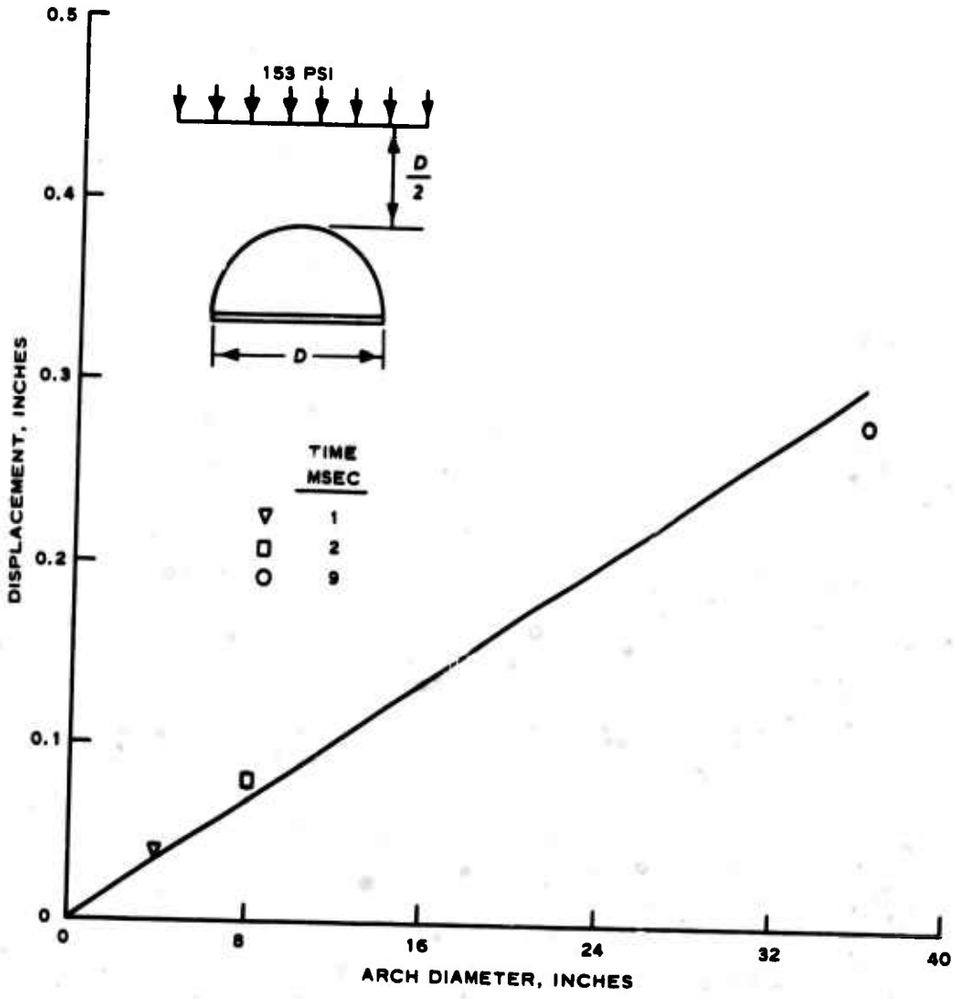

Fig. 30

Floor Displacement at Scaled Time, p_{so} = 153 psi

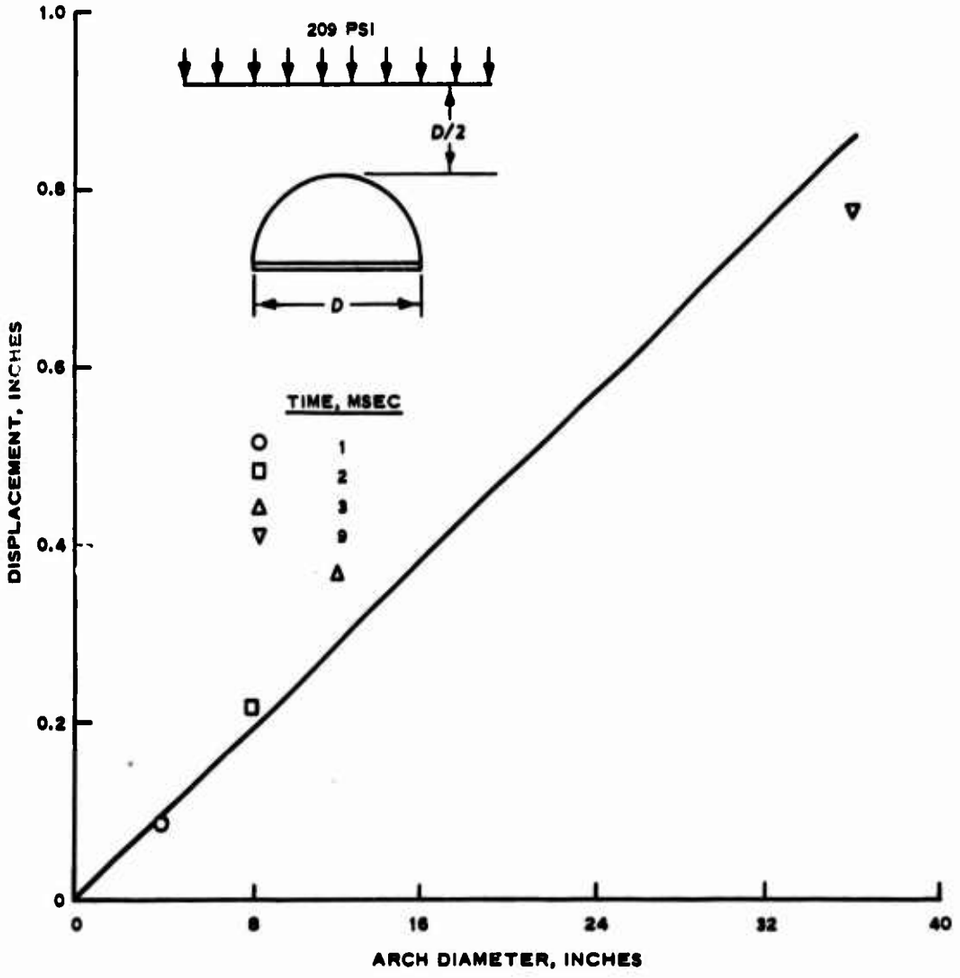

Fig. 31

Floor Displacement at Scaled Time, p_{so} = 209 psi

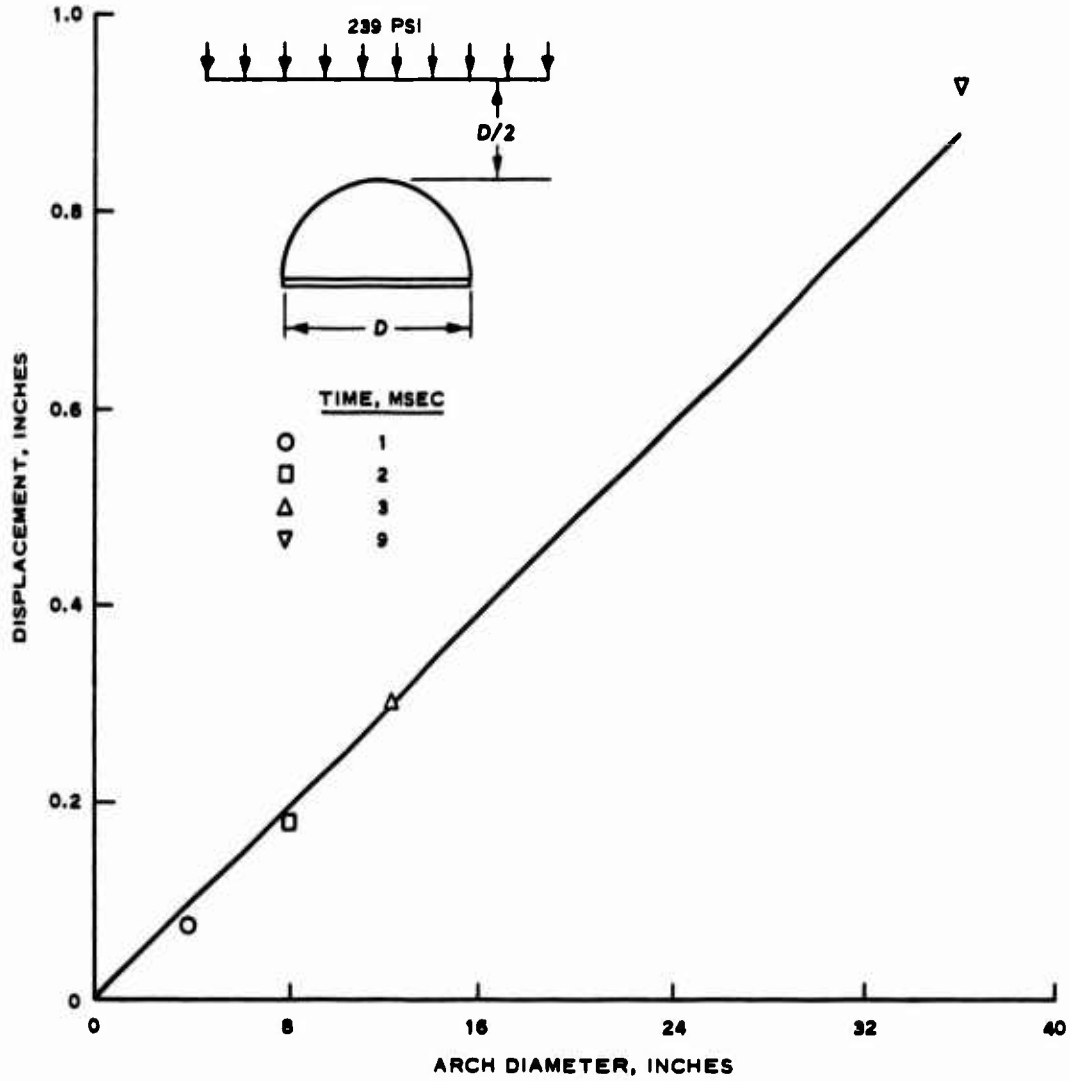

Fig. 32

Floor Displacement at Scaled Time, p_{so} = 239 psi

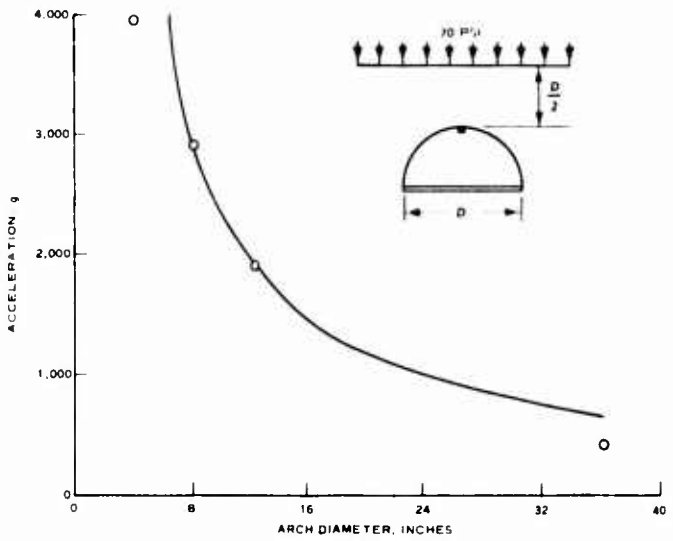

a. p_{so} = 70 psi

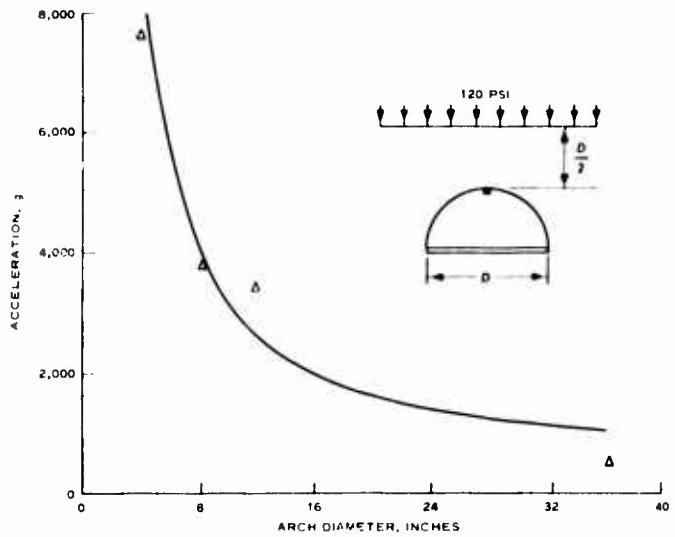

b. p_{so} = 120 psi

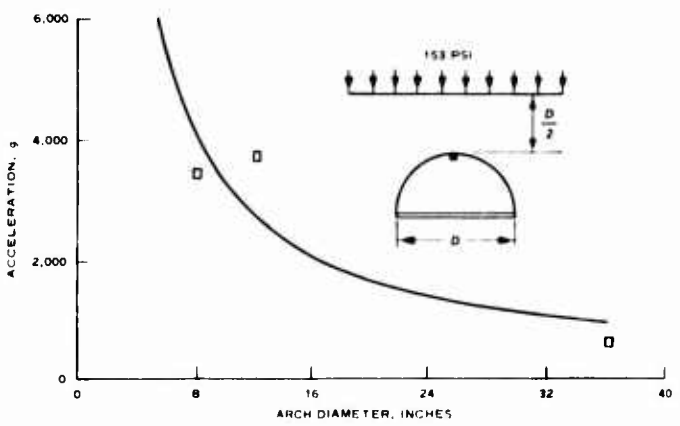

c. p_{so} = 153 psi

Fig. 33

Peak Crown Accelerations, p_{so} = 70, 120, and 153 psi

$$T = \int_0^h \sigma(y)dy$$

$$M = \int_0^h \sigma(y)ydy$$

The relation between stress and strain is approximated by a bilinear relation

$$\sigma = E\,\epsilon \text{ for } \epsilon \leq \epsilon_{yield}$$

$$\sigma = \sigma_{yield} + E'(\epsilon - \epsilon_{yield}) \text{ for } \epsilon \geq \epsilon_{yield}$$

where the units of strain are μinches/inch. The values of E, E', σ_{yield} and ϵ_{yield} are determined from Figures 48 and 49 in Appendix A.

Figures 34 through 37 show computer plots of moment and thrust time at 85 degrees from the crown for the four arches. The ordinate and abscissa of each plot have been constructed so as to maintain proper similitude relations among the four arch sizes. Thus, the plots for each parameter should be identical for all arch diameters. Except for the 4-inch-diameter arch, the magnitudes and shapes of the thrust-time plots compare favorably. The magnitudes of the thrusts were higher for the 4-inch arch, and the bending moments show considerable scatter in magnitude. DaDeppo[8] has shown by a perturbation analysis that moments in a thin metal arch are dependent on the initial deformation. The initial deformation could result from induced strain caused by the backfill or by random variations in the circularity of the arch. Other factors contributing to the scatter in the thrusts and moments could be

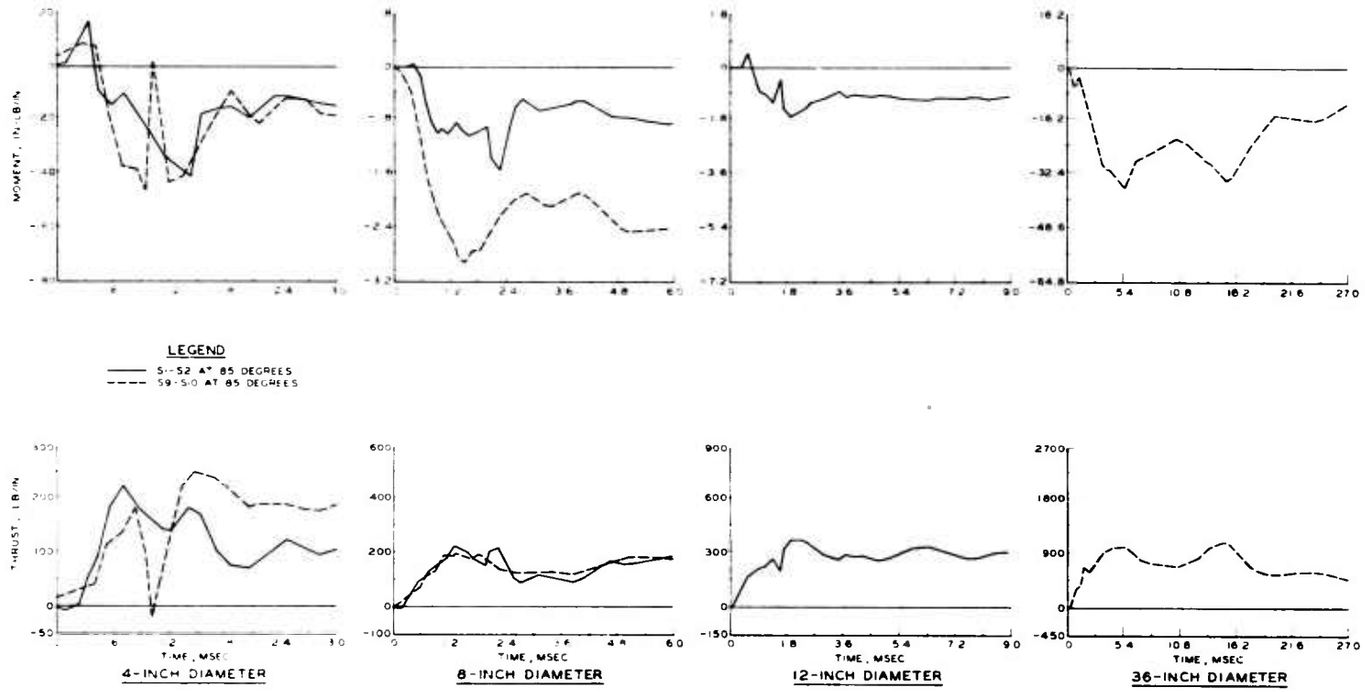

Fig. 34

Moments and Thrusts at 85° from Crown, p_{so} = 70 psi

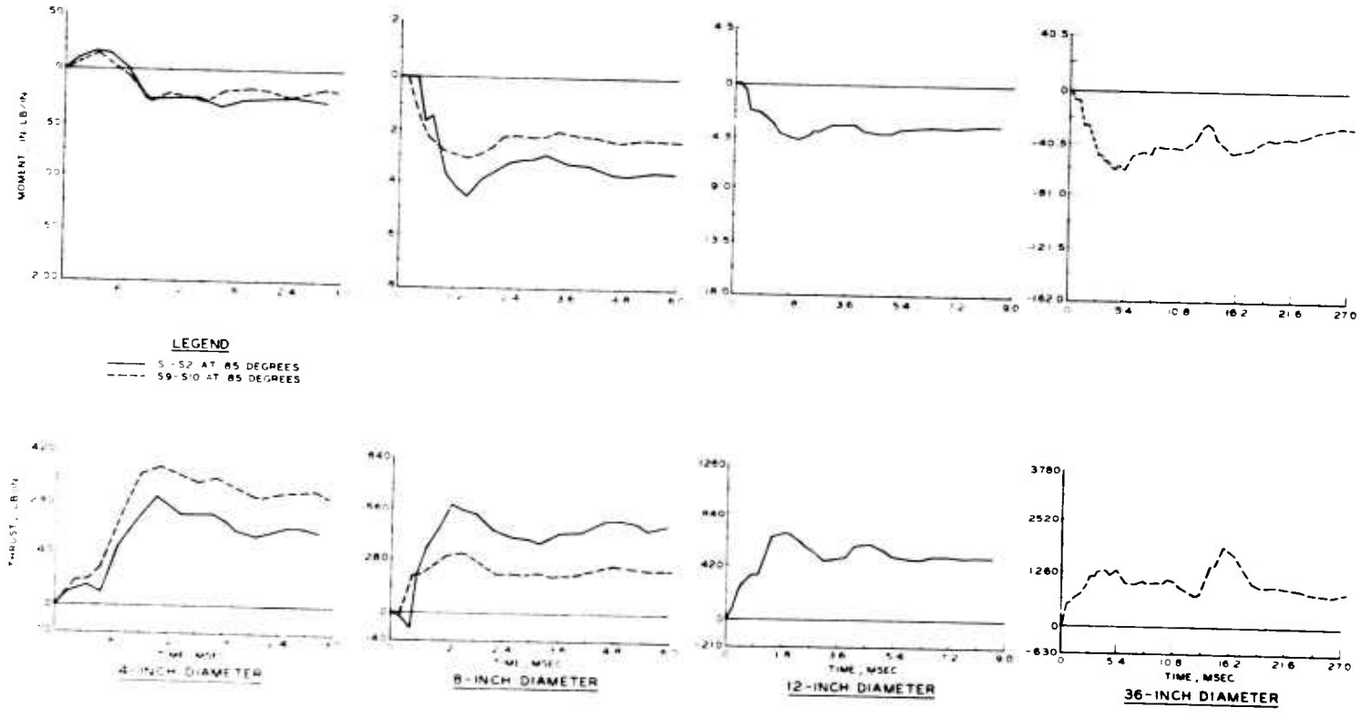

Fig. 35

Moments and Thrusts at 85° from Crown, p_{so} = 120 psi

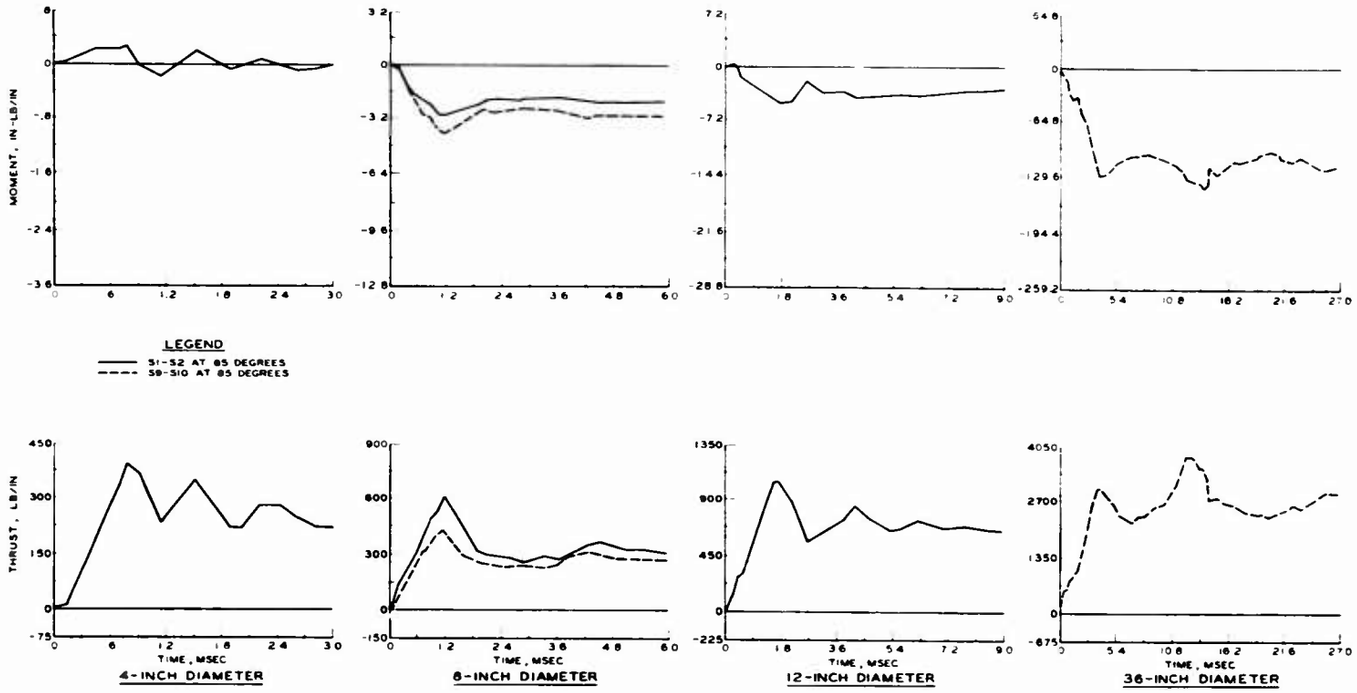

Fig. 36

Moments and Thrusts at 85° from Crown, p_{so} = 153 psi

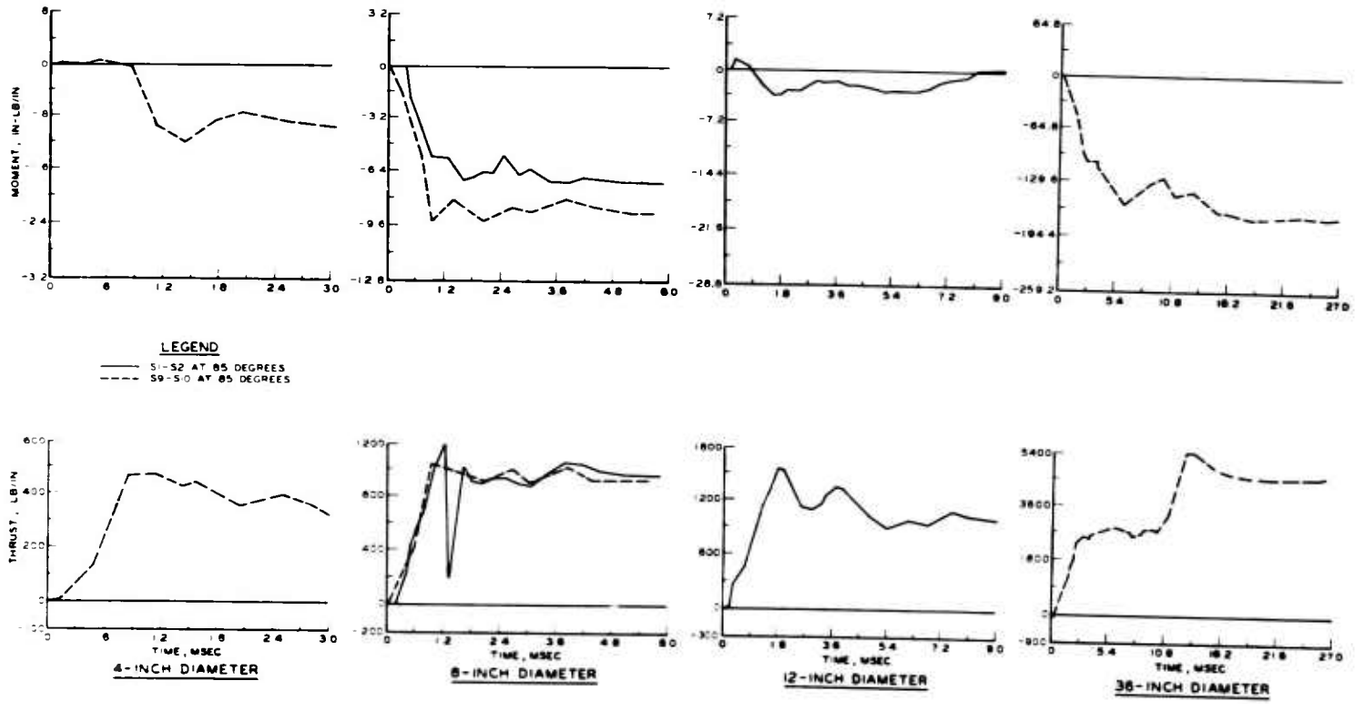

Fig. 37

Moments and Thrusts at 85° from Crown, p_{so} = 209 psi

attributed to variation in the arch thickness, change in pressure distributions with depth and to the end fixity. Although care was taken to obtain as rigid a boundary as possible, it was impossible to obtain the same amount of fixity for all four arches. Denton and Flathau's[9] tests on fixed-end metal arches showed that the thrusts and moments scaled better. Their arches were twice the thickness or eight times stiffer with length ratios up to three.

Back-to-back strain gages were placed at various locations on the arches to compute thrust and moment distributions; however, it was considered sufficient for the purpose of verifying similitude relations to present plots of maximum moments and thrusts. Inelastic strains occurred in the arches during the fourth shot (p_{so} = 209 psi), and since permanent deformations cause changes in shape and material properties any further evaluation of moment and thrust would introduce additional, and possibly significant errors.

Figures 38 through 41 show an average of the maximum values of thrust and moments at 85 degrees from the crown. Average values could only be obtained for the 4- and 8-inch-diameter arches since one gage from the pair on the 12- and 36-inch-diameter arches did not record. According to the scaling relations, thrust varies linearly with the length scale and the moment varies as the square of the length scale; hence, a straight line is drawn through the data points for thrust and a parabola through the data points for moment.

The strain distribution around the arch indicates a condition of uniform thrust and a moment distribution which increases in magnitude near the fixed ends.

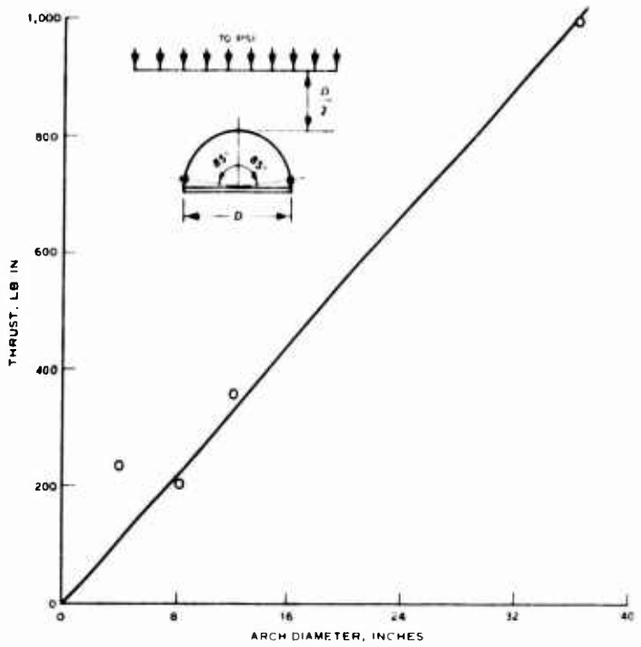

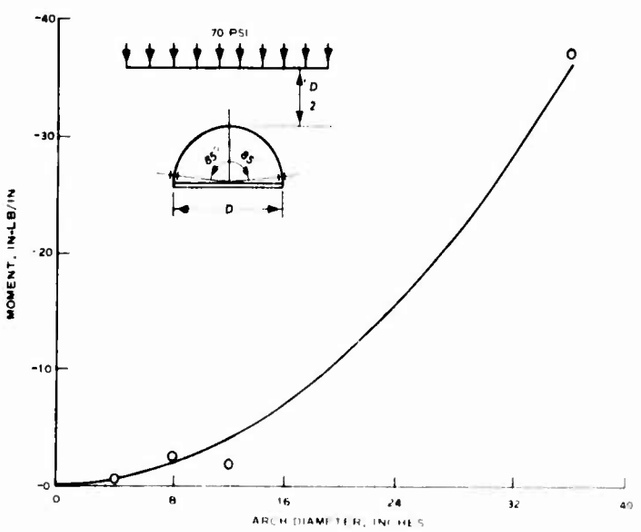

Fig. 38

Average Maximum Thrust and Moment at 85° from Crown,
p_{so} = 70 psi

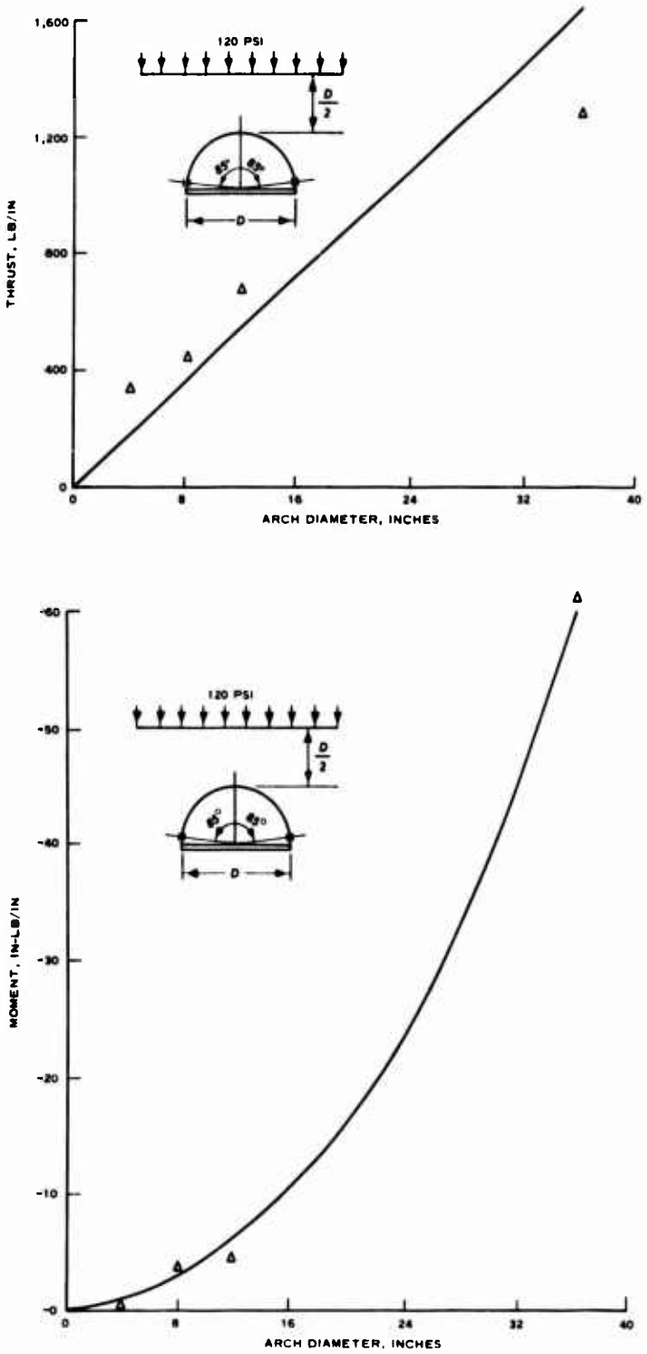

Fig. 39

Average Maximum Thrust and Moment at 85° from Crown,
p_{so} = 120 psi

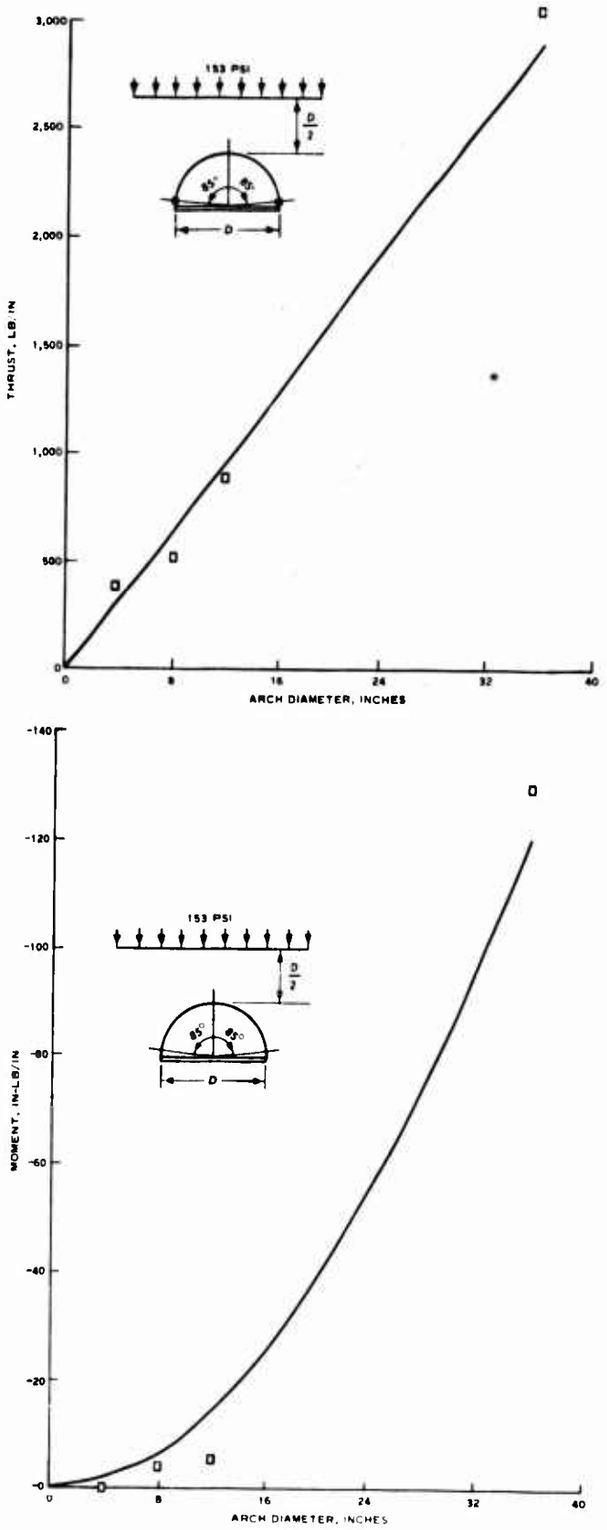

Fig. 40

Average Maximum Thrust and Moment at 85° from Crown, p_{so} = 153 psi

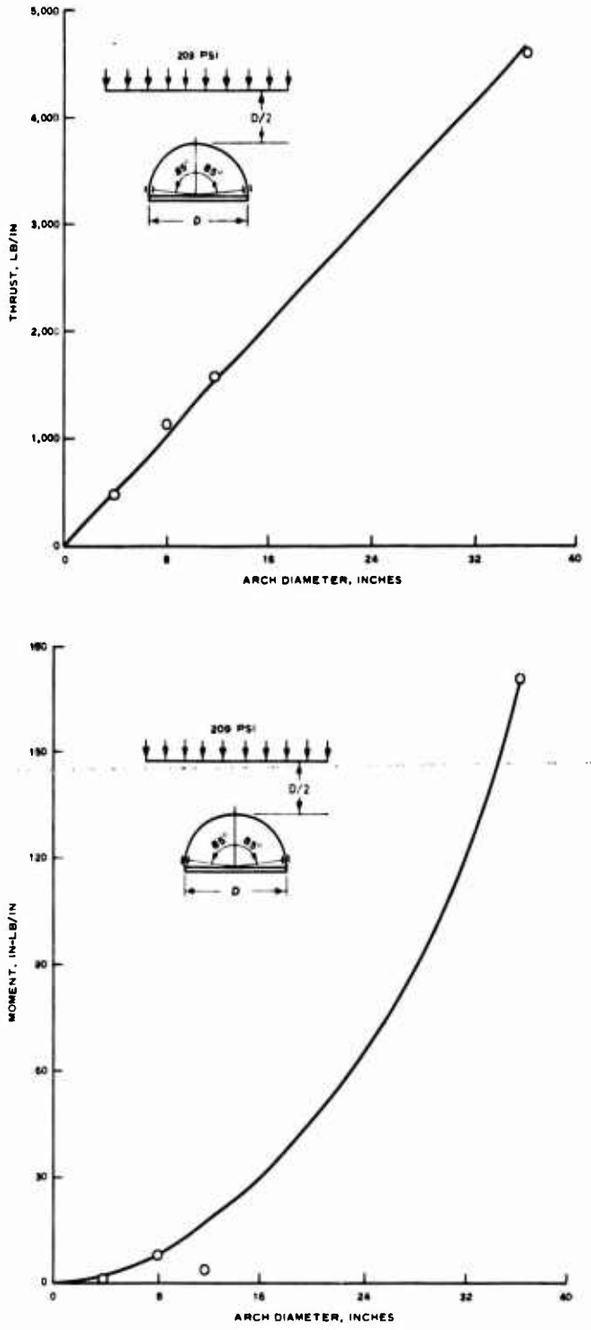

Fig. 41

Average Maximum Thrust and Moment at 85° from Crown,
p_{so} = 209 psi

The displacement data for the first three shots are not presented since the spring-loaded probes of the LVDT's separated from the crown. The oscillograph traces for the next three shots are shown in Appendix B. The probes were rigidly attached to the crown for this series of tests. The screws holding the LVDT to the mount in the 36-inch-diameter arch were sheared, and the transducer body was loose; therefore, these data should be disregarded and no plots of relative deflection of this arch are shown for any of the test structures.

Figures 42 and 43 show the end views of the failed arches. Since the arches were geometrically scaled and subjected to the same surface overpressures simultaneously, they should all have sustained the same amount of inelastic action and failed in a similar manner. The 4- and 12-inch-diameter arches buckled at the springing line and the 8-inch-diameter arch was on the verge of failure at the springing line. The bolts on one side of the 36-inch-diameter arch were sheared. The arch ring was bolted to the floor plate at each springing line with two rows of bolts, each row consisting of 16-7/16-inch-diameter steel bolts. Had the floor plate of the 36-inch-diameter arch been grooved and secured by a single row of bolts like that of the 4-, 8-, and 12-inch-diameter arches, it could not have failed in this manner but would have developed a local buckle similar to the other three arches.

Prior to buckling, the arch crown deformed inward with an outward bulge developing at approximately the 85-degree sections where the strain gages on the inside measured high compressive

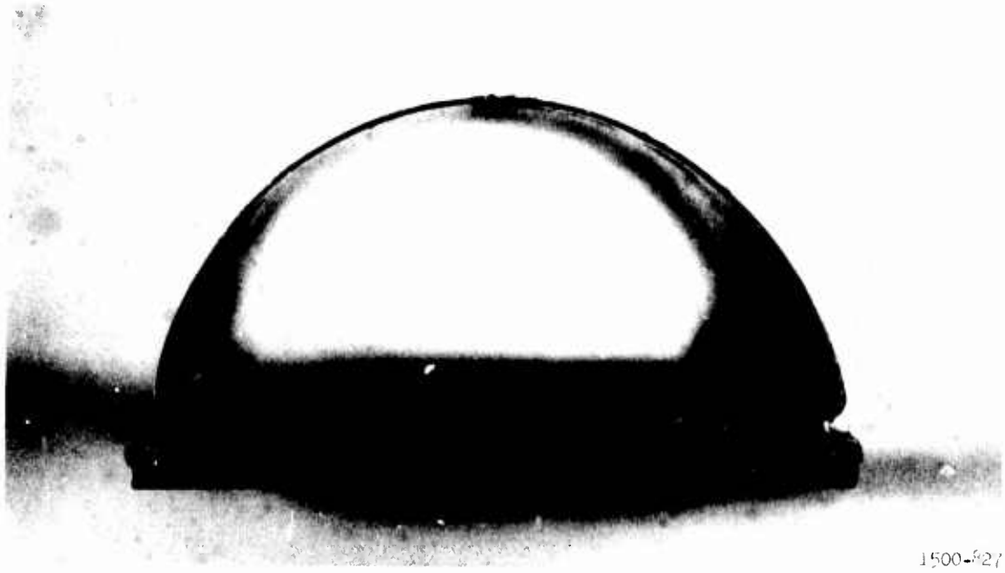

1500-827

a. Four-Inch-Diameter Arch

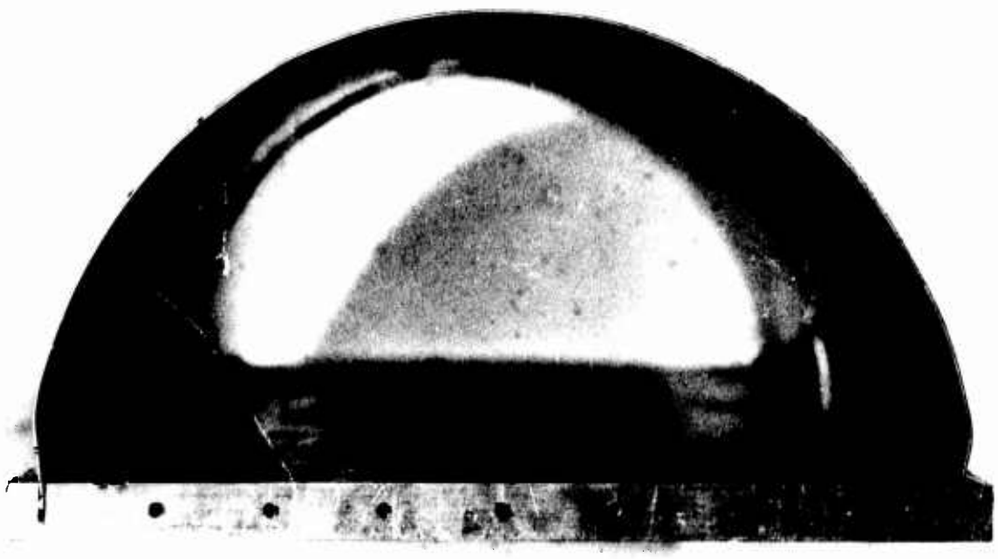

1500-820

b. Eight-Inch-Diameter Arch

Fig. 42

End Views of 4- and 8-Inch-Diameter Arches

a. Twelve-Inch-Diameter Arch

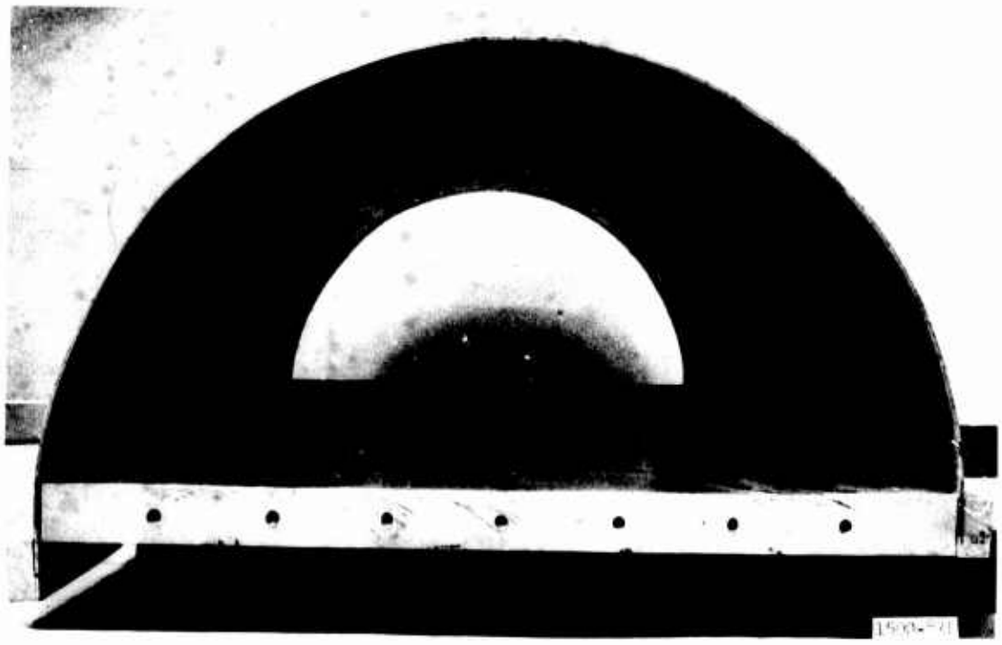

b. Thirty-Six-Inch-Diameter Arch

Fig. 43

End Views of 12- and 36-Inch-Diameter Arches

strains and the gages on the outside measured significantly smaller compressive strains or tensile strains. This trend is indicated by the 8-inch-diameter arch shown in Figure 42.

VI

SUMMARY, CONCLUSIONS, AND RECOMMENDATIONS

A. Summary

The general objective of this investigation was to verify similitude relations for buried semicircular fixed-end metal arches subjected to surface airblast overpressures. Two series of tests, each consisting of three shots and a total of 411 channels of instrumentation, were performed in the LBLG. The independent variables associated with the geometry and the material properties were carefully controlled to satisfy the scaling relations. The variations of preshot and postshot soil densities, within the capabilities of the measuring technique, were insignificant. The variables associated with the specific weight, and the rise and decay times of the overpressure were distorted. The effect of the distortion was apparently negligible.

The results obtained from these tests extend a previous study by Denton and Flathau[9] by increasing the length scale to 9 and by conducting tests on eight times more flexible arches in and beyond the elastic range of response.

B. Conclusions

The parameters that were verified can be subdivided into the motion of the arch floor and the internal forces and moments. The floor motion, measured by its acceleration, velocity, and

displacement, scaled closely for the four arches. The variation from the predicted curves can be attributed more to transducer and system response than to any distortions in the models. The variations in thrust and moment from the predicted curves can be associated more with scale effects and model distortions.

From the observed and calculated results of the tests, the following specific conclusions are applicable to the conditions of this study (see Figures 17 through 43):

1. The variables considered in developing the scaling relations in the elastic and inelastic ranges of response were adequate for the test conditions and the material used.

2. The accelerations, velocities, and displacements of a prototype can be predicted for length scales of up to 9.

3. Based on four tests, the maximum thrust in a prototype can be predicted with reasonable accuracy for length scales of up to 9; however, predicting the maximum bending moments for length scales of 9 could lead to significant error. The results indicate that a length scale of 4-1/2 would be more suitable when predicting values for moment.

4. From the results of the last test, surface overpressure causing excessive inelastic action and localized buckling at the springing line can be predicted.

5. These results appear to indicate that small scale models can be used for other structural and soil materials when subjected to air induced blast loads for length scales up to nine, provided

that all design conditions relevant to the response of the structure are satisfied.

C. Recommendations

The ultimate goal of model design and testing should be to predict the behavior of a prototype in the field. Tests of scale models of prototype systems already tested in the field should be undertaken in the laboratory or under field conditions to evaluate modeling techniques.

An investigation should be conducted of the effect of distorting duration time if the structure response is dependent on the duration time. This would be the case if the ratio of the pulse duration time to the natural period of the structure were near unity.

Since prototype installations in the field would be in naturally occurring soil, investigations of modeling procedures in soil other than dry sand should be conducted.

A statistical study should be conducted for a length scale of nine in an effort to determine the number of tests on the model to predict with a specified level of confidence the response of a prototype.

APPENDIX A

SUPPORT INVESTIGATIONS

A. Sand Properties

The sand used in the test series is locally known as Cook's Bayou sand. Standard soil tests[18] conducted included gradation, specific gravity, maximum and minimum laboratory dry unit weight, and consolidated-drained direct shear. The curves showing the physical properties of Cook's Bayou sand have been presented by Kennedy et al[15] and are shown herein. The one-dimensional compression and wave propagation tests were conducted under contract by the United Research Service Corporation.[11]

The gradation curve (Figure 44a) shows that a negligible percentage of the sand specimen is finer than the No. 200 sieve. The sand is uniform fine sand classified as SP in the Unified Soil Classification System. Its specific gravity is 2.65 and its maximum and minimum laboratory dry unit weights are 110.3 and 93.3 pcf. The angle of friction increases from 34.5 to 42.0 degrees as the dry unit weight increases from 98.5 to 109 pcf (Figure 44b). The photomicrograph of the sand (Figure 44c) shows that subround shapes predominate. Figures 45 and 46 show static and dynamic one-dimensional compression stress-strain relations for the sand specimen. Comparison of the static and dynamic data indicates that no significant effects result from loading rates.

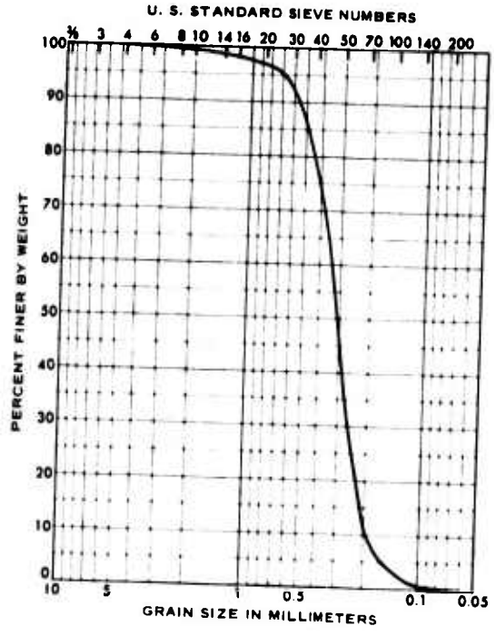

a. Gradation Curve

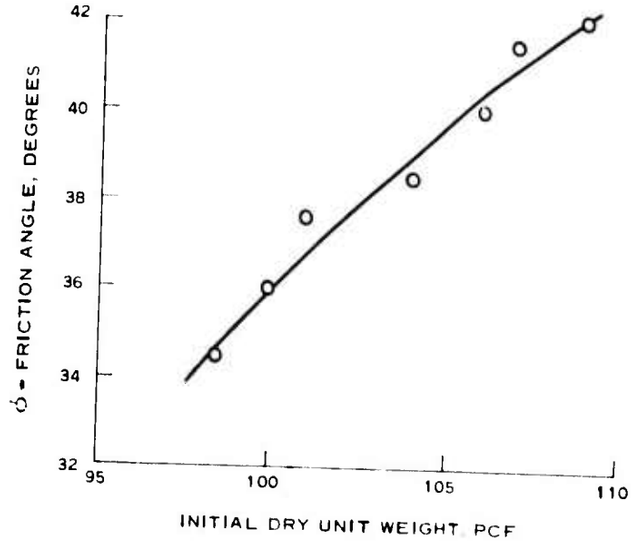

b. Consolidated-Drained Direct Shear Test Results

c. Photomicrograph 25X Showing Sub-rounded Shape of Grains

Fig. 44

Gradation, Angle of Friction, and Shape of Cook's Bayou Sand

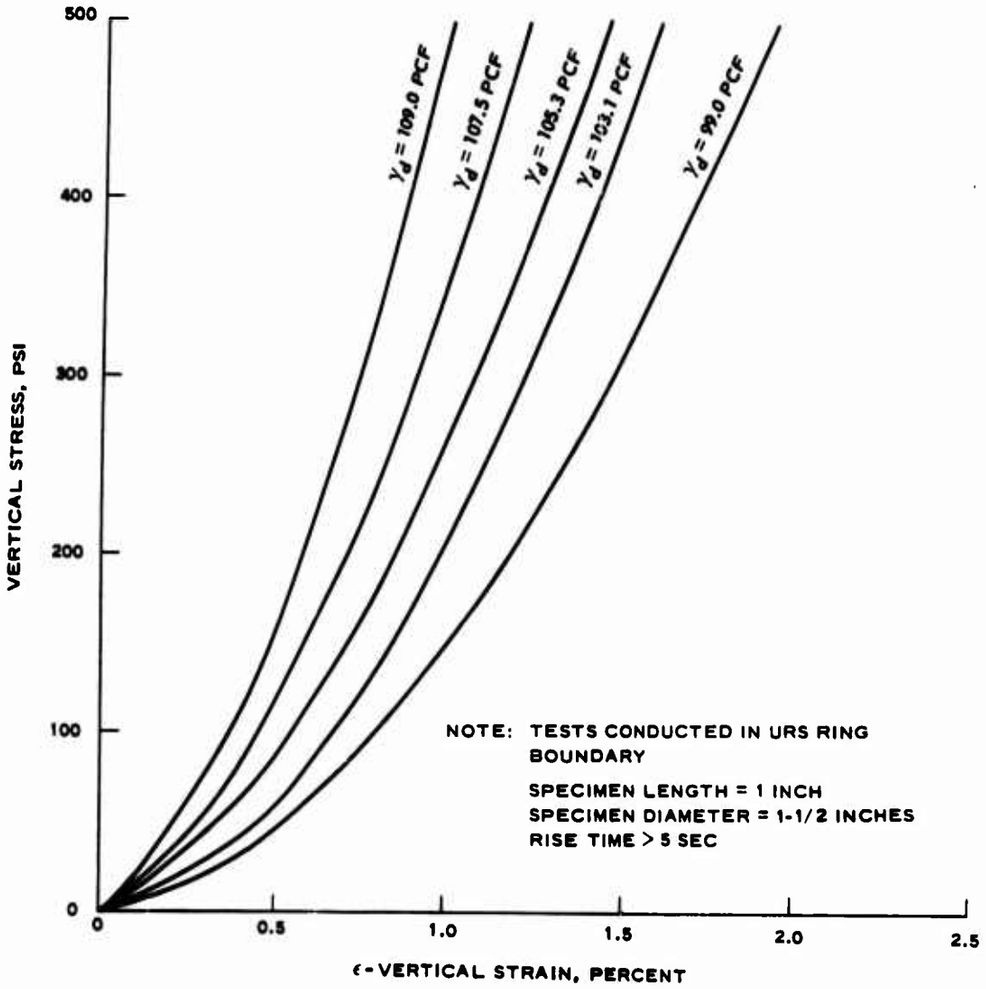

Fig. 45

Results of Static One-Dimensional Compression Tests on Cook's Bayou Sand

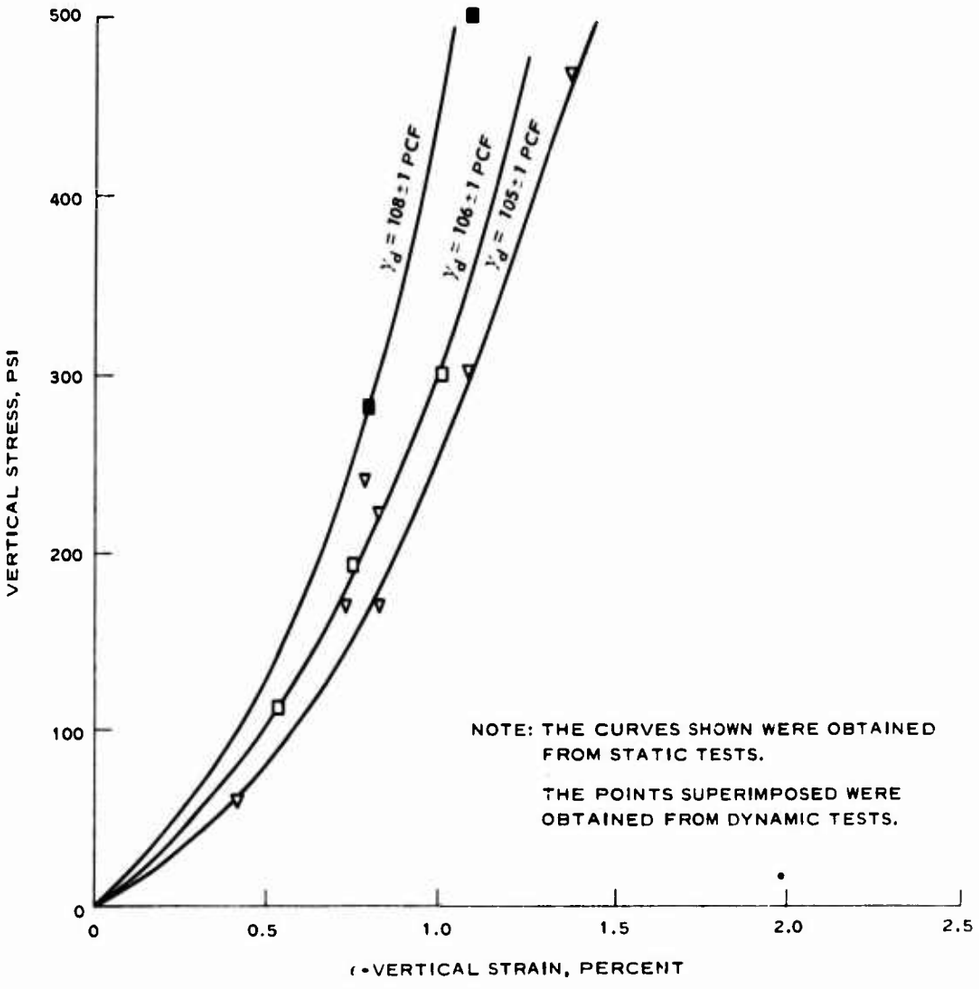

SYMBOL	DRY UNIT WEIGHT γ_d PCF	TYPE TEST	RISE TIME SEC
———	SEE CURVES	STATIC ONE-DIMENSIONAL COMPRESSION	12.0
▽	107.0 ± 0.5	DYNAMIC ONE-DIMENSIONAL COMPRESSION	0.001
□, ■	106.5 ± 0.5	WAVE PROPAGATION	0.0002

Fig. 46

Comparison of Static and Dynamic One-Dimensional Stress-Strain Data for Cook's Bayou Sand

Preshot and postshot densities of the sand were determined at various locations. A box density device which takes a sample 12 inches long, 4 inches wide, and 2 inches deep was used. Density test locations shown in Figure 47 are for the first series of tests and the values are tabulated below. No significant variations in preshot and postshot densities were observed. The density variation for the second series was similar to the first and is not shown.

Location	Depth Below Surface, in.	Density pcf
	Pretest	
1	6	110.4
2	6	109.1
3	10	111.3
4	10	109.0
5	4	108.9
6	4	109.3
7	16	108.9
8	16	110.7
	Posttest	
1	4	105.8
2	4	109.2
3	6	108.5
4	6	111.2
5	2	108.1
6	2	109.5
7	18	108.9
8	18	110.6

B. Structure Material Properties

Two tensile specimens cut from a 1/4-inch-thick plate of

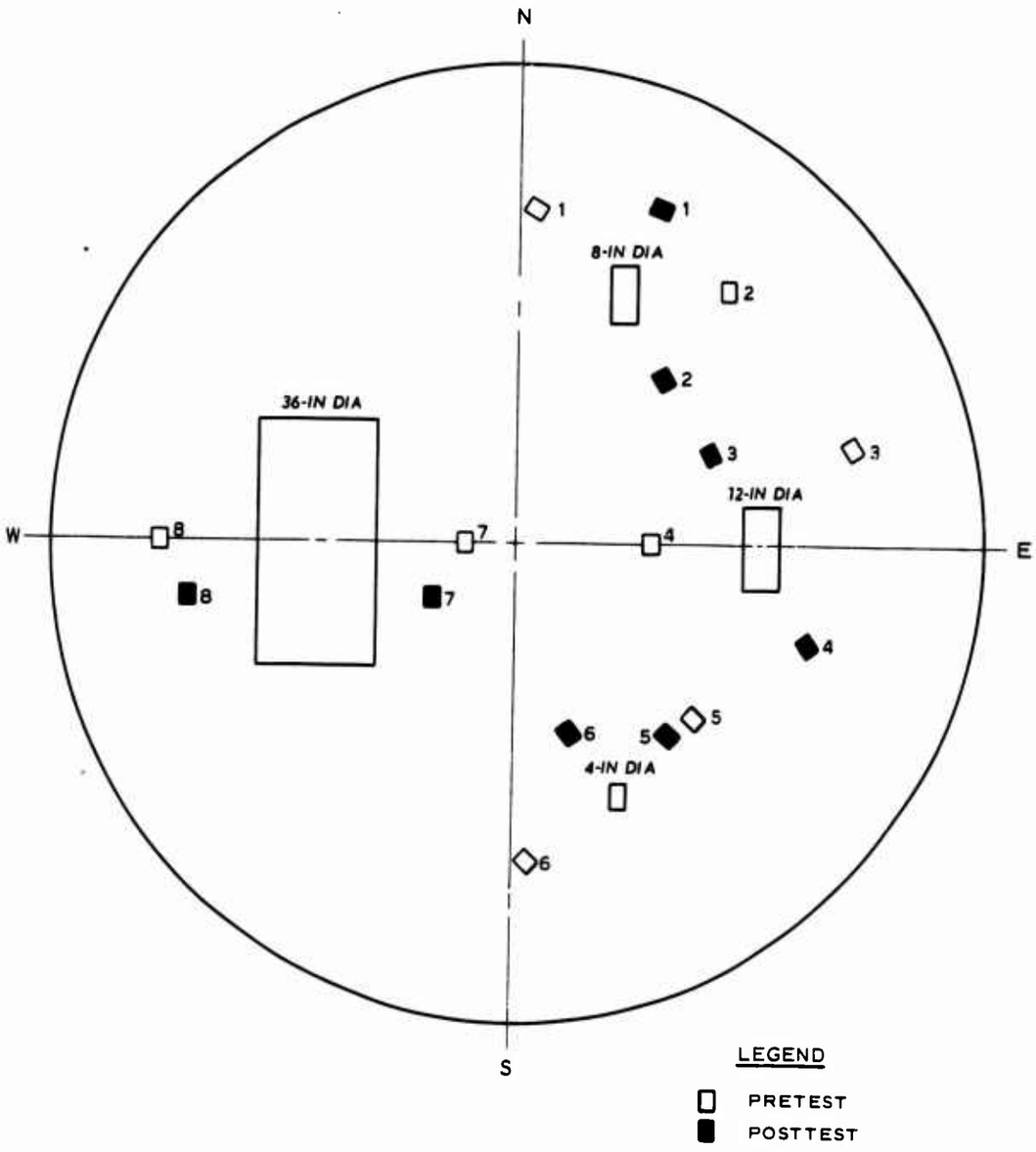

Fig. 47

Location of Density Tests in LBLG

5086-H32 aluminium alloy were tested statically with the load axis parallel and perpendicular to the direction of rolling. The partial stress-strain curves are shown in Figures 48 and 49. Dynamic tests[7] on similar alloys have shown no significant change in material properties due to rapidly applied loads.

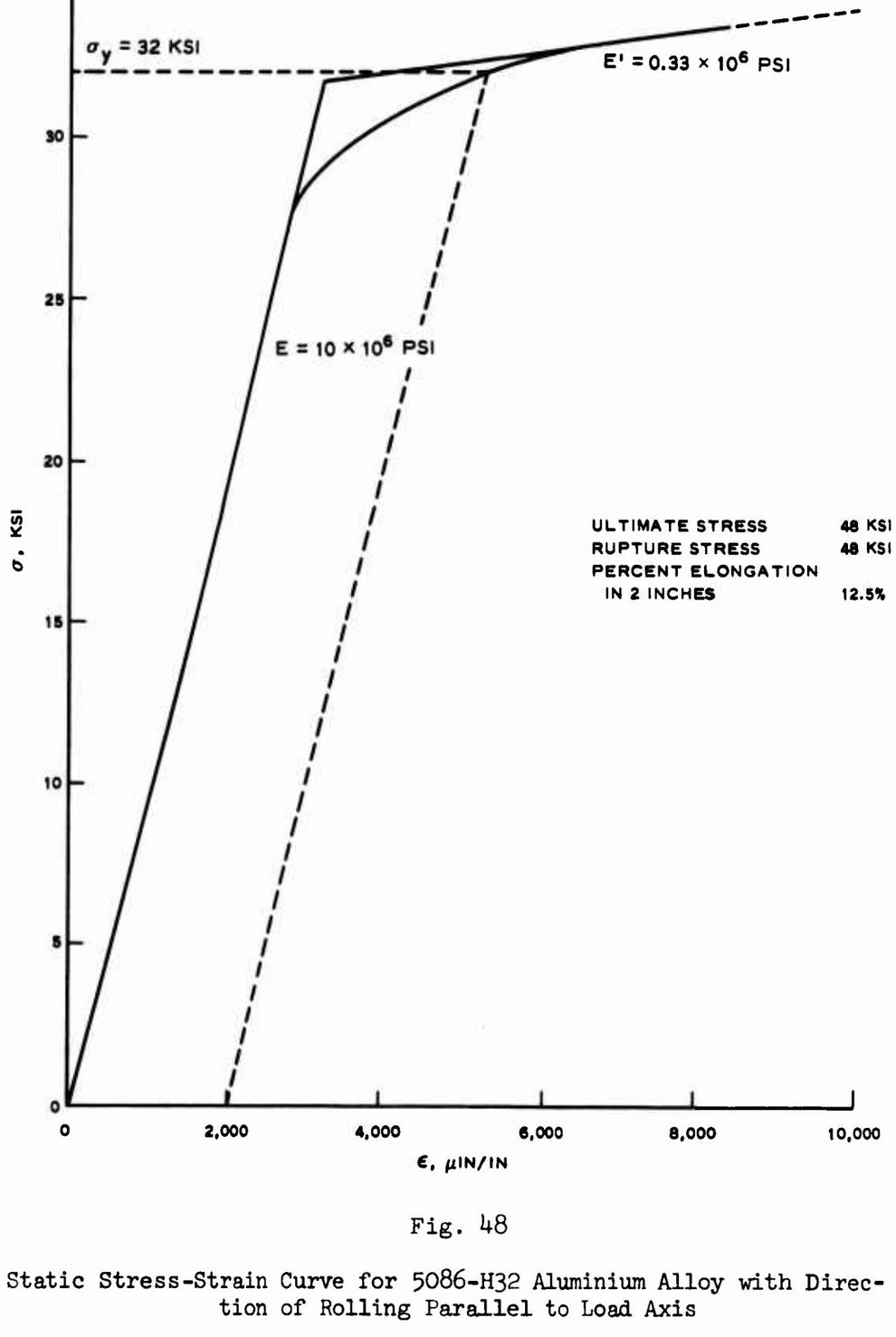

Fig. 48

Static Stress-Strain Curve for 5086-H32 Aluminium Alloy with Direction of Rolling Parallel to Load Axis

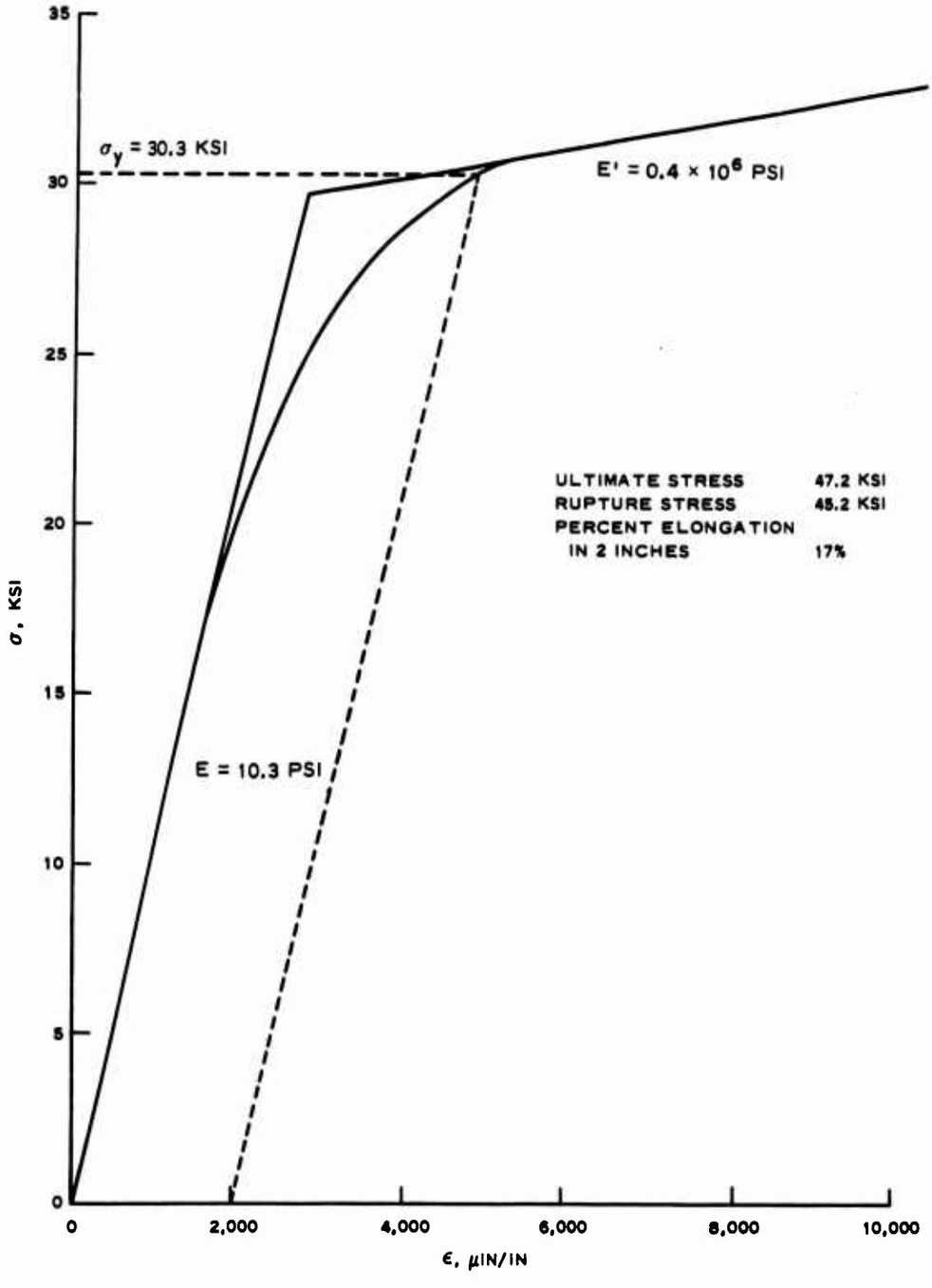

Fig. 49

Static Stress-Strain Curve for 5086-H32 Aluminium Alloy with Direction of Rolling Perpendicular to Load Axis

APPENDIX B

SELECTED OSCILLOGRAPH RECORDS

Tracings and photographic reproductions of records are presented herein. Calibration factors are noted in the labels on the left side for each trace in terms of inches of record deflection at full scale, and a graphic scale is included for each trace.

The alphabetic notations SS, S, PS, PB and W_o refer to records from soil-stress gages, strain gages, surface pressure gages, bonnet pressure gages, and deflection gages, respectively. The number preceding the alphabetic notation indicates arch diameter, and the numerical or alphabetical designations following indicate their locations on the structure or in the free field.

Figures 50 through 61 are tracings of the records for the first three tests on the 4-, 8-, 12- and 36-inch-diameter arches. The traces show the soil stress data on either side of each arch at its crown level, strain values on the inside and outside surfaces of the arches, and surface and bonnet pressures. The time base is shown by a 1000-cps trace and by timing lines 10 msec apart. The detonation of the explosive is shown by the zero-time trace. Figure 62 shows condensed-time surface pressures and Figures 63 through 65 show expanded-time crown accelerations traced from magnetic tape playbacks.

Figures 66 through 77 are photographic reproductions of the

oscillograph records for the next three shots on the 4-, 8-, 12-, and 36-inch-diameter arches. The traces show the soil stresses at the crown level of each arch, strain values on the inside and outside surfaces at the crown and at 5 degrees from the springing line of the arch, crown displacement relative to the floor, and the pressures at the sand surface and in the bonnet. The time base is shown by a 1000-cps trace and by timing lines 10 msec apart. The detonation of the explosive is shown by the discontinuity in the zero-time trace. For the first shot in this series the zero-time trace malfunctioned. Figure 78 shows condensed-time surface pressures traced from magnetic tape playbacks.

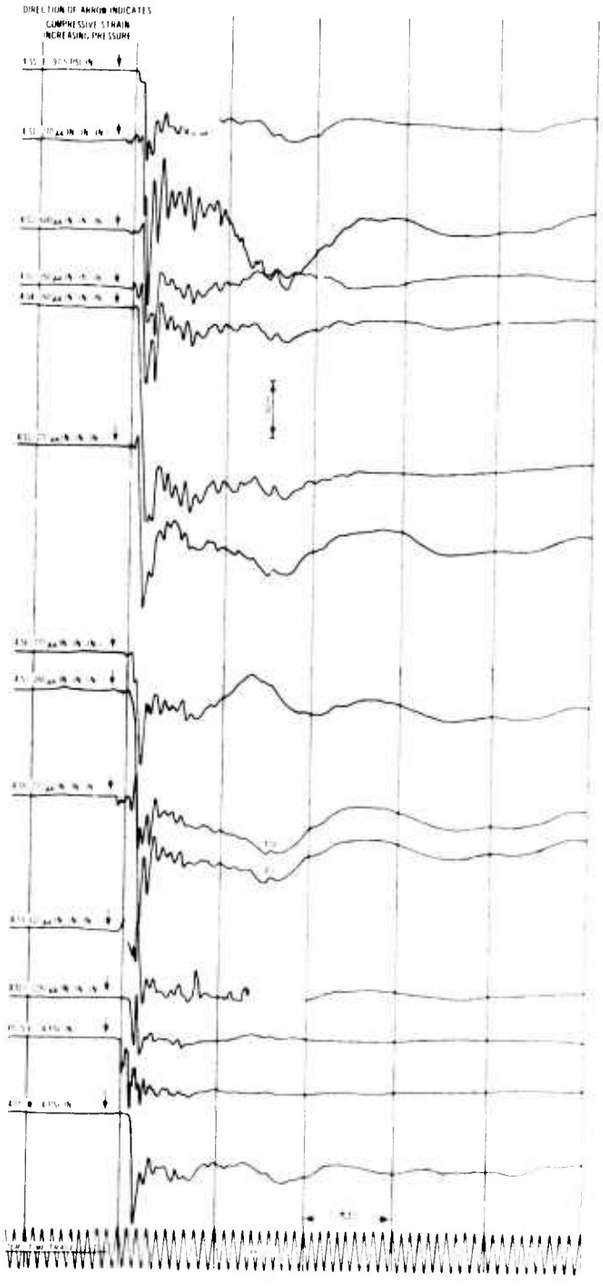

Fig. 50

Tracing from Recorder 1, Test 1

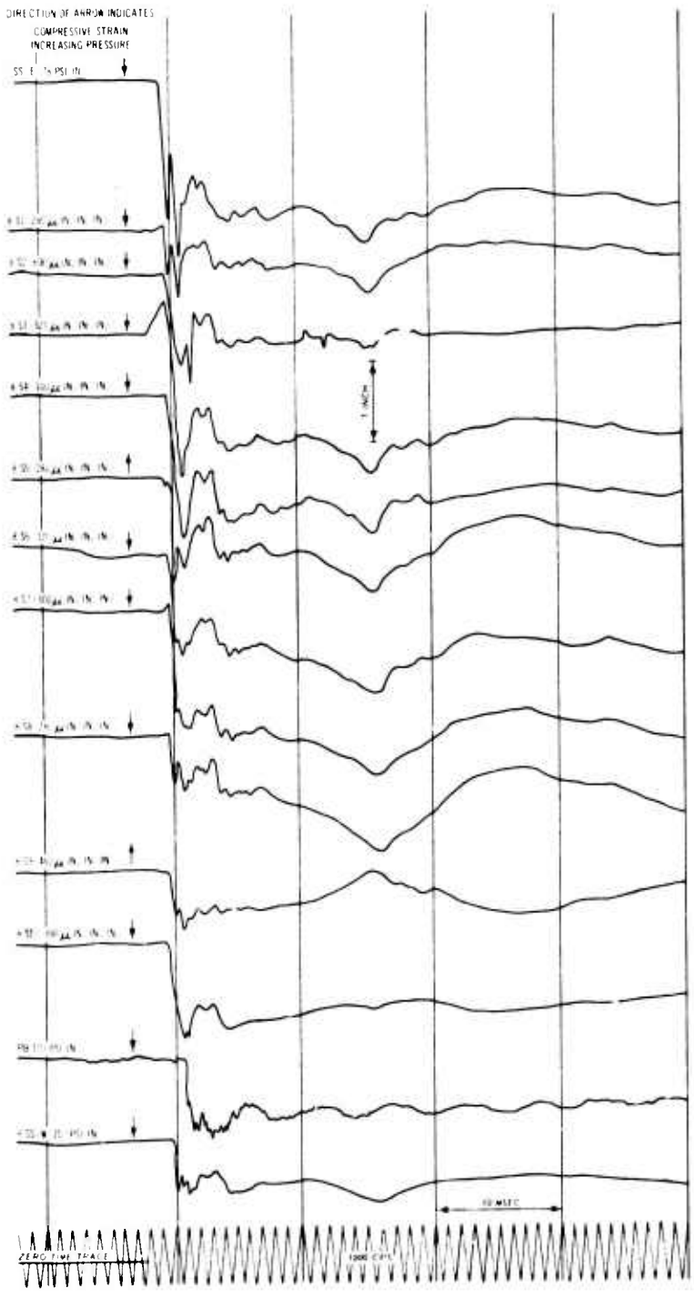

Fig. 51

Tracing from Recorder 2, Test 1

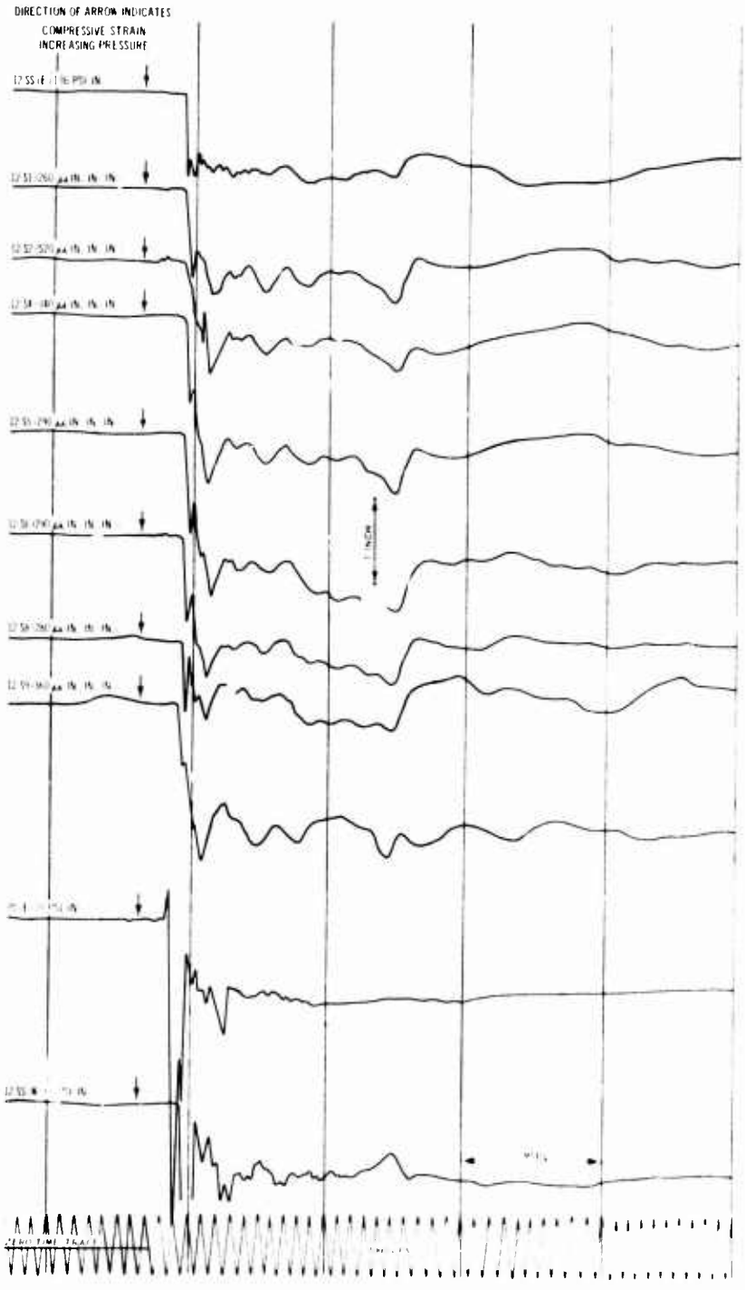

Fig. 52

Tracing from Recorder 3, Test 1

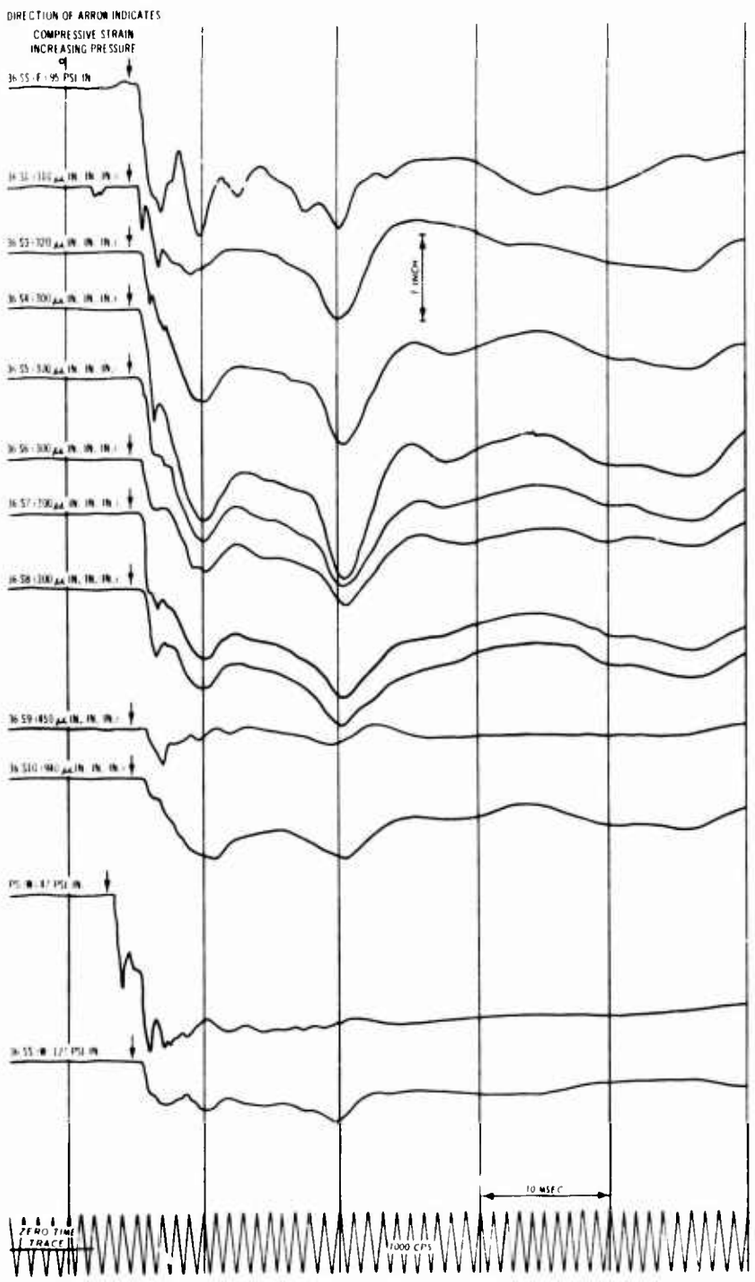

Fig. 53

Tracing from Recorder 4, Test 1

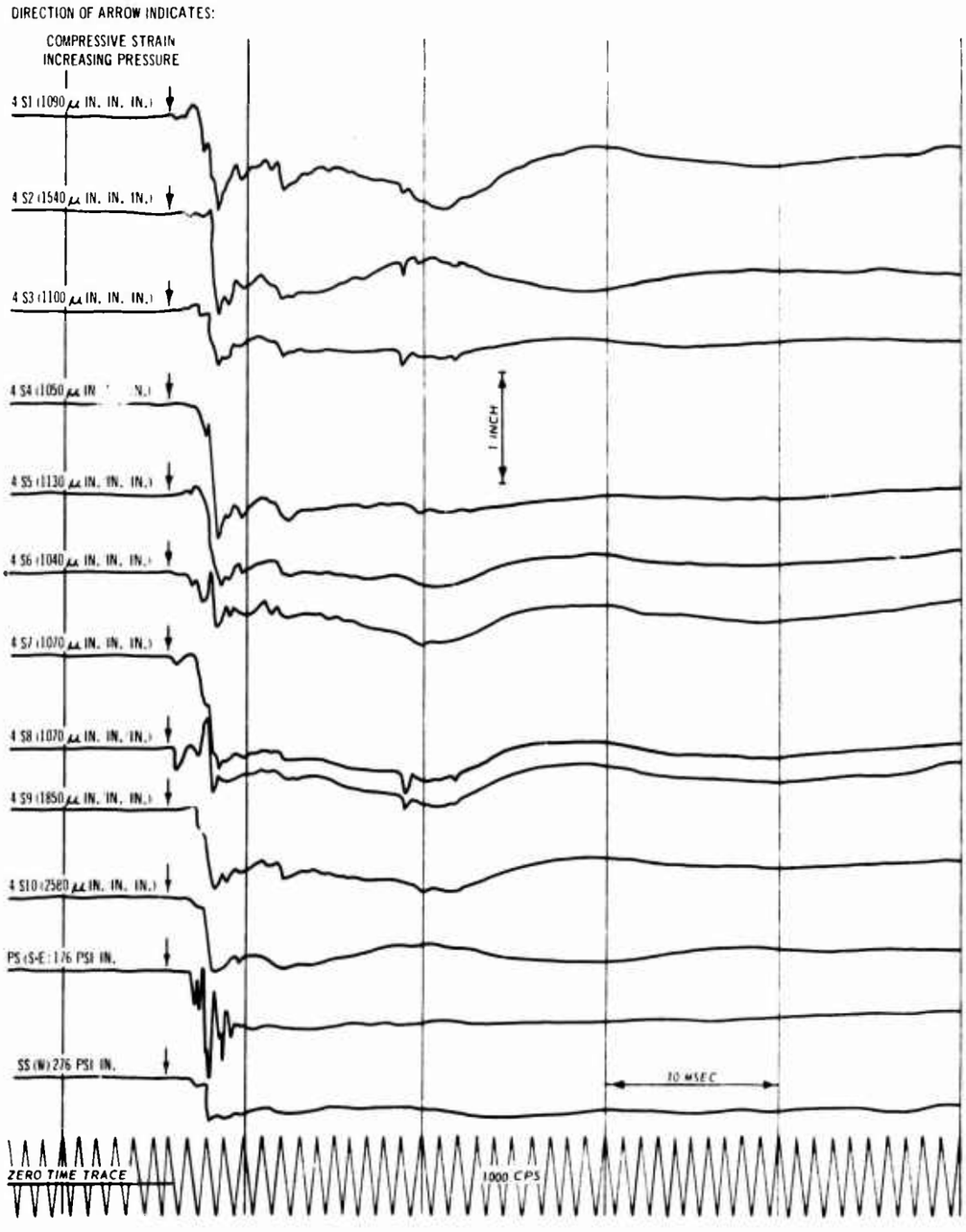

Fig. 54

Tracing from Recorder 1, Test 2

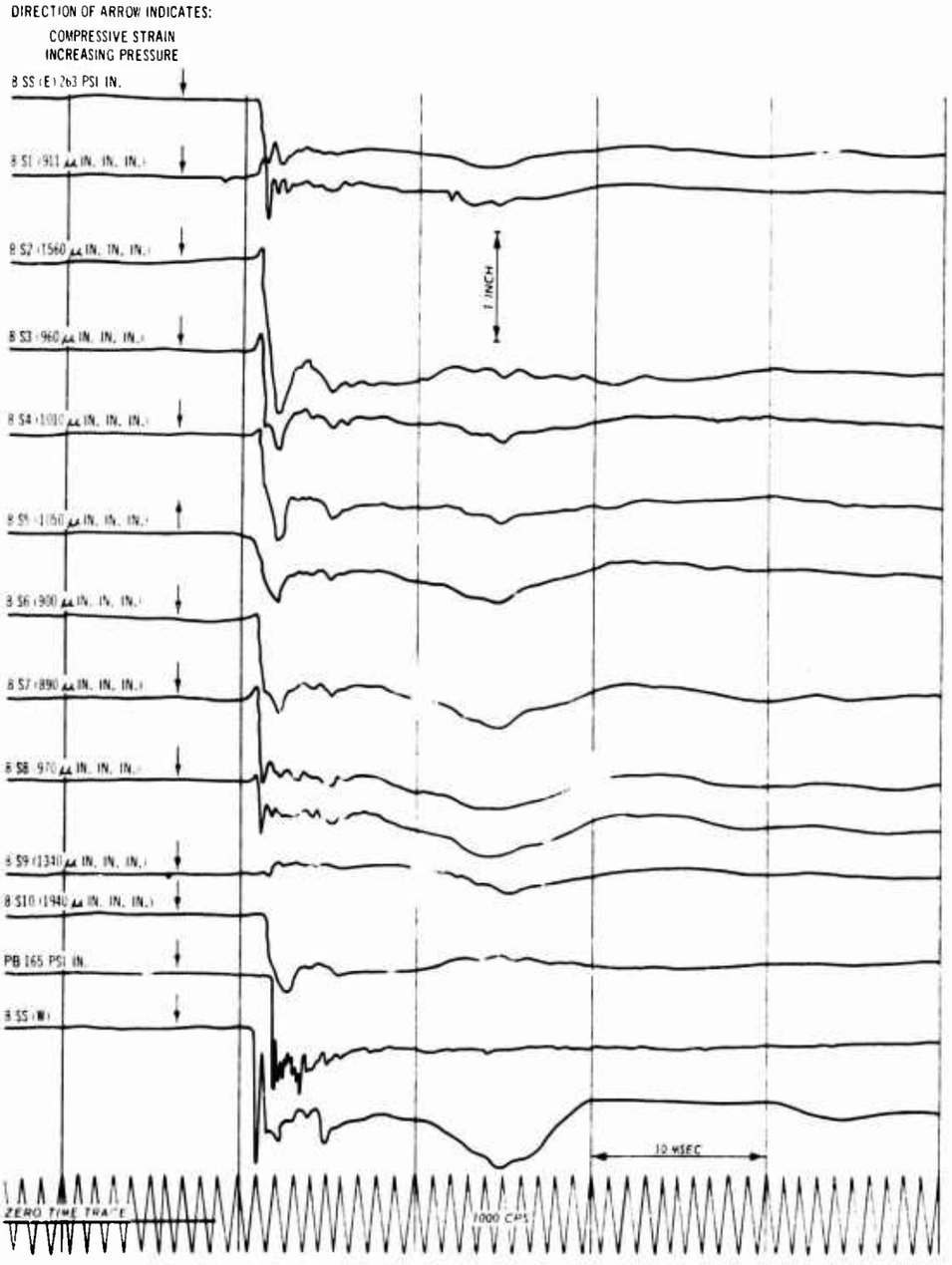

Fig. 55

Tracing from Recorder 2, Test 2

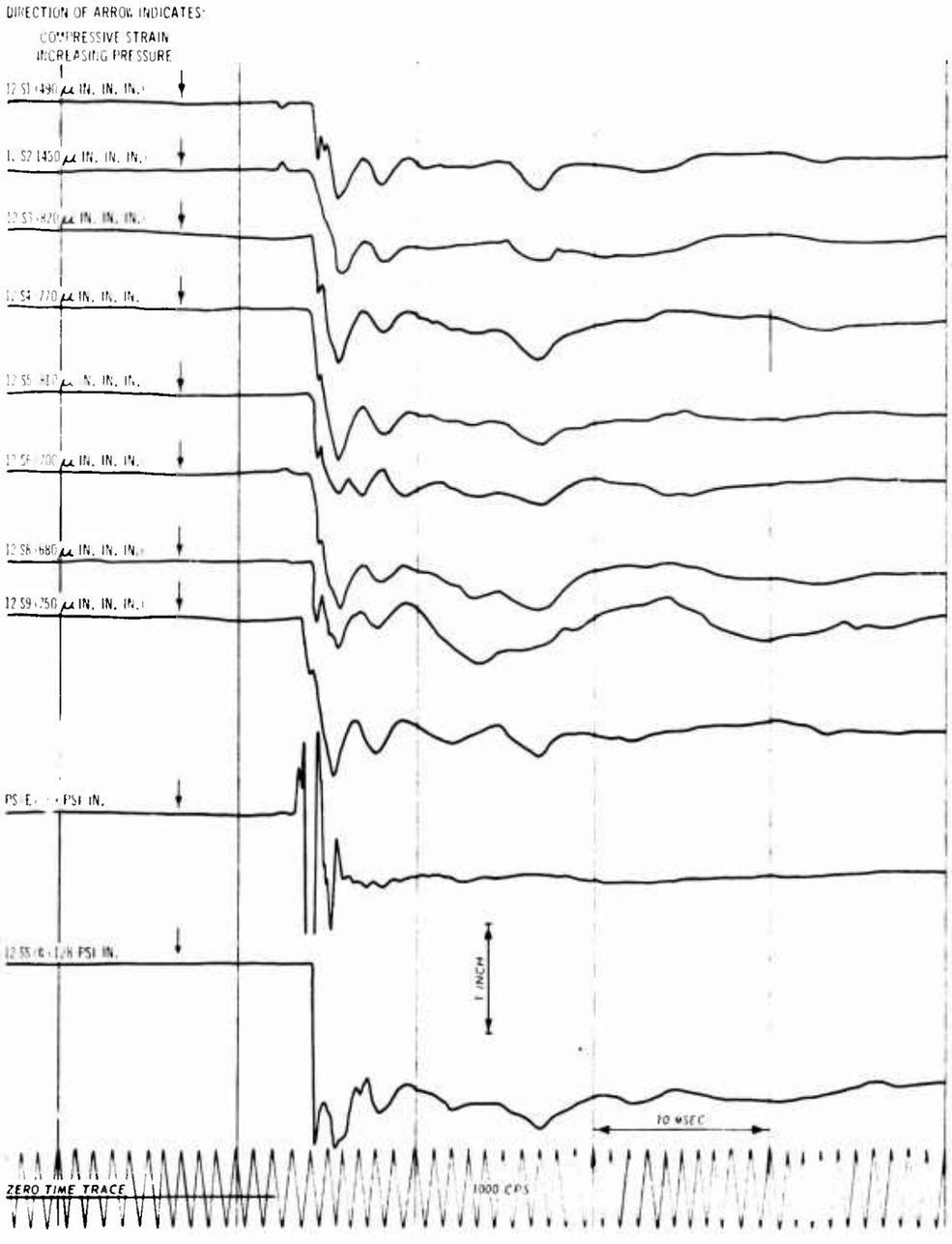

Fig. 56

Tracing from Recorder 3, Test 2

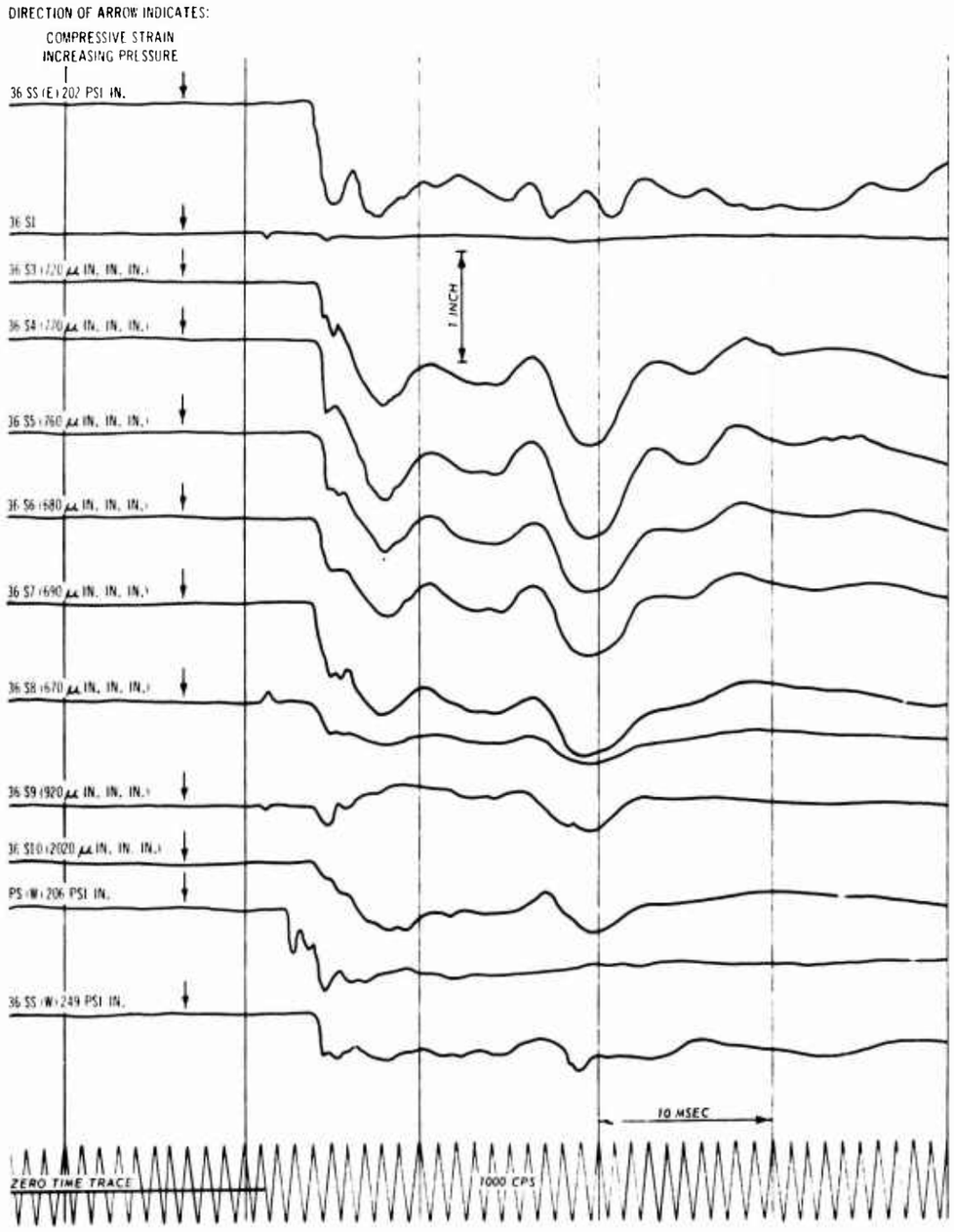

Fig. 57

Tracing from Recorder 4, Test 2

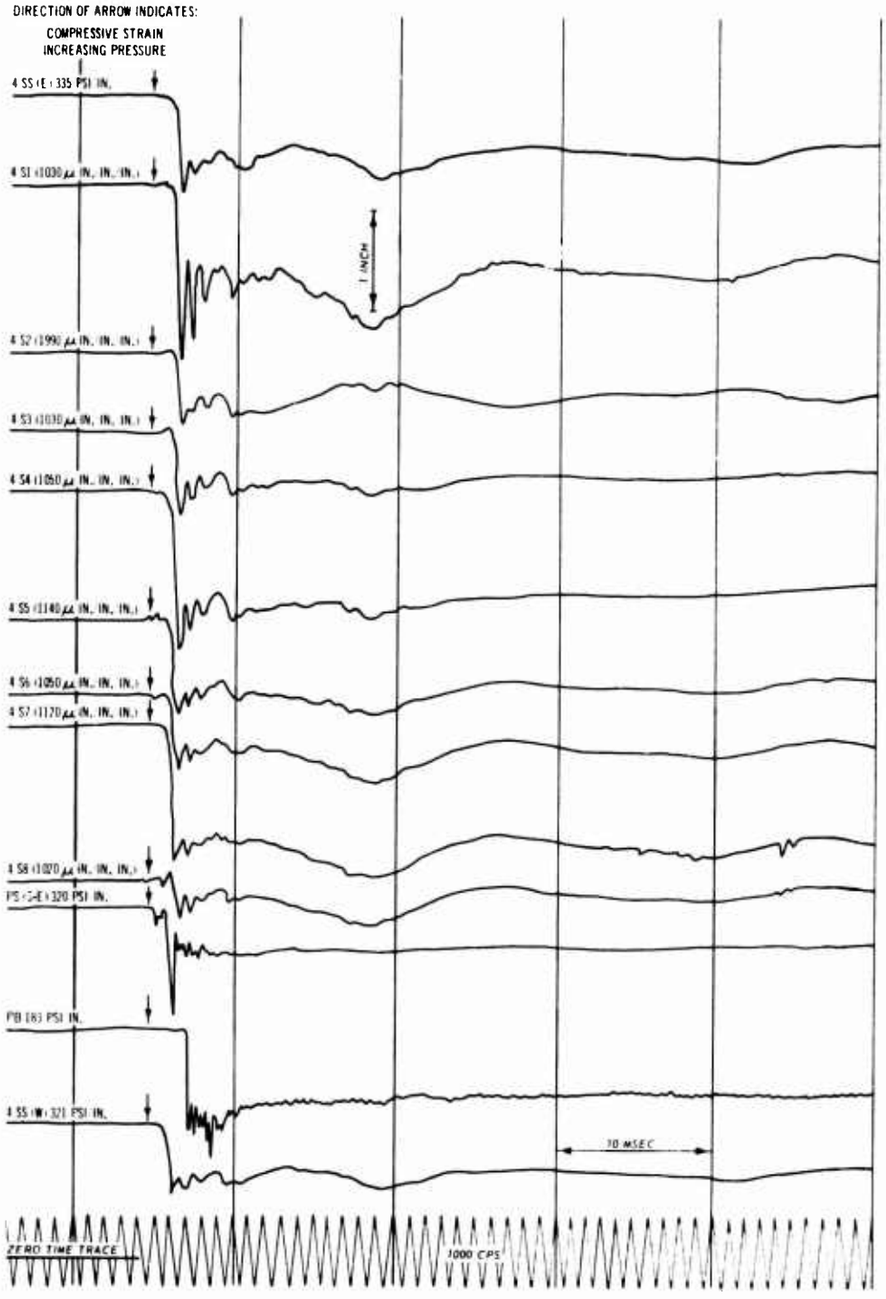

Fig. 58

Tracing from Recorder 1, Test 3

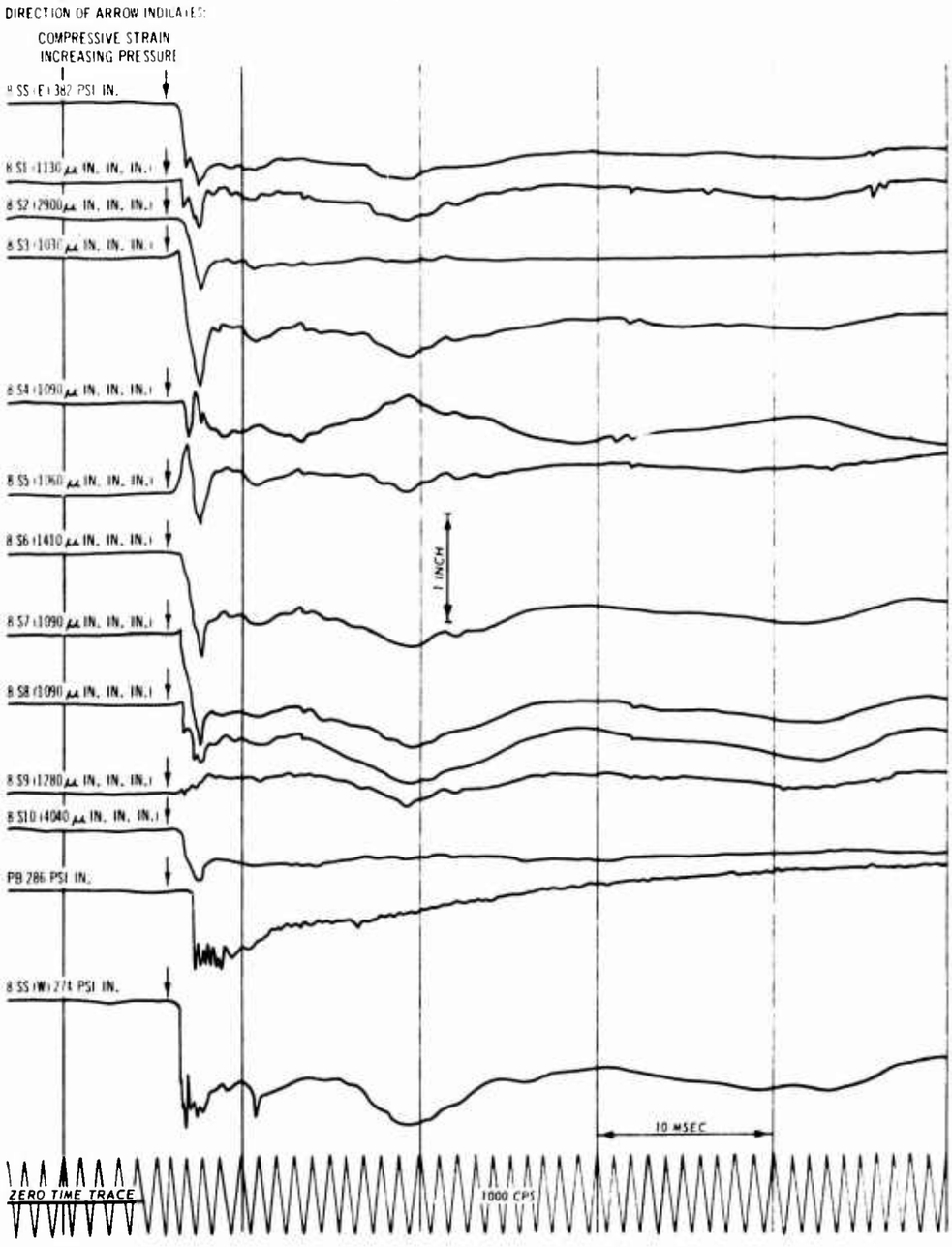

Fig. 59

Tracing from Recorder 2, Test 3

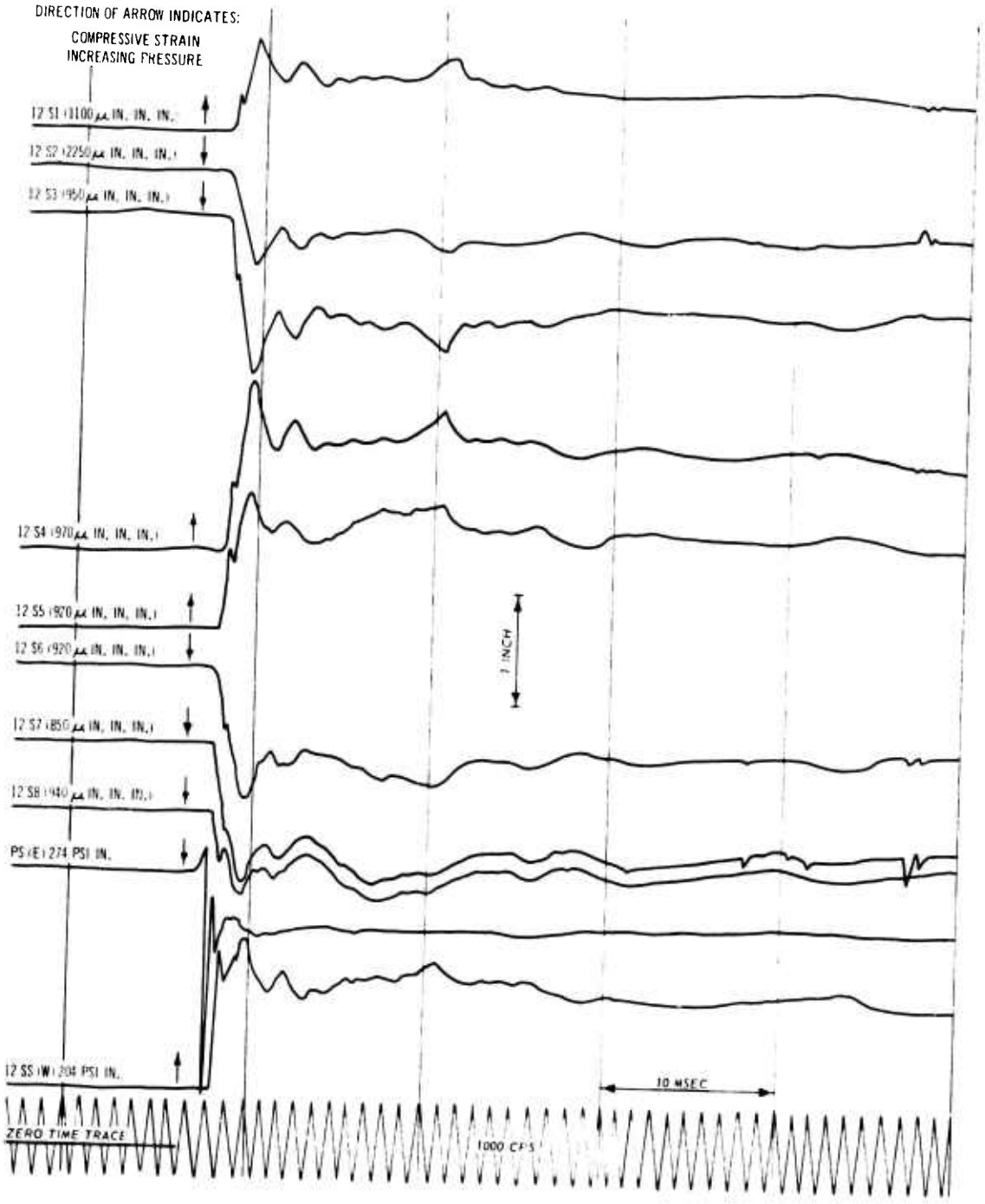

Fig. 60

Tracing from Recorder 3, Test 3

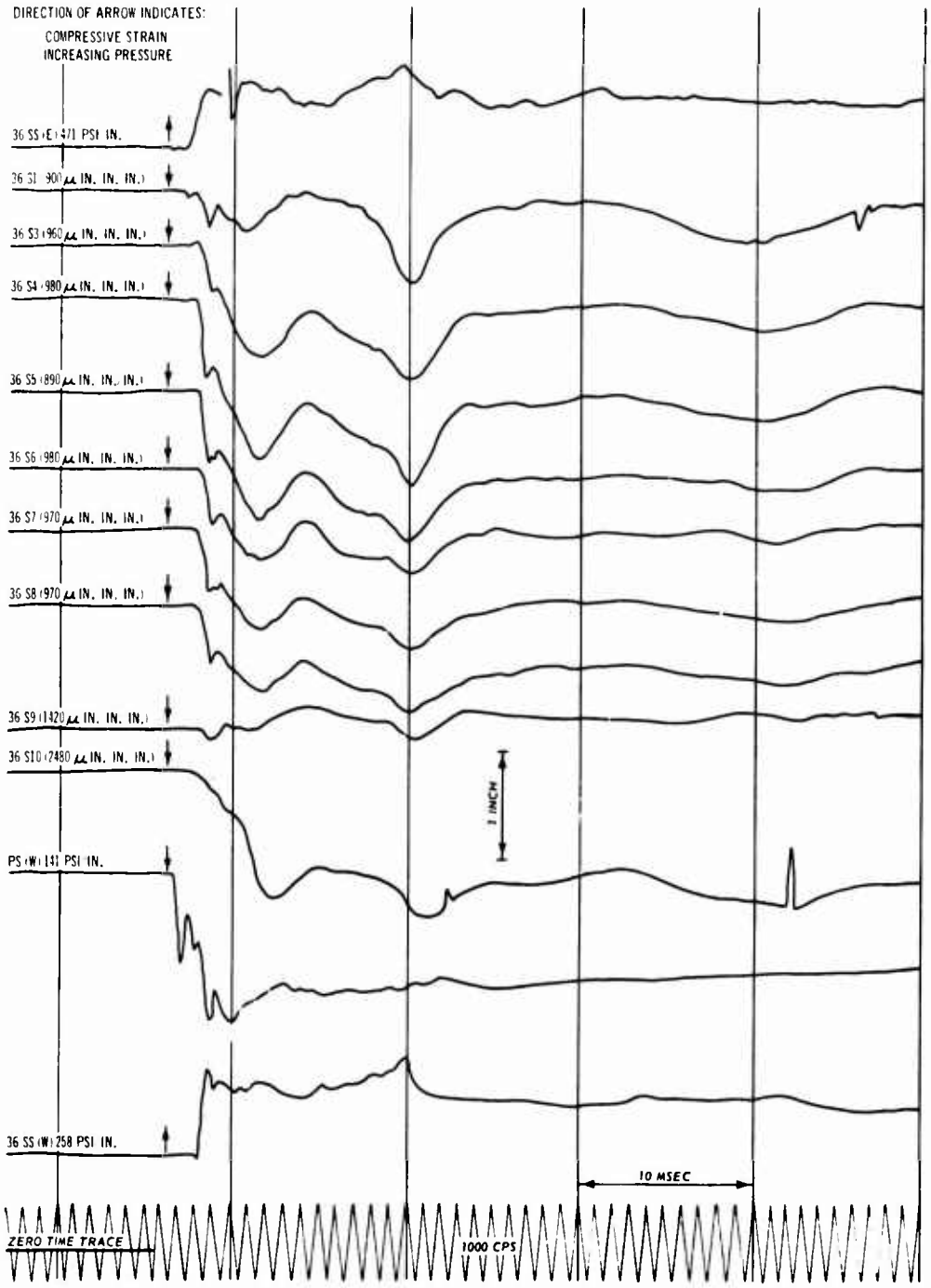

Fig. 61

Tracing from Recorder 4, Test 3

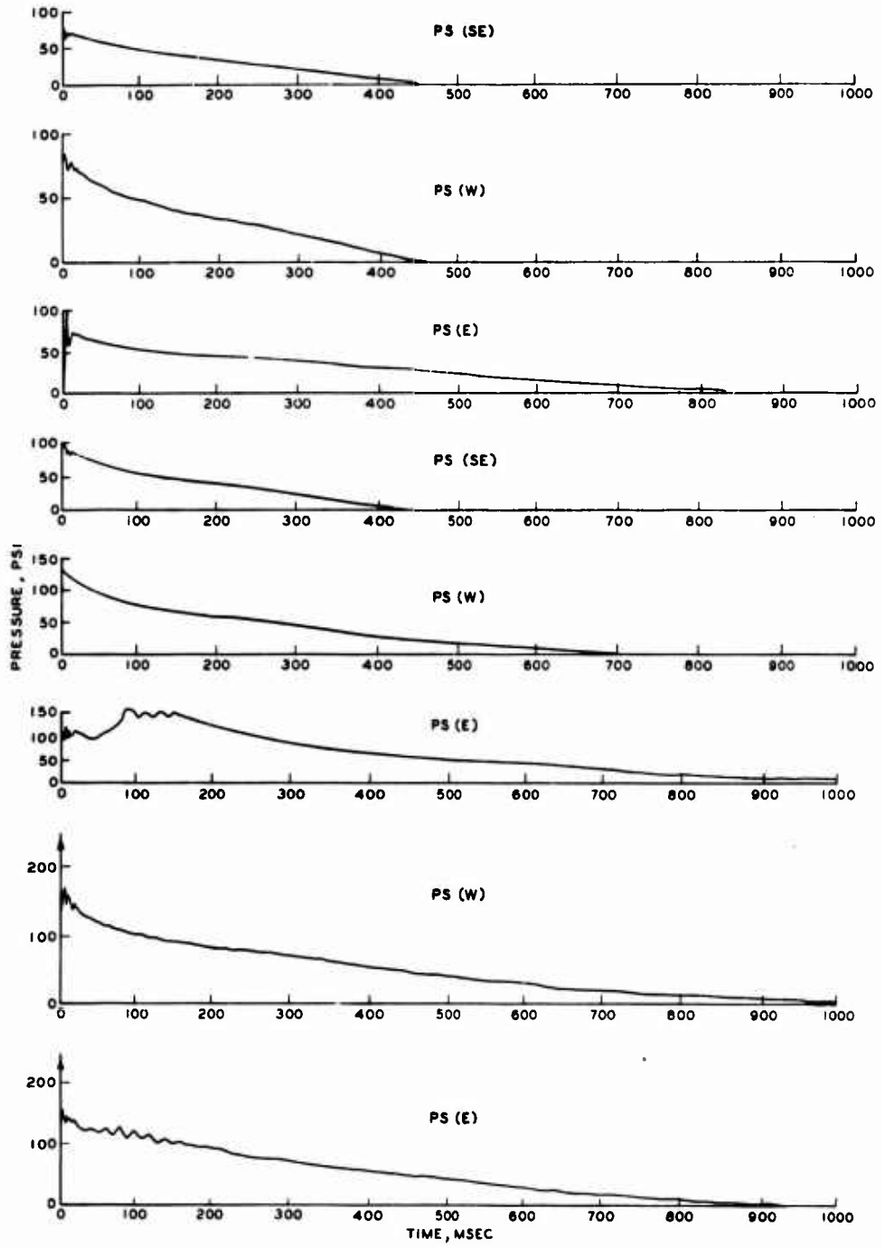

Fig. 62

Condensed-Time Surface Pressure Records for Tests 1, 2, and 3

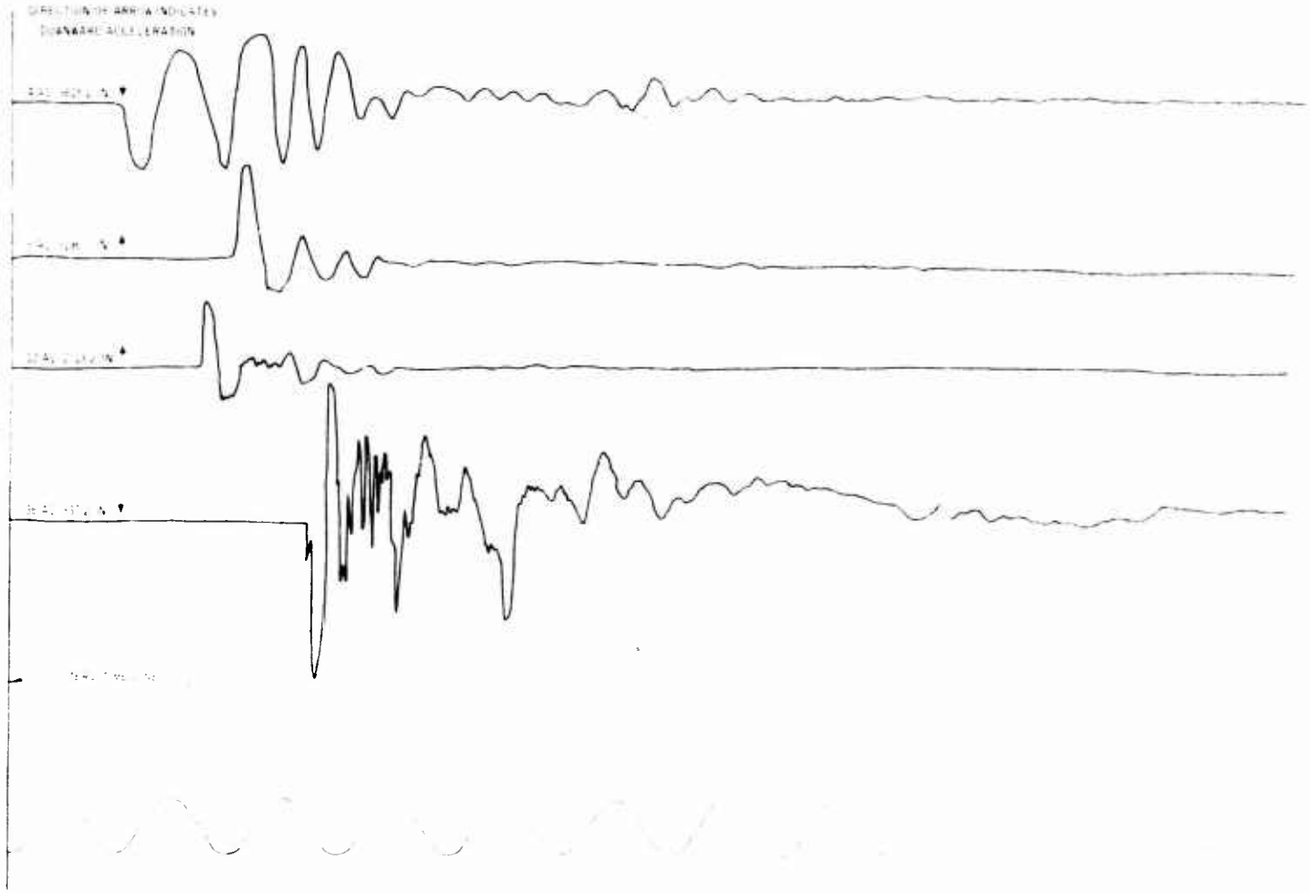

Fig. 63

Expanded-Time Crown Acceleration Records for Test 1

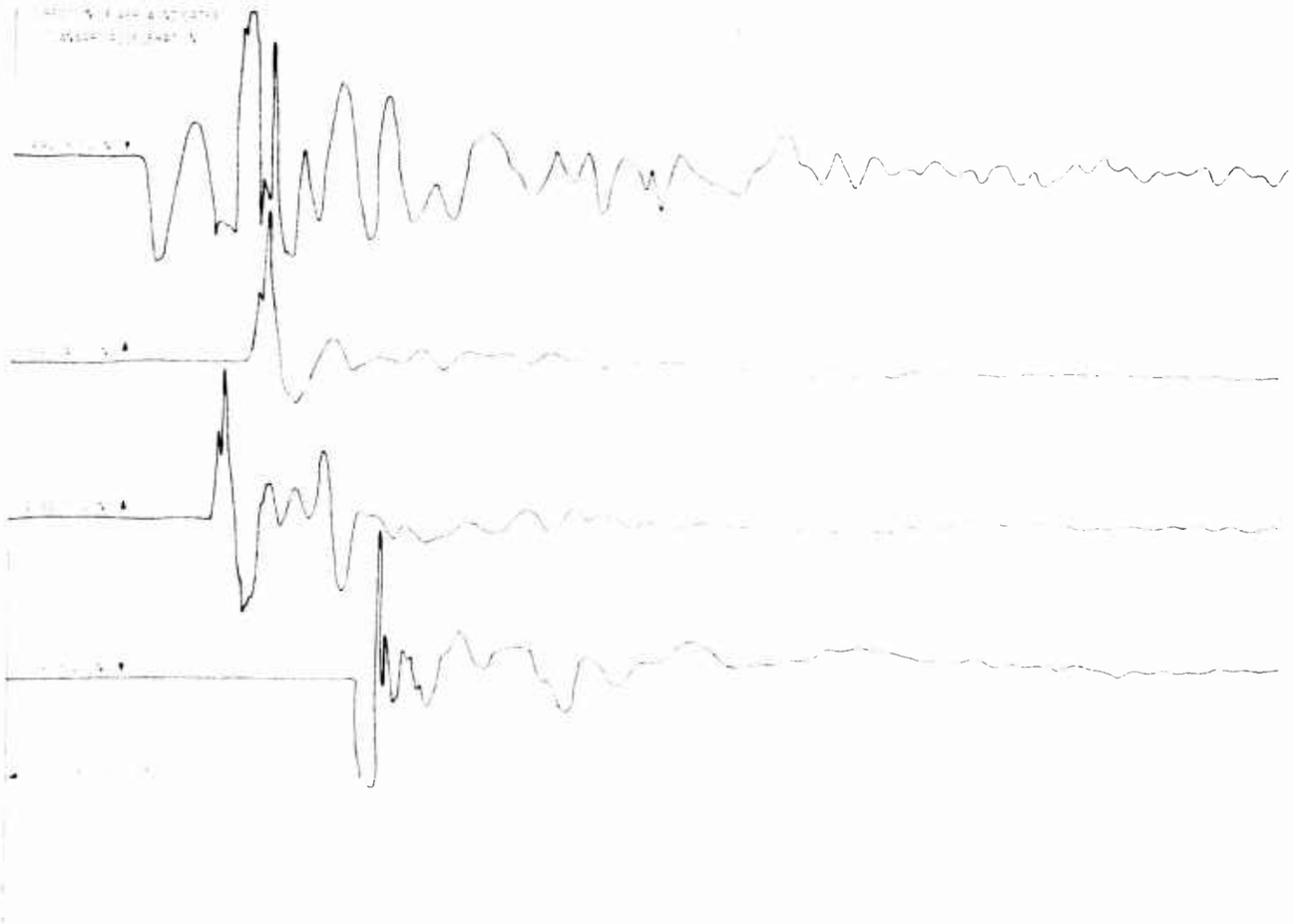

[illegible]

[illegible]- [illegible] Acceleration Records for Test [illegible]

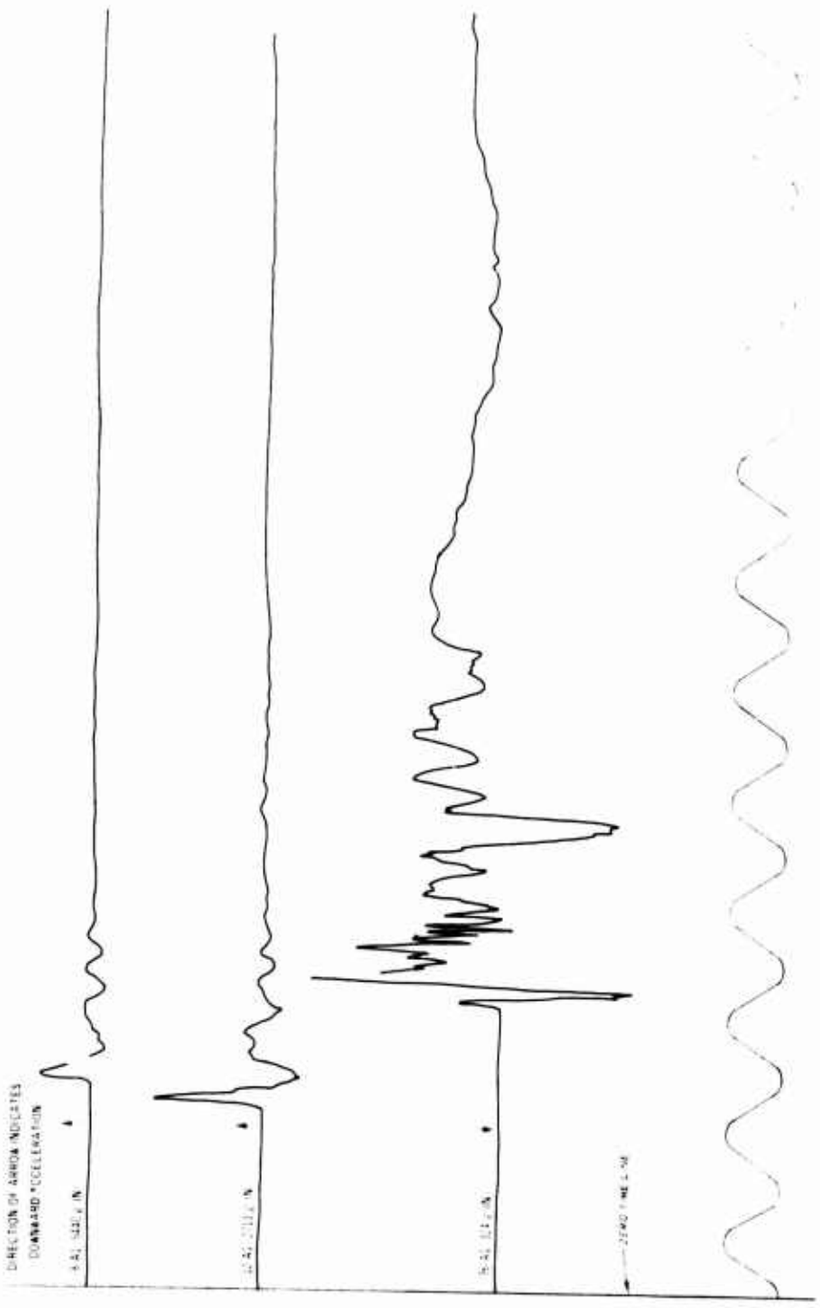

Fig. 65

Expanded-Time Crown Acceleration Records for Test 3

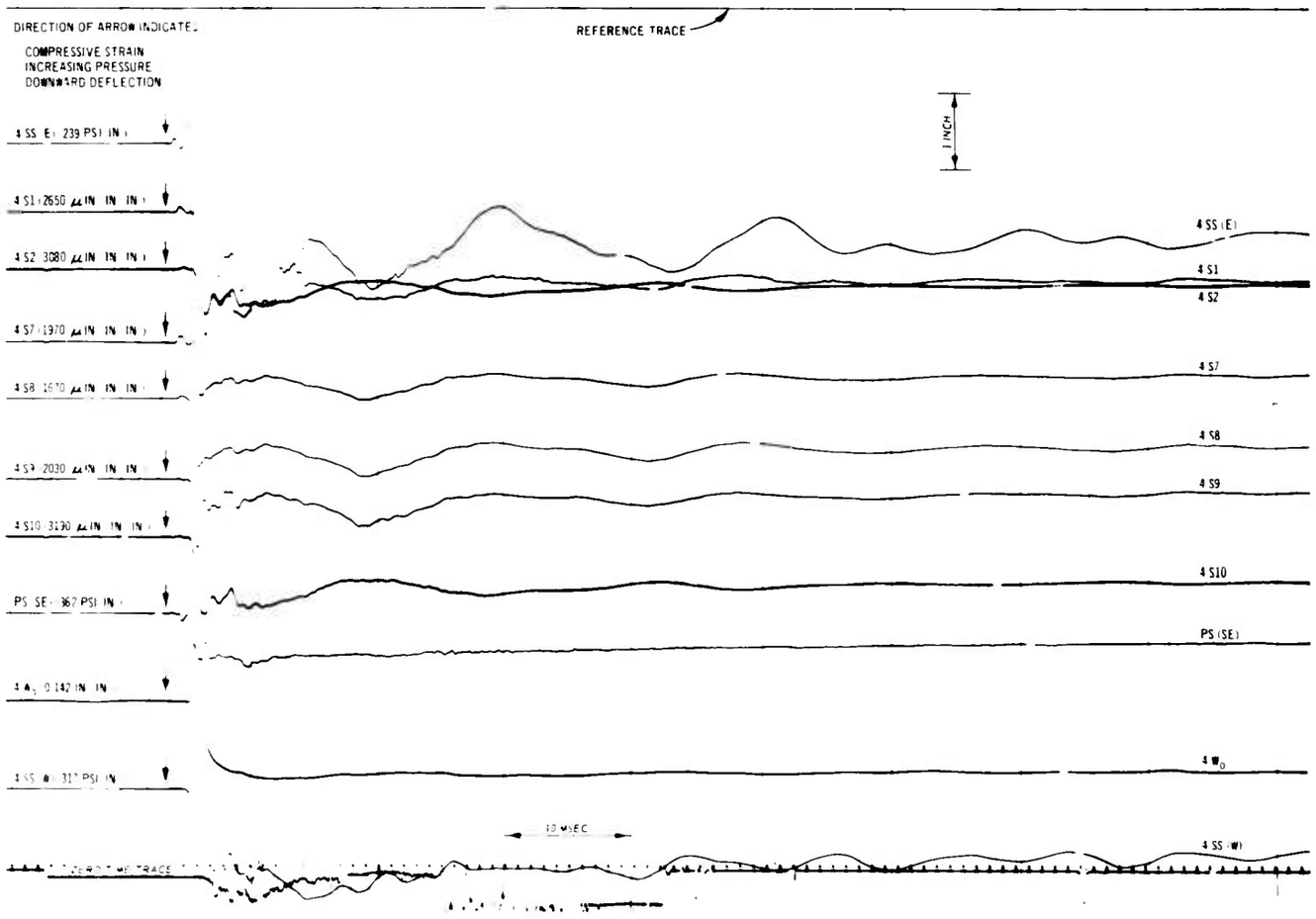

Fig. 66

Record From Oscillograph 1, Test 4

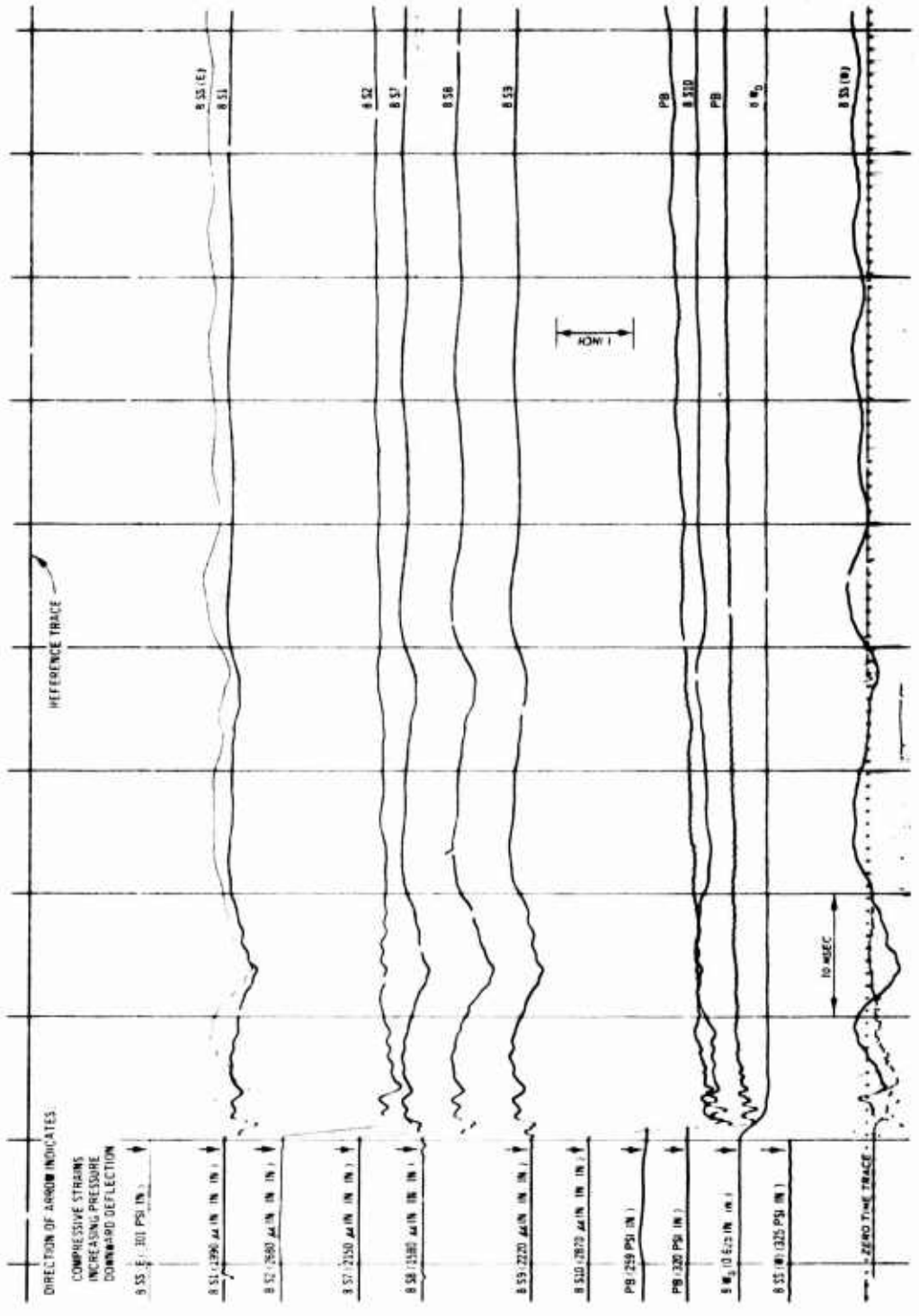

Fig. 67

Record from Oscillograph 2, Test 4

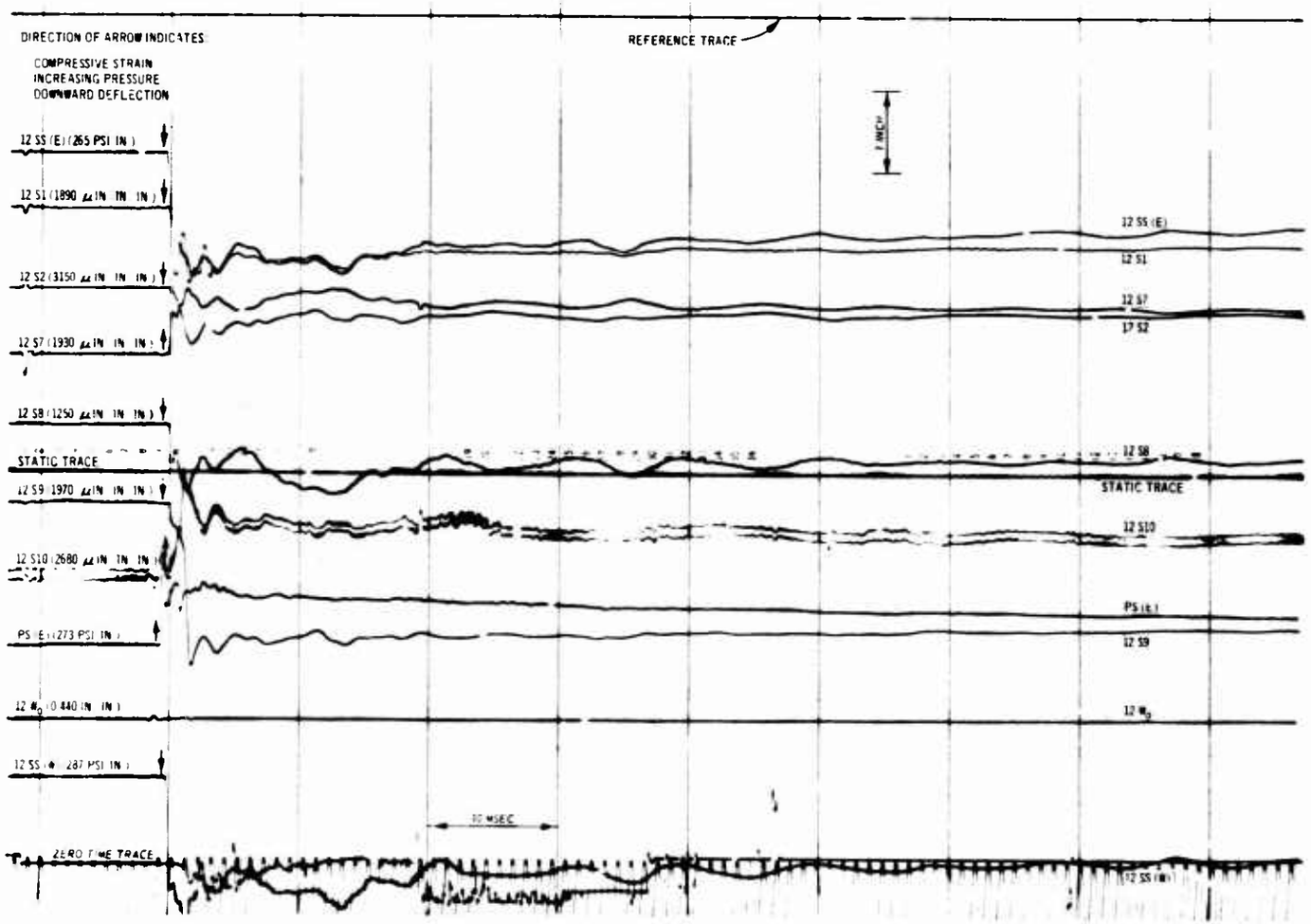

Fig. 68

Record From Oscillograph 3, Test 4

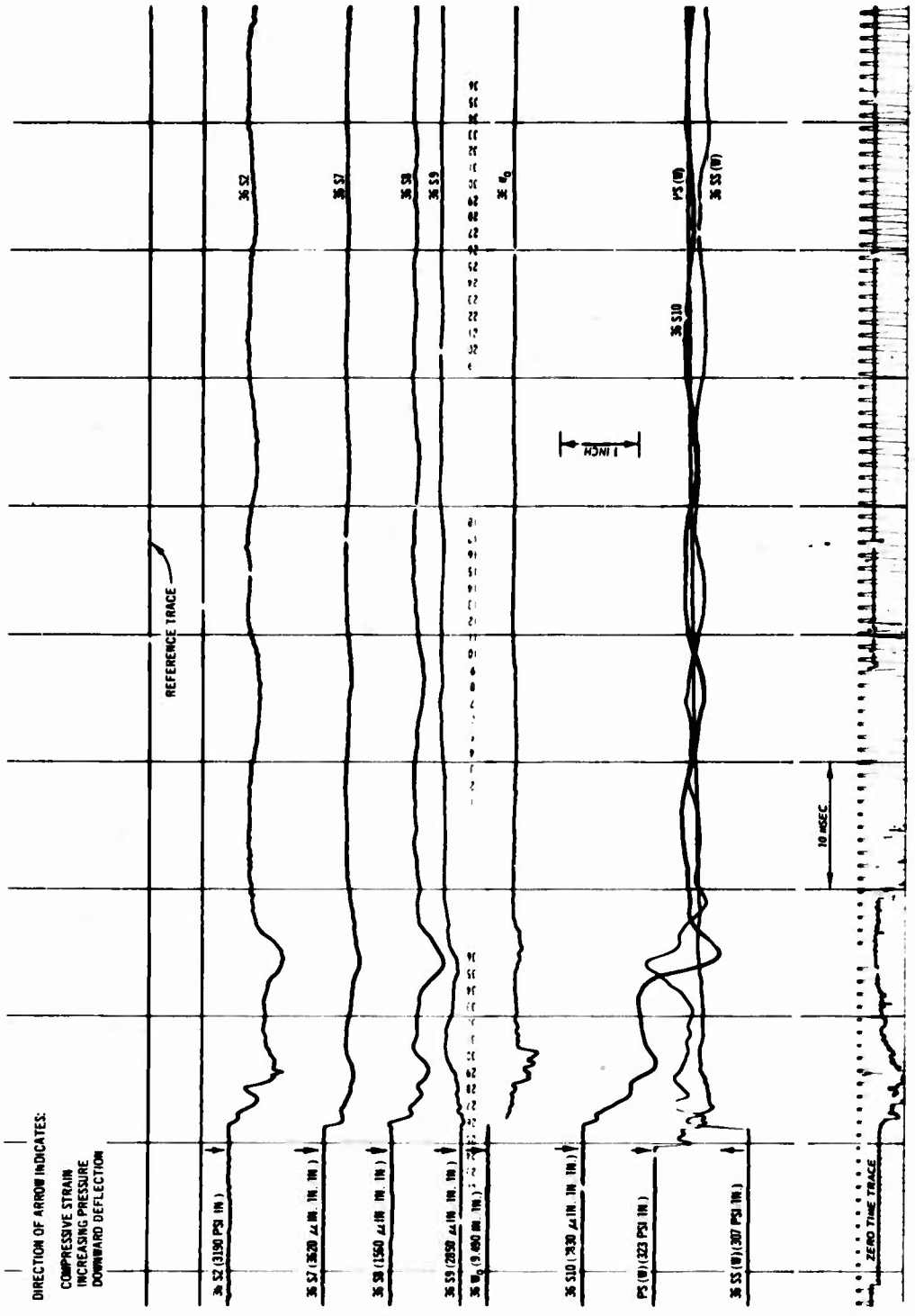

Fig. 69

Record from Oscillograph 4, Test 4

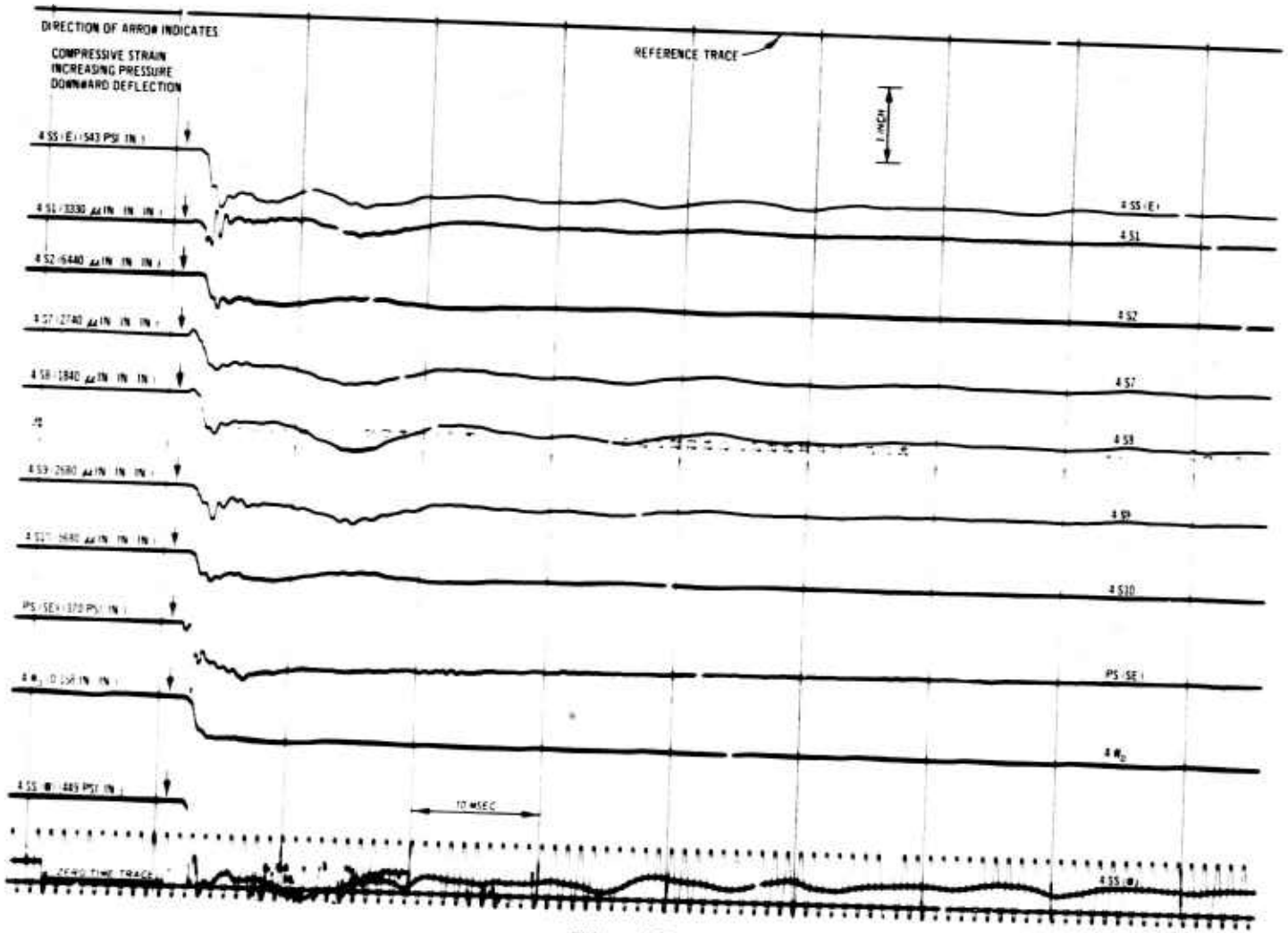

Fig. 70

Record from Oscillograph 1, Test 5

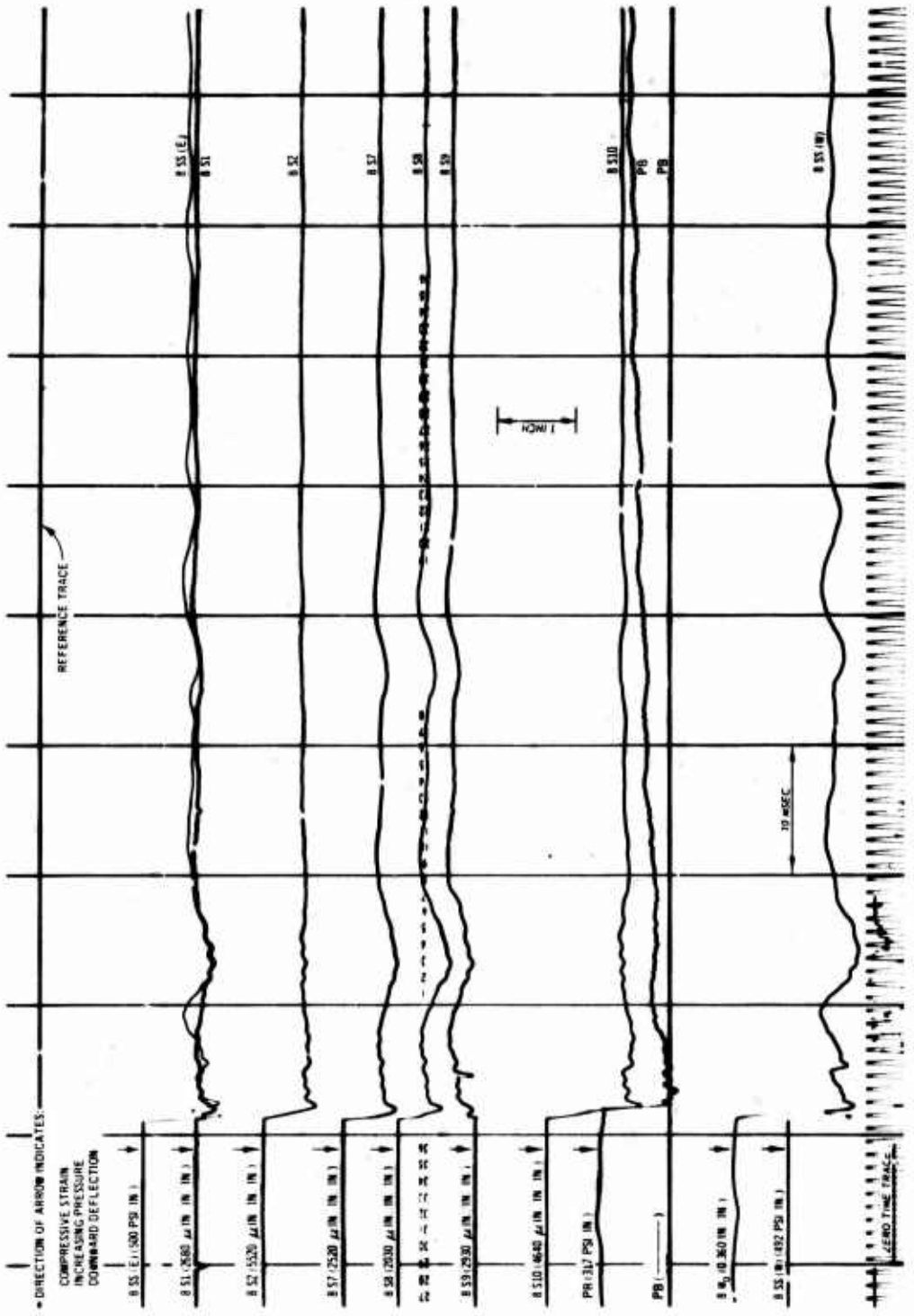

Fig. 71

Record from Oscillograph 2, Test 5

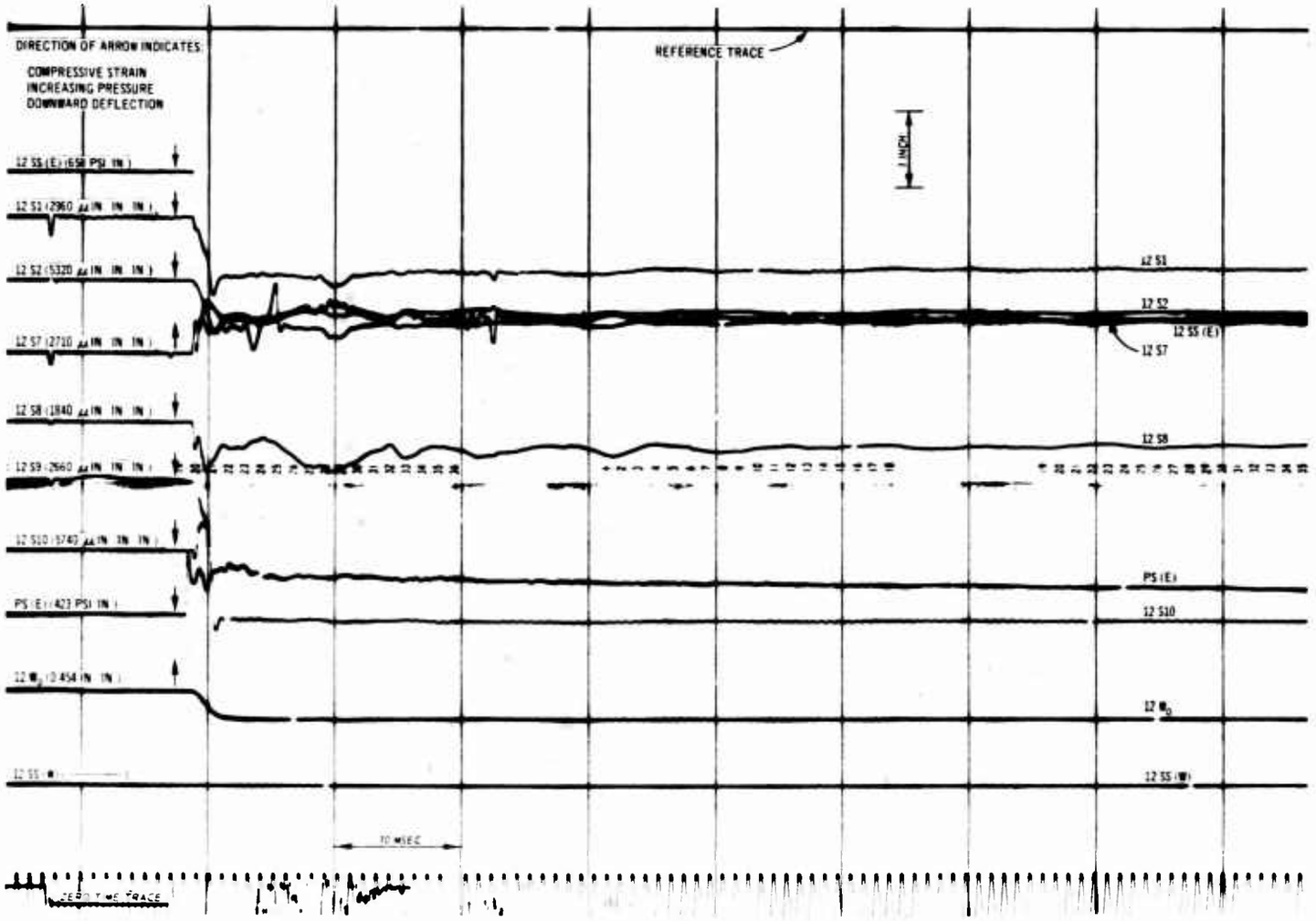

Fig. 72

Record from Oscillograph 3, Test 5

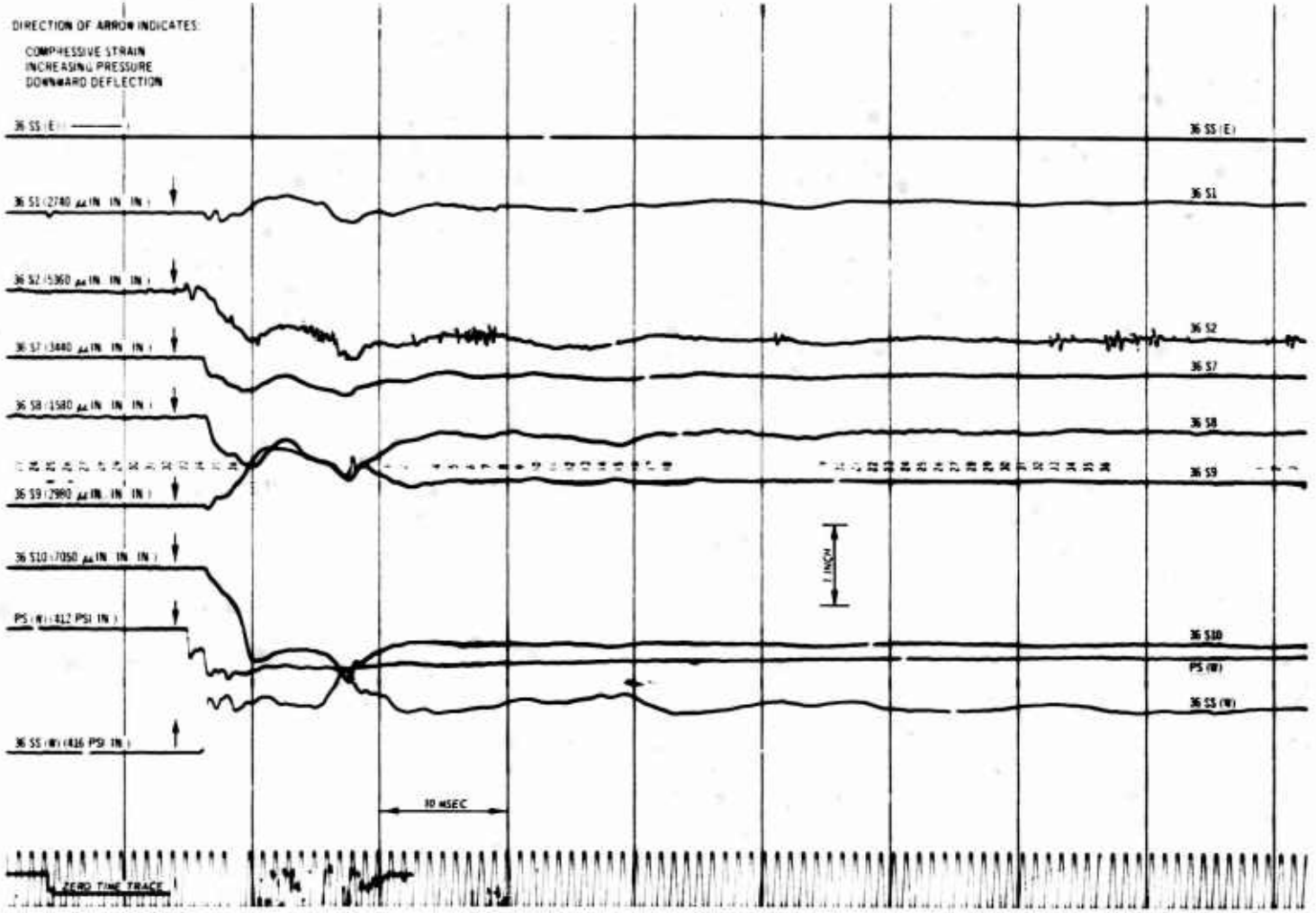

Fig. 73

Record from Oscillograph 4, Test 5

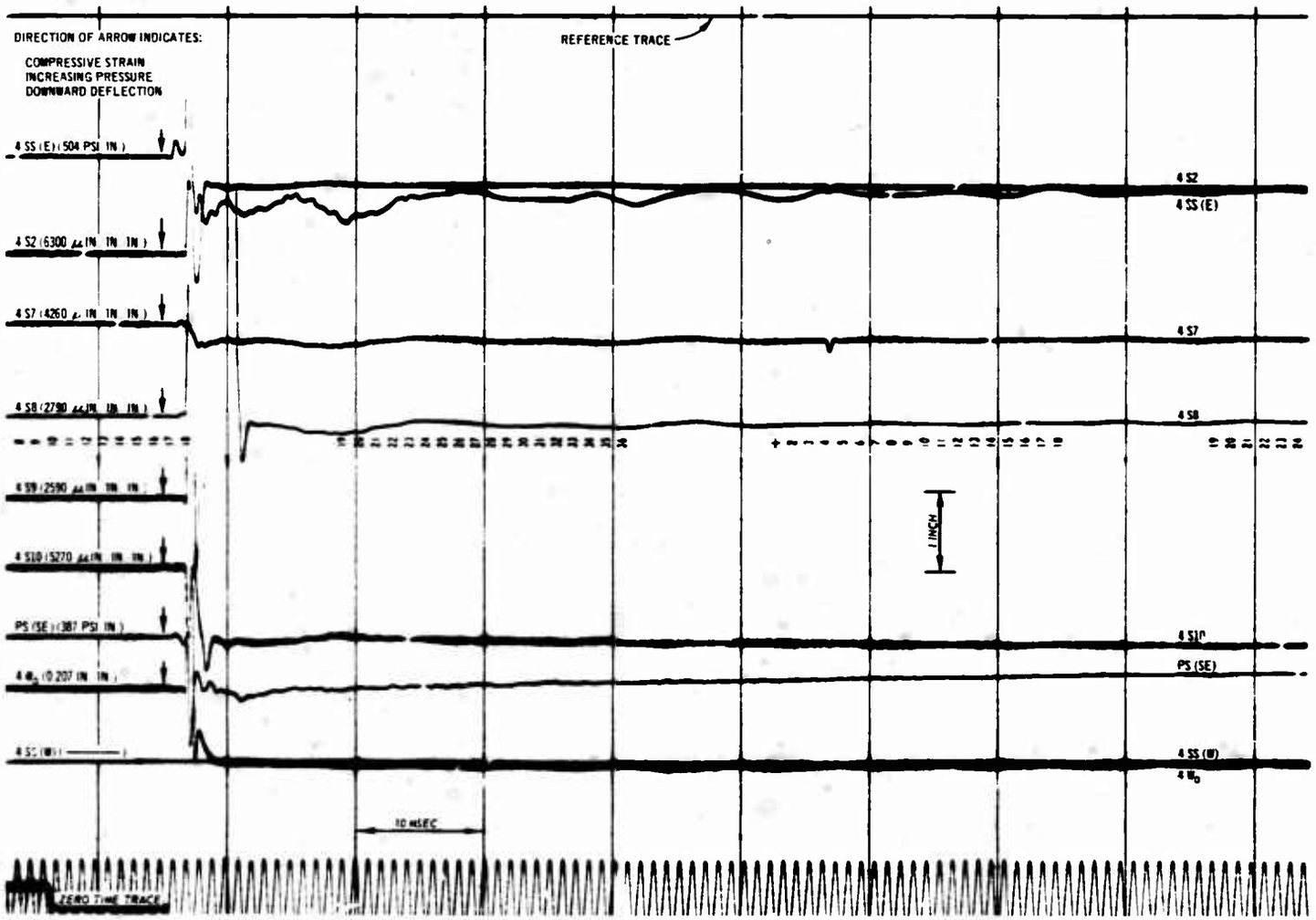

Fig. 74

Record from Oscillograph 1, Test 6

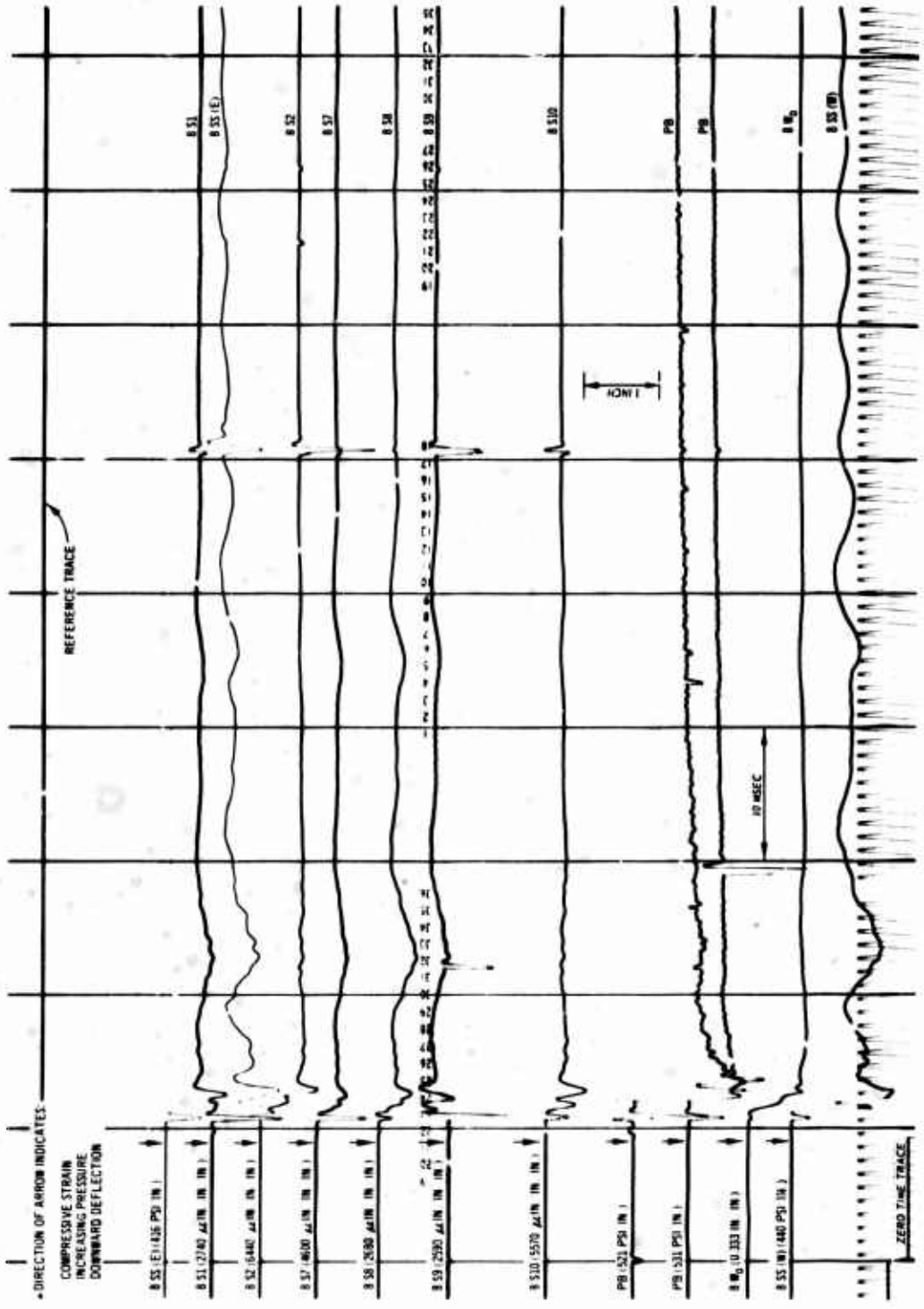

Fig. 75

Record from Oscillograph 2, Test 6

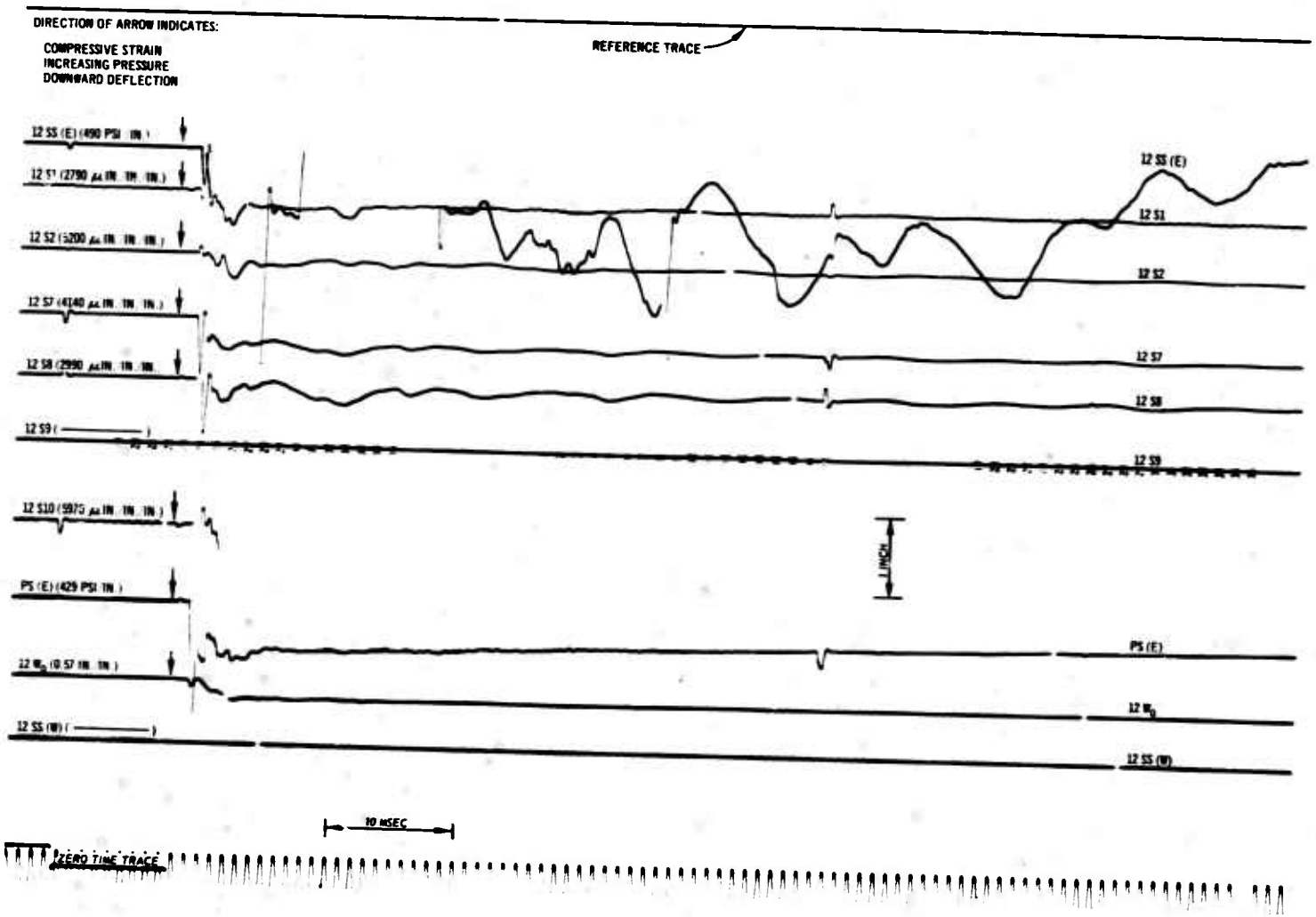

Fig. 76

Record from Oscillograph 3, Test 6

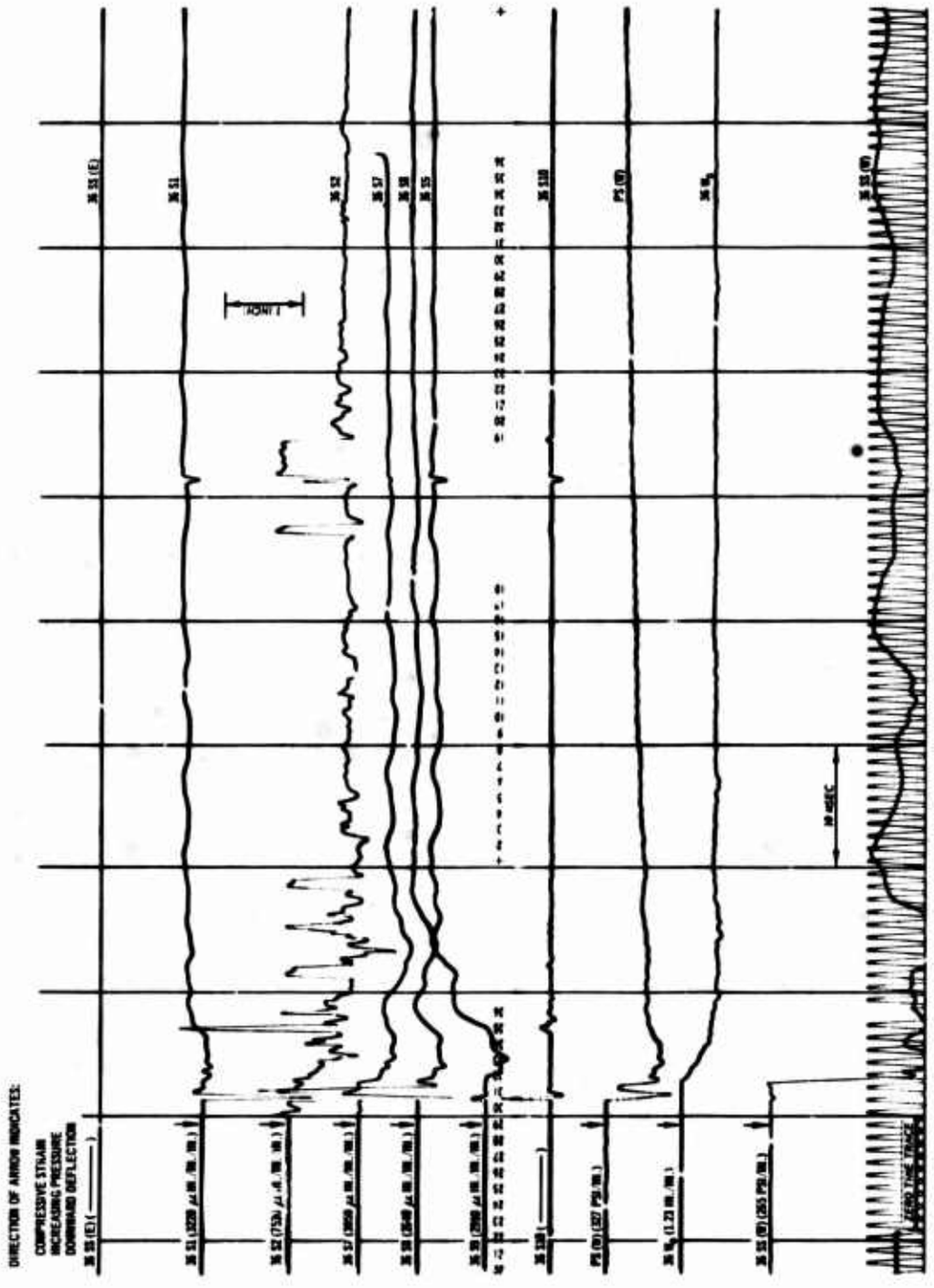

Fig. 77

Record from Oscillograph 4, Test 6

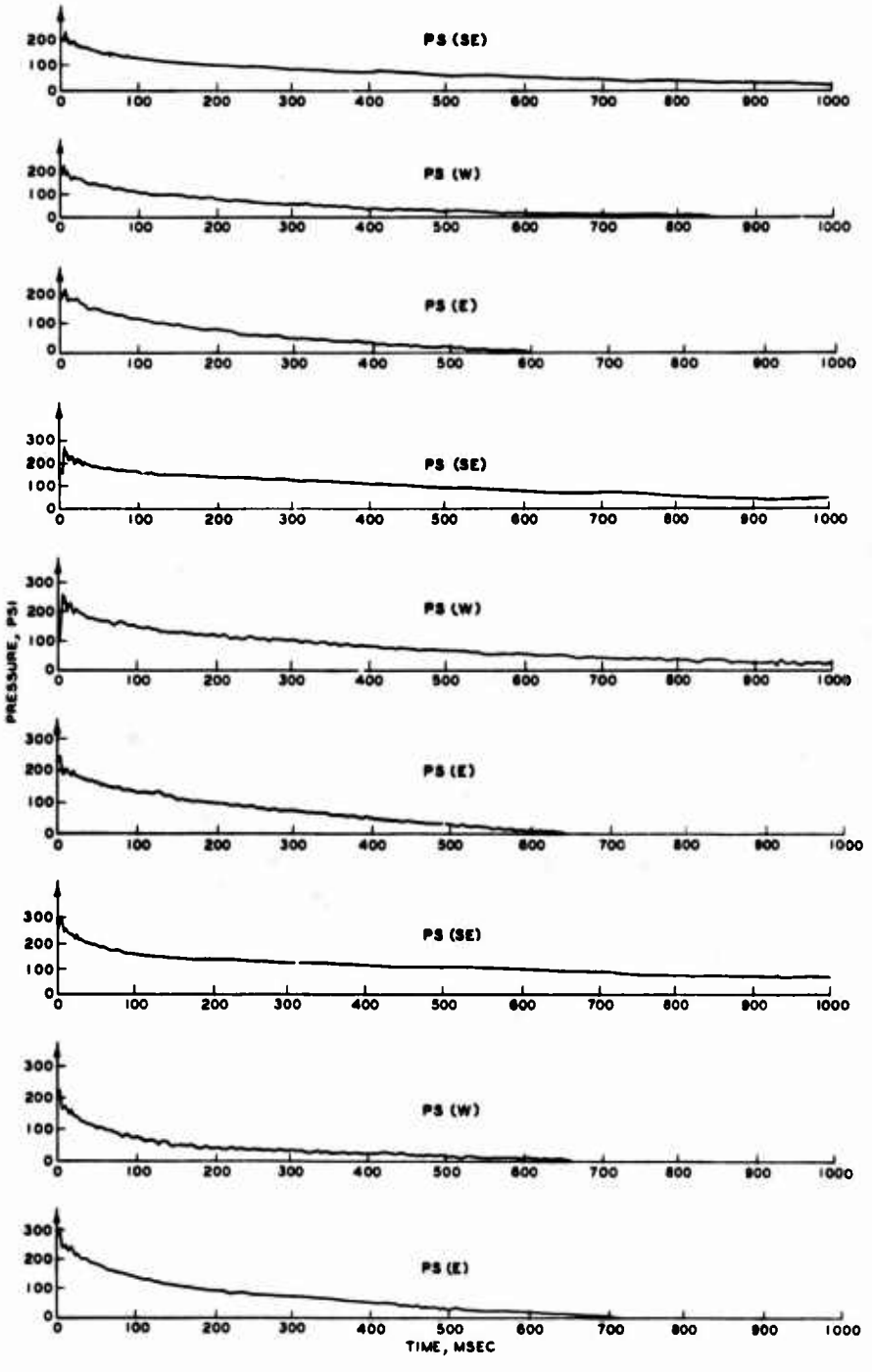

Fig. 78

Condensed-Time Surface Pressure Records
for Tests 4, 5, and 6

BIBLIOGRAPHY

1. Ahlers, E. B. Experimental Methods of Determining the Behavior of Underground Structures Under Dynamic Loads. Chicago: Armor Research Foundation of Illinois Institute of Technology, November 1961.

2. Albritton, G. E. Description, Proof Test, and Evaluation of Blast Load Generator Facility. Technical Report No. 1-707, December 1965. Vicksburg, Miss.: U. S. Army Engineer Waterways Experiment Station, CE.

3. Allgood, J. R., and others. Blast Loading of Small Buried Arches. Technical Report R216, Type C, April 1963. Port Hueneme, Calif.: U. S. Naval Civil Engineering Laboratory.

4. Baker, W. E. "Modeling of Large Transient Elastic and Plastic Deformations of Structures Subjected to Blast Loading." Journal of Applied Mechanics, Transactions of the American Society of Mechanical Engineers, Vol 27 (September 1960).

5. Baker, W. J. Wave Propagation Studies in Laterally Confined Columns of Sand. Technical Report No. AFWL-TR-66-146, June 1967. Kirtland Air Force Base, N. Mex.: Air Force Weapons Laboratory.

6. Buckingham, E. "On Physically Similar Systems." The Physical Review, Vol IV, No. 4 (October 1914).

7. Cowell, W. L. Dynamic Tests of Structural Aluminum Alloys. Technical Report R 478, September 1966. Port Hueneme, Calif.: U. S. Naval Civil Engineering Laboratory.

8. DaDeppo, D. A. Influence of Initial Deformation on the Bending of Arches. A Preliminary Study, TN-462, February 1963. Port Hueneme, Calif.: U. S. Naval Civil Engineering Laboratory.

9. Denton, D. R., and Flathau, W. J. "Model Study of Dynamically Loaded Arch Structures." Journal of the Engineering Mechanics Division, American Society of Civil Engineers, Vol 92, No. EM3 (June 1966).

10. Design of Structures to Resist Nuclear Weapons Effects. American Society of Civil Engineers, Manual of Engineering Practice No. 42, 1961.

11. Durbin, W. L. Study of the Dynamic Stress-Strain and Wave-Propagation Characteristics of Soils; Measurements of Stress-Strain, Peak Particle Velocity, and Wave-Propagation Velocity in Three Sands. Contract Report No. 3-91, February 1965. Vicksburg, Miss.: U. S. Army Engineer Waterways Experiment Station, CE, and Burlingame, Calif.: United Research Services Corporation.

12. Flathau, W. J., Brechenridge, R. A., and Wiehle, C. K. Blast Loading and Response of Underground Concrete Arch Protective Structures (U). Project 3.1, Operation PLUMBOB, WT-1420, June 1959. Vicksburg, Miss.: U. S. Army Engineer Waterways Experiment Station, CE, and Port Hueneme, Calif.: U. S. Naval Civil Engineering Laboratory.

13. Flathau, W. J., and Meyer, G. D. Static and Dynamic Tests of Buried Unreinforced Concrete Arches. Miscellaneous Paper No. 1-809, April 1966. Vicksburg, Miss.: U. S. Army Engineer Waterways Experiment Station, CE.

14. Jones, G. H. S. The Use of Models in the Study of the Blast Effects of Simulated Nuclear Weapons. Technical Paper No. 132, April 1958. Ralston, Alberta, Canada: Suffield Experiment Station.

15. Kennedy, T. E., Albritton, G. E., and Walker, R. E. Initial Evaluation of the Free-Field Response of the Large Blast Load Generator. Technical Report No. 1-723, June 1966. Vicksburg, Miss.: U. S. Army Engineer Waterways Experiment Station, CE.

16. Kennedy, T. E., and Hendron, A. J., Jr. The Dynamic Stress-Strain Relation for a Sand as Deduced by Studying its Shock-Wave Propagation Characteristics in a Laboratory Device. Miscellaneous Paper No. 1-831, July 1966. Vicksburg, Miss.: U. S. Army Engineer Waterways Experiment Station, CE.

17. Kolsky, H. Stress Waves in Solids. 2nd ed. New York: Dover Publications, Inc., 1963.

18. Laboratory Soil Testing. EM 1110-2-1906, 1965. Washington: U. S. Army, Office of the Chief of Engineers.

19. Langhaar, H. L. Dimensional Analysis and Theory of Models. New York and London: John Wiley and Sons, Inc., 1960.

20. Meyer, G. D., and Flathau, W. J. Static and Dynamic Tests of Unreinforced Concrete Fixed-End Arches Buried in Dry Sand. Technical Report No. 1-758, February 1967. Vicksburg, Miss.: U. S. Army Engineer Waterways Experiment Station, CE.

21. Murphy, G. Similitude in Engineering. New York: Ronald Press Co., 1950.

22. Murphy, G., and Young, D. F. A Study of the Use of Models to Simulate Dynamically Loaded Underground Structures. Technical Documentary Report No. 62-2, January 1962. Kirtland Air Force Base, N. Mex.: Air Force Special Weapons Center.

23. Murphy, G., Young, D. F., and Martin, C. W. Use of Models to Predict the Dynamic Response of Dynamically Loaded Underground Structures. Technical Documentary Report 63-3064, November 1963. Kirtland Air Force Base, N. Mex.: Air Force Special Weapons Laboratory.

24. Study of the Use of Models to Simulate Dynamically Loaded Underground Structures. Technical Documentary Report No. 62-3, February 1962. Kirtland Air Force Base, N. Mex.: Air Force Special Weapons Center, and Niles, Ill.: American Machine and Foundary Company, Mechanics Research Division.

25. Tener, R. K. Model Study of a Buried Arch Subjected to Dynamic Loading. Technical Report No. 1-660, December 1965. Vicksburg, Miss.: U. S. Army Engineer Waterways Experiment Station, CE.

26. USAEWES, Semiannual Progress Report for FY 1966, Including Long Range Plans (FY 68-72) for DASA Protective Structures Subtasks Conducted by the U. S. Army, compiled by U. S. Army Engineer Waterways Experiment Station, Vicksburg, Mississippi, February 1966.

ABSTRACT

The objective of the study was to investigate and verify model-to-prototype scaling relations for blast-loaded buried arches that respond elastically and inelastically. Four geometrically similar, semicircular, aluminum alloy arches with 4-, 8-, 12-, and 36-inch diameters were buried in dense, dry sand and subjected to airblast-induced loads on the surface. The tests were conducted in the Large Blast Load Generator located at the U. S. Army Engineer Waterways Experiment Station. The results of two series of tests, each consisting of three repeated shots, ranging from 70 to 300 psi, are presented.

Within the range of parameters investigated, the scaling of the dependent variables was adequately verified. These variables included acceleration, velocity, displacement, thrust, and bending moment.

VITA

Jimmy Piroshaw Balsara was [redacted] He attended Karachi University where he received the degree of Bachelor of Engineering (Civil) in June 1961.

In September 1961 he accepted a part-time instructor's appointment in the Department of Civil Engineering at Duke University where he pursued graduate work in civil engineering. He received the Master of Science degree from Duke University in September 1963 and continued his graduate program leading to a Doctor of Philosophy degree in the Department of Theoretical and Applied Mechanics at West Virginia University, where he also taught undergraduate mechanics courses as a part-time instructor. In June 1966 he accepted an appointment at the U. S. Army Engineer Waterways Experiment Station as a project engineer.

APPROVAL OF EXAMINING COMMITTEE

Eugene F. Smith

Edward F. Byars

H. F. Harrell

E. L. Kay

James Mc Elderry (Chairman)

Date 1 December 1967

BLANK PAGE

Unclassified
Security Classification

DOCUMENT CONTROL DATA - R & D

(Security classification of title, body of abstract and indexing annotation must be entered when the overall report is classified)

1. ORIGINATING ACTIVITY (Corporate author) U. S. Army Engineer Waterways Experiment Station Vicksburg, Mississippi	2a. REPORT SECURITY CLASSIFICATION Unclassified 2b. GROUP

3. REPORT TITLE
SIMILITUDE STUDY OF FLEXIBLE BURIED ARCHES SUBJECTED TO BLAST LOADS

4. DESCRIPTIVE NOTES (Type of report and inclusive dates)
Final report

5. AUTHOR(S) (First name, middle initial, last name)
Jimmy P. Balsara

6. REPORT DATE January 1968	7a. TOTAL NO. OF PAGES 159	7b. NO. OF REFS 26
8a. CONTRACT OR GRANT NO. b. PROJECT NO. c. NWER Subtask 13.010 d.	9a. ORIGINATOR'S REPORT NUMBER(S) Technical Report No. 1-807 9b. OTHER REPORT NO(S) (Any other numbers that may be assigned this report)	

10. DISTRIBUTION STATEMENT
This document has been approved for public release and sale; its distribution is unlimited.

11. SUPPLEMENTARY NOTES Report was also submitted as dissertation for partial fulfillment for degree of Doctor of Philosophy to the faculty of the Graduate School of West Virginia University, Morgantown, W. Va.	12. SPONSORING MILITARY ACTIVITY Defense Atomic Support Agency Washington, D. C.

13. ABSTRACT

The objective of the study was to investigate and verify model-to-prototype scaling relations for blast loaded buried arches that respond both elastically and inelastically. Four geometrically similar, semicircular aluminum alloy arches with 4-, 8-, 12-, and 36-inch diameters were buried in dense dry sand and subjected to air-blast-induced loads on the surface. The tests were conducted at the Large Blast Load Generator located at the U. S. Army Engineer Waterways Experiment Station. The results of two series of tests, each consisting of 3 repeated shots, ranging from 70 to 300 psi, are presented. Within the range of parameters investigated, the scaling of the dependent variables were adequately verified. These variables included acceleration, velocity, displacement, thrust, and bending moment.

DD FORM 1 NOV 68 1473 REPLACES DD FORM 1473, 1 JAN 64, WHICH IS OBSOLETE FOR ARMY USE.

Unclassified
Security Classification

Unclassified
Security Classification

14. KEY WORDS	LINK A		LINK B		LINK C	
	ROLE	WT	ROLE	WT	ROLE	WT
Arches						
Blast						
Similitude						
Soil dynamics						

Unclassified
Security Classification